Alma Mater Studiorum - Università di Bologna

DOTTORATO DI RICERCA IN GEOFISICA

Ciclo XXX

Settore Concorsuale: 04/A4

Settore Scientifico Disciplinare: GEO/12

Effects of tidal motion on the Mediterranean Sea General Circulation

Presentata da:

Valentina Agresti

<div style="display:flex; justify-content:space-between;">

Coordinatore Dottorato:

Supervisore:

</div>

Prof. Nadia Pinardi   **Prof. Nadia Pinardi**

Esame finale anno 2018

Acknowledgments

Firstly, I would like to express my sincere gratitude to my advisor Prof. Nadia Pinardi for the continuous support of my Ph.D study and related research, for her contagious enthusiasm and for her immense knowledge on Oceanography. I could not have imagined having a better advisor for my Ph.D study.

Besides my advisor, I would like to thank the Prof. Florent Lyard for his insightful comments and encouragement. His knowledge on tidal modelling has given a huge contribution to this work.

My sincere thanks also go to all the colleagues of the INGV Operational Oceanography Team of Bologna, especially to Emanuela Clementi, Gelsomina Mattia, Damiano Delrosso and Davide Padeletti. Without their precious support it would not be possible to conduct this research. Likewise I am grateful to Patrick Marsaleix, Damian Allain, Rachid Benchila and Jérôme Chanut for giving me precious suggestions to improve this work, during the visiting period I have spent at LEGOS, in Toulouse.

I would like to thank all my friends for supporting me spiritually and to make my life intense and fun. Antonio Ricchi deserves a special thank, for his continuous encouragements during the last three years.

I would like to thank my partner Angelo, he knows why. Last but not the least, I would like to thank my mother, my sisters and my nephews Leonardo, Frida, Cecilia and Alice, who are a great source of inspiration for me.

This thesis is dedicated to the memory of my father.

Abstract

The study of tides and their interactions with the complex dynamics of the Mediterranean Sea represents a crucial and important challenge in ocean modelling. In this work, the main semidiurnal and diurnal tides have been implemented in the NEMO model, with a horizontal resolution of 1/24°, never achieved so far in this regional configuration. Both the equilibrium tide and the Atlantic tides contribute to tidal propagation in this semi-enclosed Sea. Consequently a Mediterranean Sea tidal configuration requires high resolution to solve the Strait of Gibraltar and a careful nesting on a global tidal model. On this purpose, a modelling chain is used in this work, to downscale tidal currents to the Med Sea model lateral open boundary. Tides are also very sensitive to both a reliable bathymetry and coastline, especially at the Strait of Gibraltar and to an appropriate calibration of the parameterization of the bottom friction. A barotropic-equivalent model is used to set up the configuration and to perform several sensitivity tests, then the tidal forcing is added to a complete and realistic baroclinic tidal model, which allows to study the interactions of tides with the complex dynamic of the basin. In general, modelled M2, S2, K1 and O1 waves result in good agreement with the observations. The assessment in coastal area is based mainly on a comparison with a control set of tide gauges, while the modelled tidal solutions with NEMO are compared with the altimetry derived harmonics and with the FES2014 global tidal model solutions. This study confirms that the interaction of the barotropic tide with the topography of the Strait of Gibraltar generates an internal tidal variability which produces an enhancement of vertical mixing at the entrance of the Mediterranean Sea. Consequently saltier and colder waters are found on the surface layer in most part of the Western Mediterranean basin and higher salinity characterizes the Modified Atlantic water entering in the Eastern basin, when tides are prescribed. Tides are also responsible for the intensification of different gyres, especially in the southern part of the basin, where mesoscale and semi-permanent gyres are present. The strength of this Mediterranean tidal model is its capability to simulate from the synoptic scale to the mesoscale, an essential characteristic to understand properly the dynamics of the Mediterranean Sea and despite their moderate intensity, the important role that tides play.

Contents

viii

Chapter 1

Introduction

1.1 General characteristics of the Mediterranean Sea

The Mediterranean Sea can be defined as a mid-latitude, semi-enclosed, marginal sea character-ized by high salinities, temperatures and densities. It is connected to the global ocean through the narrow Strait of Gibraltar and it is composed by two basins that are connected by the shallow Strait of Sicily, that has a maximum depth of $500\ m$. In turn, the Adriatic and the Aegean Sea are two marginal seas, connected to the eastern basin respectively through the Strait of Otranto and Crete. Both the Mediterranean Sea geography and bathymetry are very complex and the dynamical features of the basin are strongly influenced by them.

Since the net evaporation exceeds the precipitation and the river inflow, the Mediterranean Sea is characterized by a negative heat and fresh water budgets that correspond to a net loss of about $5\ W/m^2$ and $0.7\ m/yr$. This unbalance is the driver of an anti-estuarine circulation through the Strait of Gibraltar. In fact the negative budget is compensated by water supply from the Atlantic Sea that enters on the the Mediterranean Sea surface layer, while colder and saltier waters outflows through the bottom layer (Lascaratos and Nittis, 1998).

The flow exchange at Gibraltar Strait controls the circulation in the overall basin with a decadal time scale. The other two physical processes responsible for the Mediterranean Sea anti-estuarine circulation that happen at different timescales are the buoyancy fluxes at the surface, due to freshwater and heat fluxes, that are forcings of variable scales, from seasonal to decadal. They are responsible of the overturning circulation and control the water mass formation processes. On the other hand, the wind stress plays an important role, forcing the circulation at a sub-basin scale and with a strong seasonal variability. These three forcings, their connexions and interactions are widely described by Pinardi and Navarra (1993).
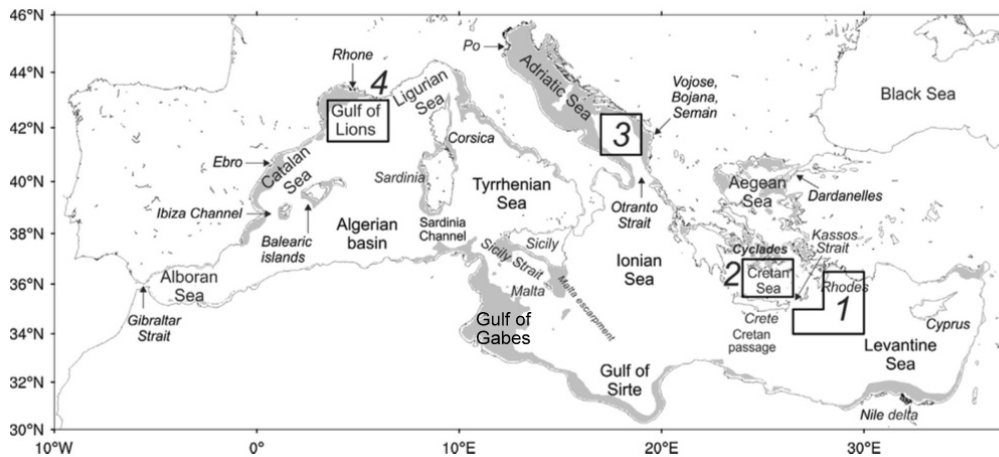
FIGURE 1.1: Mediterranean basin geometry and nomenclature for major seas and areas. The four boxes (1 - 4) show the water mass formation areas. Reproduced from Pinardi et al. (2015).

The water mass formation is an uncommon ocean dynamic process, characterizing the Mediterranean Sea, which deserves much attention. The stratification of waters in the basin is characterized by the surface layer fresher Atlantic water up to 100 m of depth which overlies the Levantine Intermediate Water, formed in the Levantine basin, populating the layer between 200 and 600 m. The deep water masses, found at depth greater than 1500 m remain separate between the eastern and western basins. In fact, the Western Mediterranean Deep Waters (WMDW) and the Eastern Mediterranean Deep Waters (EMDW) are formed in the Gulf of Lyon area and the South Adriatic Sea, respectively, even if the EMDW can also form in the Rohodes Gyre and in the Cretan Sea (Fig. 1.1). A schematic of the vertical distribution of water in the basin is shown in Figure 1.2.

A recent exhaustive description of the Mediterranean Sea circulation structure and dynamics is provided by Pinardi et al. (2015). This analysis is derived from a 23-year-long reanalysis of the ocean circulation carried out by Adani, Dobricic, and Pinardi (2011). The multi-decadal mean flow emerging from this analysis is consistent with the previous findings with the Northern basin dominated by cyclonic gyres and the Southern one characterized by anticyclonic gyres and eddies. Besides this circulation pattern, more defined open ocean, free jet intensified structures are evident. This work documents, for the first time, a clear picture of the Northern Ionian Reversal phenomenon.

Among the previous works, assessing the dominant mesoscale circulation component of the Mediterranean Sea, characterized by semi-permanent and persistent eddies, we mention the ones of Robinson et al. (1992) and Ayoub, Le Traon, and De Mey (1998).

Mediterranean Sea water masses: vertical distribution
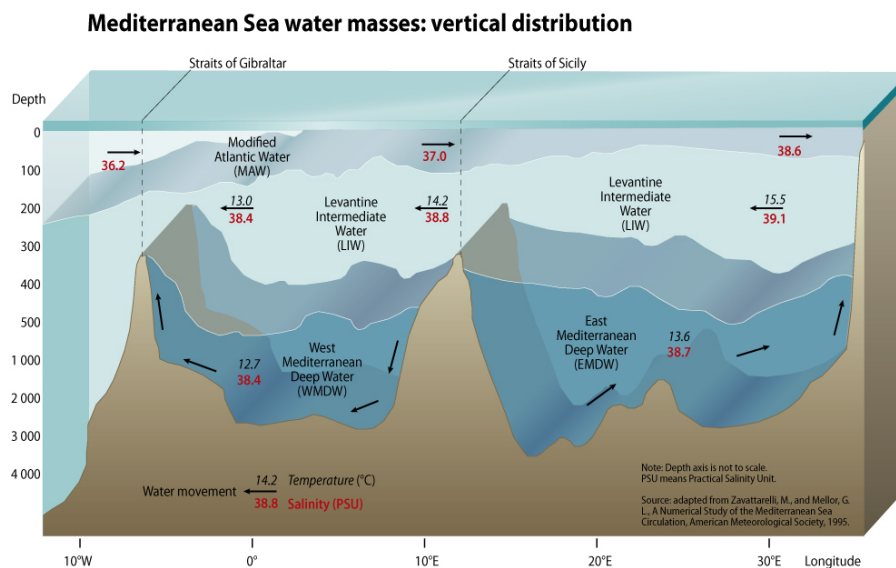
FIGURE 1.2: Vertical distribution of Mediterranean Sea water masses. Adapted from Zavatarielli and Mellor (1995) and reproduced from http://www.grida.no/resources/5885.

For what concerns the surface circulation of the Mediterranean basin, the Atlantic Water Current dominates the surface mean eastward flow with several complex meandering structures on both sides. These structures can be appreciated in Figure 1.3.
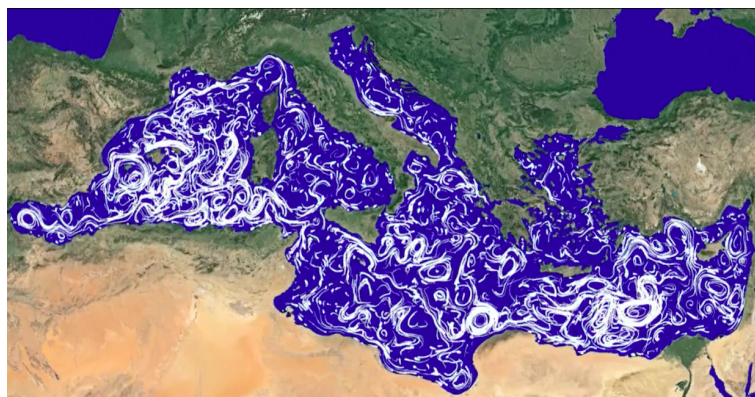
FIGURE 1.3: Mediterranean Sea Surface currents. Reproduced from http://oceanop.bo.ingv.it/multimedia/.

Figure 1.4 shows the surface and intermediate circulation structures in the Mediterranean Sea, the grey areas indicating the velocity amplitudes greater than 0.1 m/s and 0.05 m/s respectively. More precisely, from the panel (a) of this figure it is possible to see the Atlantic Water (AW) flowing into the Mediterranean Sea and, following an overall cyclonic path, meandering around the Alboran anti-cyclonic gyres, spreading northward as far as the Balearic Islands. On the other hand, the Algerian current flows along the African Coast and then bifurcates, partly entering the Eastern basin through the Sicily Channel and partly proceeding to the northwest along the

Tyrrhenian Coast and recirculating westward as the Northern Current. The inflow into the Levantine basin describes a major cyclonic basin wide gyre developing unstable eddies along the Southern Coast and then being transformed into the salty and warm Levantine Intermediate Water (LIW) off the Turkish Coast, where the structure of the Rhode gyre is also evident.

The newly formed LIW occupies the layer between 200 and 300 m. This current (Figure 1.4, panel (b)) recirculates westward spreading into the Ionian basin and the Southern Adriatic Sea. A second branch directs toward the Tyrrhenian Sea and after a cyclonic circulation constrained by the Sardinian, in turn this current bifurcates with a branch that directs toward the Gulf of Lyon (where the LIW can take part of deep water formation processes) and another one that reach directly the Strait of Gibraltar.

1.2   Mechanism of tides and their characteristics in the Mediterranean Sea

1.2.1   Tidal harmonics

Tides are regular and predictable oceanic waves that cause large variations in the sea level, especially in coastal areas. These periodical oscillations of the sea surface are caused by the gravitational attraction of celestial bodies, in particular the Sun and the Moon.

The response of the ocean to the tide-raising forces of the Moon and the Sun is in the form of long waves, thus propagating through the ocean following the physics of these waves, interacting with each other and with the local peculiarities of the system, such as its geometry and bathymetry. These characteristics, together with the Earth's rotation, are determining factors of tidal magnitude and propagation which are: large ranges in shallow shelf seas and a cyclonic propagation around the ocean basins.

The history of developing tidal concepts and prediction is discussed in the work of Pinardi et al. (2017) in which the authors highlight the importance of tides from many points of view. First, the prediction of tides is very important since they can participate to the generation of coastal floods events by the interaction with tsunamis, storm surges and wind waves. Furthermore, tides form strong currents in many shallow-shelf seas, hence their correct prediction is crucial to navigation purposes.
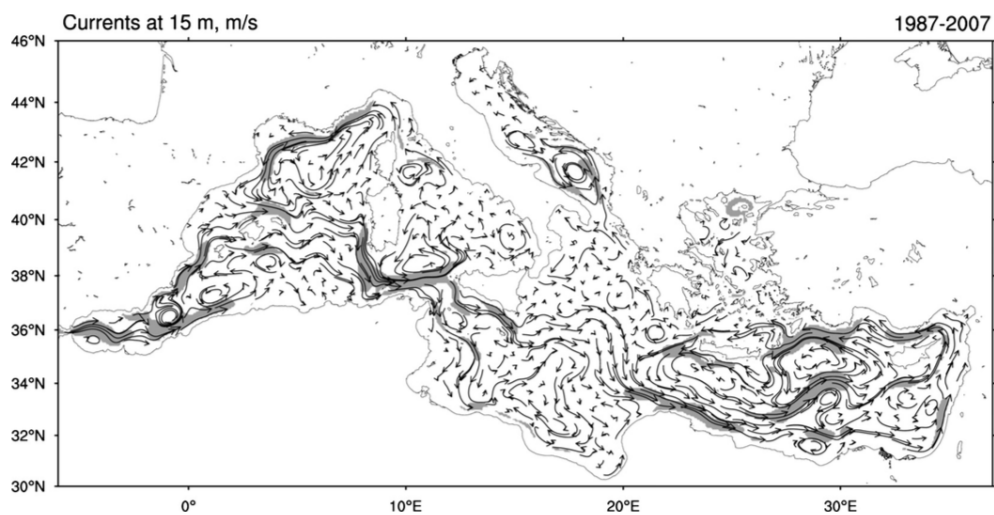
(a) Surface Mediterranean Sea currents at 15 m
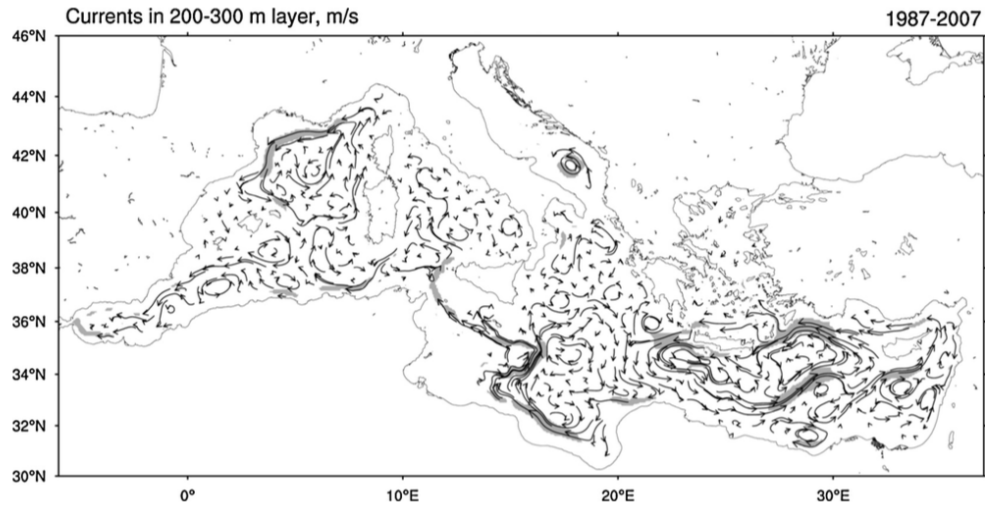
(b) Intermediate Mediterranean Sea currents at 200 m

FIGURE 1.4: 1987 - 2007 time mean circulation from the reanalysis. Reproduced from Pinardi et al. (2015).

Tides are also the object of modern research, having been identified as a primary source of energy to mix the interior ocean. It has been demonstrated that the barotropic tidal energy is converted into heat through a series of important mixing processes. More precisely when the barotropic tides flow over rough topographic features, a portion of the barotropic energy is lost directly through local mixing, while the other portion is converted into baroclinic energy through the generation of internal (baroclinic) tides. This generated baroclinic energy either dissipates locally or radiates into the open ocean, and then cascades into smaller scales along the internal wave spectrum and finally turns into deep ocean turbulence (Kang, 2012).
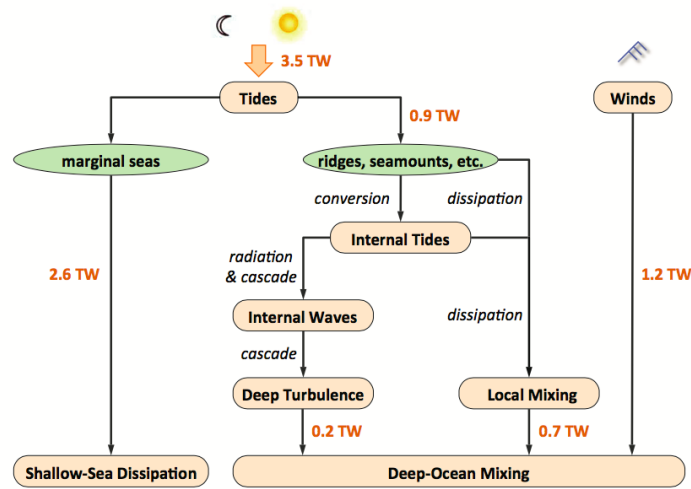
FIGURE 1.5: Global energy flux budget based on Munch and Wunsch (1998).
Reproduced from Kang (2012)

In Figure 1.5 the energy flux budget described by Munk and Wunsch (1998) is reperesented. Tides and winds are the two major sources of energy to mix the ocean. Tides contribution is of 3.5 TW of energy of which 2.6 TW are dissipated in shallow marginal seas and 0.9 TW are lost in the deep ocean. The winds provide 1.2 TW of additional mixing power to maintain the global abyssal density distribution. Those results are confirmed by the work of Egbert and Ray (2000) and Egbert and Ray (2001), who raise the interest in internal tides as a major source of energy for deep-ocean mixing.

The mathematical description of tidal waves is based on a sum of cosine functions (Eq. 1.1) which represent the fluctuation of the tidal sea level in time.

$$\eta\left(t\right) = \sum_{k=1}^{n} A_k \cos\left(w_k t + \phi_k\right) \tag{1.1}$$

where η is the tidal sea elevation, A_k and ϕ_k are the amplitude and the phase, namely the tidal harmonics, w_i is the frequency and the index k is associated to each tidal harmonic.

The tidal harmonics allow to predict the tidal sea elevation $\eta(t)$ at any location, forward or backward in time. They are obtained by means of the harmonic analysis which allows to break down the tidal signal into a series of much simpler waves described by their amplitude and phase. The frequency of each tidal wave is known, being related to the astronomical motion of the Earth-Moon-Sun system.

The relative motions of the Earth, Moon and Sun cause the tides to vary in a fortnightly cycle:

- *Spring tides* occur when the Sun, Earth and Moon are in line, so that lunar and solar gravitational forces work together.

- *Neap tides* occur when the Moon is a quarter of the way around its orbit from the previous spring tide, so that lunar and solar gravitational forces partially cancel each other out

This spring-neap cycle is due to the combination of the two main semidiurnal tidal components that are the lunar M2 and the solar S2 harmonics. In fact, for their periods of 12 hours and 24 minutes and 12 hours, they move respectively in and out of phase over a 14.8 days cycle.

K1 and O1 are the two principle diurnal constituents which account for the declination of the Moon that changes during the solar year. Other astronomical factors, such as the ellipticity of orbits and the inclination of the lunar orbit to that of the Earth around the Sun, introduce other tidal components of lower magnitude.

1.2.2 The tides in the Mediterranean Sea

The tides in the Mediterranean are semidiurnal in nature and are the result of the combined effect of local gravitational attraction of the Moon and the Sun, the so called equilibrium tide, and the tidal forcing from the Atlantic Ocean that penetrates through the Strait of Gibraltar.

With the exception of the Adriatic Sea, the Aegean Sea and the Gulf of Gabès where tides have important ranges and are amplified by resonance phenomena (Defant, 1961), tides in the Mediterranean Sea have amplitudes of the order of few centimetres.

Figure 1.6 shows the harmonics of the main semidiurnal and diurnal tidal constituents (M2 and K1) from FES2014 global tidal model (Section 1.3.1), in the Mediterranean Sea. A description

of these two tidal components is exhaustive for an overview of tidal propagation in the Mediterranean Sea, since the other semidiurnal and diurnal tidal constituents have similar patterns but with reduced amplitudes.

According to the study of Tsimplis, Proctor, and Flather, 1995, the role of the incoming Atlantic tidal wave in the Mediterranean basin is to affect mainly the Western Mediterranean basin and to modulate the equilibrium tide in the Eastern part of the basin. This is true mostly for the semidiurnal tides with the M2 constituent reaching an amplitude of about 30 cm at the Alboran Sea. In particular the harmonic analysis of measured sea level time series at the tide gauge stations of Algeciras and Ceuta, which are placed at the entrance of the Strait of Gibraltar (figure B.1), gives amplitude values respectively of 32 cm and 30 cm.

The important tidal ranges measured in other coastal areas can be mainly attributed to the shallow bathymetry and to tidal resonance phenomena. The Gulf of Gabès has been the object of the study of Sammari, Koutitonsky, and Moussa (2006) who have analysed the tidal and low frequency variability of the measured sea level time series. The authors find that tides are responsible for most of the observed sea level variability and also that semidiurnal tides can behave as standing waves within the gulf. In fact this latter has the right dimension to entertain tidal resonance for most semi-diurnal tidal harmonics. In the work of Sammari et al., tidal amplitudes values are estimated from their measurement, with 51 cm for the M2 tidal wave and 36 cm for the S2 one, at the city of Gabès. These values are still a reference for the validation of current tidal models, due to the lack of observational data in the Strait of Sicily.

A similar study demonstrating the resonant character of tidal propagation in the Aegean Sea with both observations and a numerical model is the one of Tsimplis (1994). The author firstly defines the semidiurnal character of tides in the Aegean and Ionian Seas, finding a similar tidal propagation pattern for all the semidiurnal components from South-East to North-West with an enhancement in the North Aegean. Resonance phenomena are particluary intense at the tidal gauge stations placed in the Gulf of Corinth and in the Euripus Strait, where the highest tidal amplitude values are recored, namely 19 cm at the North Halkis tide gauge and 10.8 cm at the Posidonia tide gauge.

For what concerns the North Adriatic Sea, high amplitudes values characterize the most energetic tidal wave M2 for which the amplitude recorded at Venice and Trieste tide gauges are respectively of 23.5 cm and 26.5 cm. M2 and S2 waves propagate ciclonically in the Adriatic Sea showing a strong enhancement in the northern part of the Adriatic Sea. An amphidromic node is situated in the centre of the basin, between the Italian city of Ancona and the Croatian city of Zadar.

Also in this case, the tidal resonance plays an important role in enhancing tidal ranges. It is worth noting that the major component of tidal regime in the Adriatic Sea is linked to the astronomical tidal oscillations of the Ionian Sea, which induces forced oscillations of the Adriatic basin. Resonance phenomena are responsible for the amplification of the tidal amplitudes in the longitudinal direction, moving towards North. This suggests a tidal behaviour of the Adriatic tides very similar to that one of seiches (Cushman-Roisin et al., 2013).

Beside the convergence of phase lines in the Adriatic Sea, two other amphidrome nodes are clearly defined, one in the Balearic Sea and one in the Strait of Sicily, all characterized by a cyclonic propagation. Another degenerate amphidrome is present between the North coast of Africa and Crete.
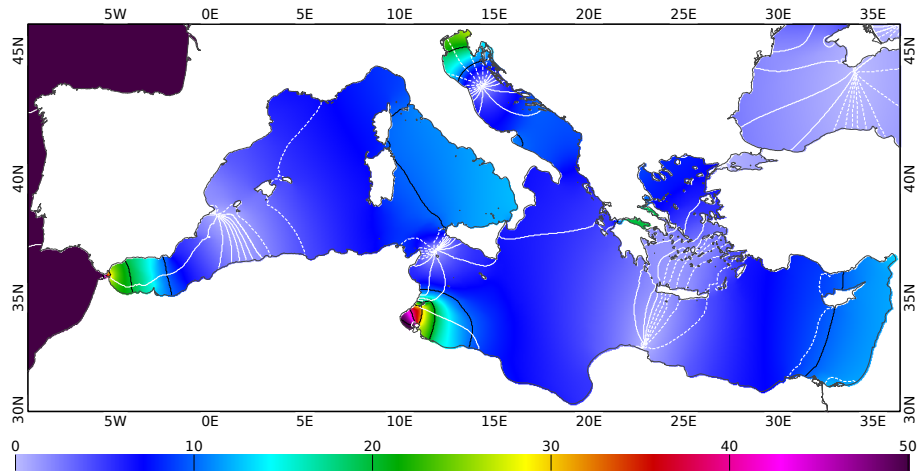
(a) M2 principal semidiurnal tidal component
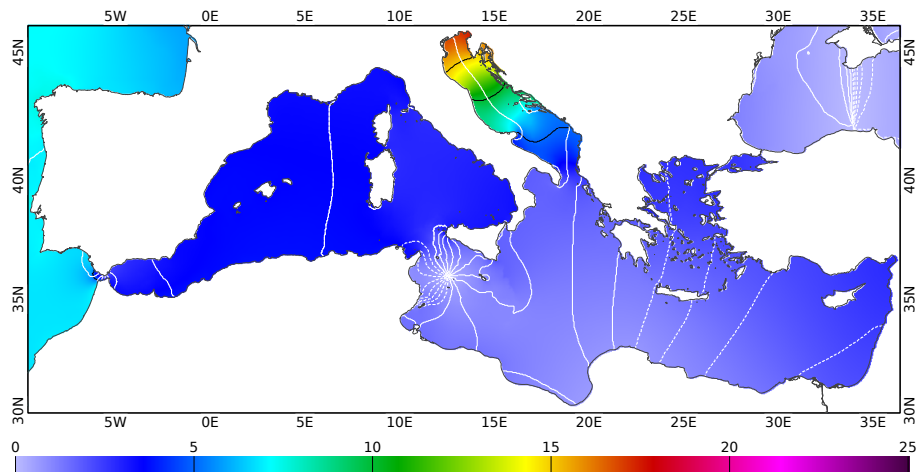
(b) K1 principal diurnal tidal component

FIGURE 1.6: Amplitude (black lines and colours) and phase (white lines) from FES2014 in the Mediterranean Sea. Panel (a) show the M2 main semidiurnal component and panel (b) shows K1 the main diurnal one.

From the comparison of the two paneles of figure 1.6 it is evident that the diurnal tidal component

K1 has remarkable amplitude values only in the Adriatic Sea. Here K1 shows a weak amplitude in the souther part of the basin, while it is enhanced moving northwards, developing isopleth lines of amplitude perpendicular to the longitudinal axis of the basin. The only amphidromic node associated to K1 tidal constituent is placed in the Strait of Sicily.

1.3   Numerical tidal models

So far, several numerical global tidal models have been developed by different Research Centres and Universities. These models found many applications in several geophysical fields, such as the de-tiding of satellite altimetry and gravimetry signals that allows the study of smaller non-tidal signals.

During the last years, many efforts have been done in order to improve the tidal models accuracy and the aim of this section is to give an overview of the state-of-the-art of numerical global tidal models. Three groups of modern global tidal models have been categorised by Arabelos et al. (2011). First, the purely hydrodynamic models that are the ones derived by solving the Laplace Tidal Equations (LTE):

$$\frac{\partial \vec{u}}{\partial t} = -f\hat{k} \times \vec{u} - g\nabla(\eta + \eta_{tide})$$
$$\frac{\partial \eta}{\partial t} = -\nabla\left(H\vec{u}\right)$$

$$(1.2)$$

where $\vec{u}$ is the depth-average current vector, t is the time, $\hat{k}$ is a unit vector that indicates the vertical direction, $f = 2\Omega\sin{(\phi)}$ is the Coriolis parameter (where ϕ is the latitude and Ω is the Earth's rotation rate), g is the gravitational acceleration, H is the still water depth, η is the surface elevation and η_{tide} is the equilibrium tide.

The empirical models are derived from the extraction of the ocean tidal signal from the satellite altimetry and are mainly used in altimetry applications, such as the ocean tide corrections.

Finally there are the assimilative models, which are derived by solving the hydrodynamic equations and are constrained by observations, through data assimilation algorithms.

The assessment of the main global barotropic ocean tide models is the object of a recent review article by Stammer et al. (2014) which describes the improvements in tidal modelling achieved since the publication of the work of Shum et al. (1997), after seventeen years. Certainly a great part of the improvements achieved in tidal modelling, during the last twenty years, is due to

the contribution of longer series of altimetry data. In addition, the increasing of the horizontal resolution, deriving from the enhanced computational power play an important role, especially in coastal area models.

In this work, the interest on global tidal assimilative models is twofold. First, due to the high accuracy the current models have reached, they can be considered a benchmark for tidal models regional solutions. On the other hand, tidal elevations and currents, extracted from a global tidal model, are prescribed at the boundary of regional configurations. For example, in this study, an accurate modelling of the Atlantic tidal wave is of primary importance.

A description of the main assimilative models used in this work and their performances is given in next section.

1.3.1   Assimilative global tidal models

In this section the two global assimilative models used in this work are described, referring to the validation performed by Stammer et al. (2014). They are FES2012 (Lyard et al., 2006) and TPXO-8 (Egbert and Erofeeva, 2002). The only difference is that here we use the last release of the Finite Element Solutions which is FES2014.

FES2012 (Carrère et al., 2012) is a finite element tidal solution, initiated by Le Provost et al. (1994). This model is based on the hydrodynamic tidal solutions of T-UGO (Toulouse-Unstructured Grid Ocean model) described in section 1.3.2 and it is built upon altimetry-derived harmonic constant assimilation using the ensemble, frequency domain SpEnOI (Spectral Ensemble Optimal Interpolation) data assimilation software.

The horizontal discretization used for FES12 is a continuous Lagrange polynomial second-order interpolation (LGP2) for elevation and discontinuous nonconforming P1 (linear approximation with nodes located at element side midpoints) for tidal currents. Resolution varies from a few kilometres in coastal areas up to about 25 km in the deep ocean and the tidal products are available on a structured grid, with a resolution of $1/6° \times 1/6°$.

The unstructured grid covers the global ocean, with the required topography based on a number of sources, including approximately 20 regional terrain models, with considerable effort devoted to improving shelf and ice-shelf seas. Ensembles were built by perturbing the main tidal parameters, such as bathymetry, bottom friction, and internal tide drag. The density of data used in assimilation was tuned as a function of depth.

	TPXO-8	FES2014
NUMERICAL METHOD	Finite Difference Model (FDM)	Finite Elements Model (FEM)
RESOLUTION	Global solutions: 1/6° x 1/6° and HR local solutions	1 464 500 triangles 2 981 213 elevation nodes 4 393 500 velocity nodes
PRINCIPLE	Best-fits, in a least-square sense, of the Lapalcian Tidal Equations and along track altimetric data	Resolution of tidal barotropic equations of T-UGOm model and the assimilation of data
ASSIMILATED DATA	TOPEX/Poseidon and Jason and tide gauges data	TOPEX/Poseidon, Jason-1, Jason-2, TPN-J1N, ERS-1, ERS-2, Envisat and tide gauges data
TIDAL PRODUCTS	Tidal elevations and currents Amplitude and phase of 13 tidal constituents distributed on a 1/6° x 1/6° grid M2, S2, N2, K2, K1, O1, P1, Q1, Mf, Mm, M4, MS4, MN4	Tidal elevations, currents and tide loading Amplitude and phase of 34 tidal constituents distributed on 1/16° x 1/16° grid M2, S2, N2, K2, K1, O1, P1, Q1, 2N2, EPS2, J1, L2, La, M3, M4, M6, M8, Mf, MKS2, Mm, MN4, MS4, MSf, MSqm, Mtm, Mu2, N2, N4, Nu2, R2, S1, S4, Sa, Ssa, T2

TABLE 1.1: Main characteristics of the global tidal models TPXO-8 and FES2014

TPXO8 is the most recent in a series of tidal solutions based on the assimilation of altimetry data into a global shallow-water model. The representer-based variational scheme is described by Egbert, Bennett, and Foreman (1994) and Egbert and Erofeeva (2002). The base global solution has a resolution of $1/6° \times 1/6°$ and respect to the previous TPXO release, thirty-three regional high resolution ($1/30° \times 1/30°$) assimilation solutions are incorporated, including all major enclosed or semi-enclosed seas and most coastal areas with significant continental shelf width. Finally thanks to a weighted average, the regional and global solutions are merged. A description of the main characteristics of TPXO-8 and of the last version of FES, and of their products is given in table 1.1.

The propagation of tides in the Mediterranean Sea is strongly affected by the complex bathymetry, the system of Straits and the huge number of islands. For this reason, among the global tidal model described, only FES and TPXO are eligible as reference models, having enough horizontal resolution to solve well this semi-enclosed Sea. In order to compare the performances of the two global models some results of the validation against tide gauge data performed by Stammer et al.

(2014) are shown hereafter.
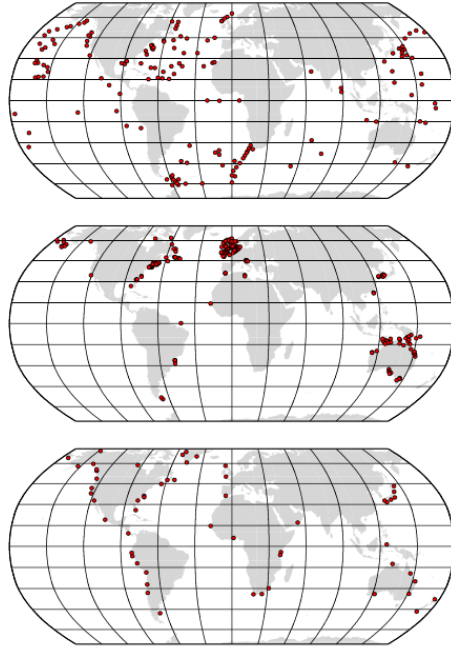
FIGURE 1.7: Station locations for the validation of global tidal model from Stammer et al. (2014). Deep - water stations (top), shelf stations (middle), coastal stations (bottom).

This analysis is performed separately, for the deep water tides, shelf tides and coastal tides since each area is influenced in a different way by the assimilation of satellite altimetry data. The most affected sites are the deep-ocean ones while the accuracy of coastal tides relies mostly on hydrodynamic modelling and accurate bathymetry. In figure 1.7 the validation sites are shown, while the results of the validation for FES2012 and TPXO-8, from the work of Stammer et al. (2014) can be appreciated in figure 1.8, for the main height diurnal and semidiurnal tidal components.

$$RMS_{difference} = \overline{\left([A_{obs} \cos(\omega t - \phi_{obs}) - A_{mod} \cos(\omega t - \phi_{mod})]^2 \right)^{\frac{1}{2}}} \qquad (1.3)$$

The equation 1.3 is the $RMS_{difference}$, where A is the amplitude, ω is the frequency, t is the time and ϕ is the phase lag. This is computed over a full cycle of the tidal constituent (ωt varying from 0 to 2π) and over all the stations locations, according to the tide gauge site (deep-water, shelf or coastal site).

The assessment of the model in deep water sites is performed against 151 measurements of bottom pressure time series. The conversion of bottom pressure amplitudes to equivalent sea

(a) Deep-water stations

(b) Shelf stations

(c) coastal stations

(d) RSS relative to deep-water, shelf and coastal stations
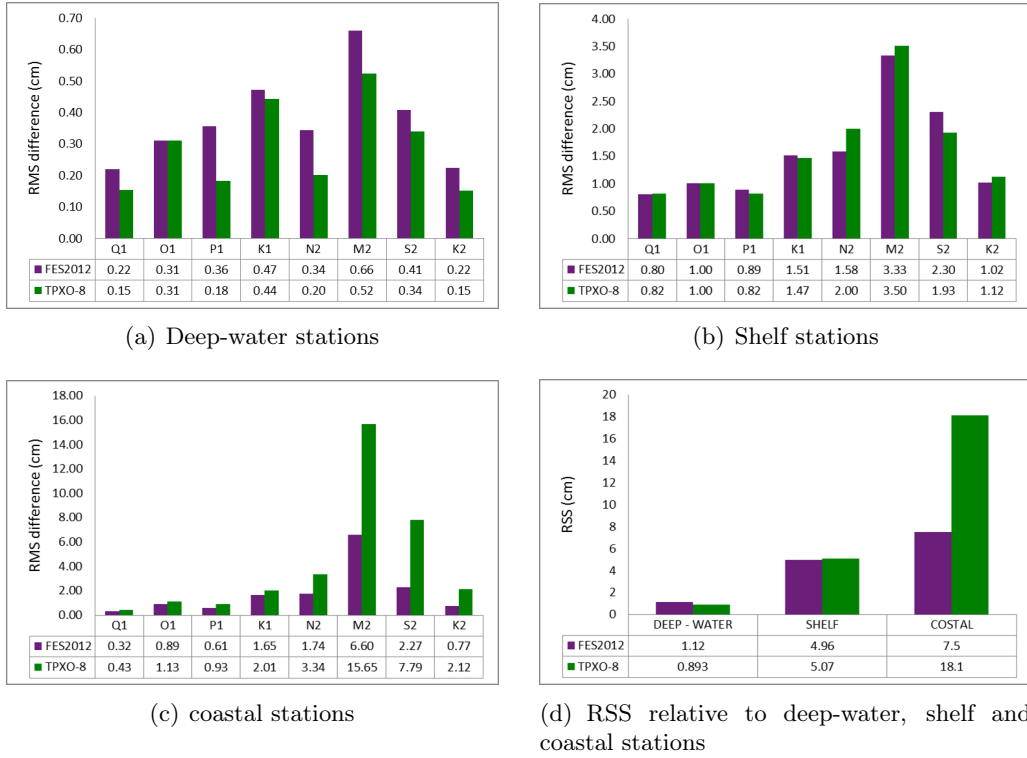
FIGURE 1.8: RMS model differences with tidal signals and RSS (cm). The results of the validation are taken from Stammer et al. (2014).

surface heights is based on a climatological ocean density at each station location. From figure 1.8 (a), it is possible to infer that TPXO-8 performs better than FES2012 at deep-water stations. Moreover, compared to coastal (Figure 1.8 (c)) and shelf (Figure 1.8 (b)) areas, the errors of deep-water sites are very low. This result can be attributed directly to the robustness of the data assimilation technique.

For what concerns the shelf stations, the comparison is done against 195 stations located in areas, generally shallower than 200 m. Among these, several stations are located in the most tidal affected areas of the Mediterranean Sea, such as the North Adriatic, the Strait of Gibraltar and the Gulf of Gabès. Compared to deep ocean sites, the accuracy at shelf station is lower, with the greater $RMS_{difference}$ associated to the principal semidiurnal component M2. In general the errors are larger for the semidiurnal tidal components and FES2012 performs better than TPXO-8. For the diurnal tidal constituents the errors are lower and comparable for the two models.

Finally the assessment of global tidal models against coastal sites is given in Figure 1.8 (c). Respect to the deep water stations, the model error can be very large in near-coastal zone where tides can reach huge tidal ranges. The 56 stations involved in this validation are well documented

and with reliable tidal harmonic constants. Also in this case, the greatest errors are associated to the most intense semidiurnal tidal components. FES2012 is more accurate than TPXO-8, for all the considered tidal waves, especially for semidiurnal ones. This trend is also evident from Figure 1.8 (d) which shows the RSS (Root Sum Squared) of all the tidal constituents. From this figure it is possible to deduce that what makes the main difference between the accuracy of the two models (FES2012 and TPXO-8) is the better performance of the Finite Element Solutions in coastal areas.

The result achieved with FES2012 in coastal areas can be attributed to the model itself, which has a better accuracy in coastal areas. In fact, the advantages of using unstructured mesh are the enhancement of resolution in regions of complex geometry together with a more realistic description of the shorelines.

1.3.2 Hydrodynamic tidal models

The numerical tidal models that do not assimilate data are obviously less accurate than the assimilative ones. Stammer et al. (2014) estimate a factor 10 between the errors associated to the two kinds of model. Due to the spatial inhomogeneity of tide gauges networks, the comparison of hydrodynamics and assimilative tidal models allows an estimation of errors distribution over all the domain. These errors can be associated to difference on both tidal amplitudes and phases.

Unlike the assimilative models, the improvements in tidal modelling in purely hydrodynamic models can derive from increasing the spatial resolution which in turn implies a better representation of the bathymetry and of the coastline. Moreover the use of more and more accurate bathymetric dataset or a composite of different ones can be responsible for a more reliable representation of tidal waves and all the physical phenomena associated.

Other modelling aspects are related to correct simulation of tides. Among these, there is the implementation of the Self-Attraction and Loading effect (SAL) that represents the modification of the Earth gravity fields accomplished by tides through mass redistribution. This feature can be considered in numerical models, by an additional term to the existing astronomical potential.

A theoretical aspects that is the object of modern research, is the understanding of tidal dissipation mechanisms. Many recent studies have addressed to the conversion of barotropic tidal energy into baroclinic motion (Egbert and Ray (2000)) and to the role of baroclinic processes in

the energy budget. This energy sink is considered in numerical models through the parametrisation of a topographic internal wave drag, some examples of this parametrisation can be found on the work of Lyard et al. (2006) and Green and Nycander (2013).

In this work, the hydrodynamic model used for simulation of tides is the last version of NEMO (Nucleus for European Modelling of the Ocean). Tidal simulation and tidal mixing parametrization capabilities are available in the NEMO numerical model. Some examples of their implementation can be found on the regional configurations of on the North European West Shelf (O'dea et al., 2012) and on the Iberia-Biscay-Ireland configuration (Maraldi et al., 2013).

In NEMO model, the tidal gravitational forcing is implemented as in the LTE equation (Eq. 1.2), representing the equilibrium tide η_{tide} with the sum of all the involved tidal waves. A different formulation is used if tides are diurnal or semidiurnal, according to the equation 1.4.

$$\eta_{tide} = \sum_k \eta_{semidiurnal} + \sum_k \eta_{diurnal}$$
$$\eta_{semidiurnal} = g A_k \left(\cos^2 \phi\right) \cos\left(\omega_k t + 2\lambda + V_{0k}\right) \tag{1.4}$$
$$\eta_{diurnal} = g A_k \left(\sin 2\phi\right) \cos\left(\omega_k t + \lambda + V_{0k}\right)$$

where A_k is the amplitude, ω_k is the pulsation, V_{0k} is the astronomical phase of the wave k. λ an ϕ are the longitude and the latitude respectively. The discussion of long term tides is neglected at this stage.

At the open lateral boundaries (olb), tides are prescribed by adding the tidal elevation and velocity to the non tidal ones (Eq.1.5).

$$\eta_{olb} = \eta_{slow} + \sum_k A_{\eta k} \cos\left(\omega_k t + \phi_{\eta k}\right)$$
$$U_{olb} = U_{slow} + \sum_k A_{uk} \cos\left(\omega_k t + \phi_{uk}\right) \tag{1.5}$$
$$V_{olb} = V_{slow} + \sum_k A_{vk} \cos\left(\omega_k t + \phi_{vk}\right)$$

In the equation 1.5 $A_{\eta k}$ and $\phi_{\eta k}$ are the amplitude and the phase of tidal elevation and A_{uk}, A_{vk}, ϕ_{uk} and ϕ_{vk} are the amplitudes and phases associated to the tidal zonal and meridional currents. These tidal harmonics can be assessed from the observations or from an assimilative model such as FES and TPXO. The k index in equations 1.4 and 1.5 refers to the tidal wave, in

Tidal wave	description
M2	Principal lunar semidiurnal tidal constituent
N2	Larger lunar elliptic semidiurnal tidal constituent
2N2	Lunar elliptic semidiurnal second-orded tidal constituent
S2	Principal solar semidiurnal tidal constituent
K2	Lunisolar semidiurnal tidal constituent
K1	Lunisolar diurnal tidal constituent
O1	Lunar diurnal tidal constituent
Q1	Larger lunar elliptic diurnal tidal constituent
P1	Solar diurnal tidal constituent
M4	Shallow water overtide of the principal lunar tidal constituent
Mf	Lunar fortnightly tidal constituent
Mm	Lunar monthly tidal constituent
Msqm	Long period tidal constituent
Mtm	Long period tidal constituent
S1	Solar diurnal tidal constituent
MU2	Varational tidal constituent
NU2	Larger lunar evectional tidal constituent
L2	Smaller lunar elliptic semi diurnal tidal constituent
T2	Larger solar elliptic tidal constituent

TABLE 1.2: Tidal waves implemented in NEMO model (version 3.6)

the last available version of NEMO model (v. 3.6), 19 tidal constituent can be considered. They are listed in table 1.2.

More details on the tidal constituent in table 1.2 can be found on Hicks and Schureman (1984).

The other ocean hydrodynamic model used in this work is TUGOm, the Toulouse Unstructured Grid Ocean model (ex-Mog2D, Lynch and Gray (1979)). T-UGOm is based on unstructured meshes and it has been run in time-stepping mode and frequency domain mode. Frequency domain 2-D governing equations are derived from the classical shallow-water continuity and momentum equations, as described in Lyard et al. (2006).

T-UGOm numerical scheme is based on both on finite elements, with a triangle mesh discretisation and on finite volumes, with a quadrangle one. In the latter the discretisation for elevations and currents is based on a Arakawa C-like grid.

1.4 Overview of dissertation and objectives

The objective of this work is to build a robust tidal configuration of the Mediterranean Sea, using the numerical model NEMO with 1/24° of horizontal resolution and with 141 vertical levels. As pointed out by Sannino et al. (2014), despite the key role played by the exchange at

the Strait of Gibraltar on the Mediterranean Thermoaline Circulation, none of the ocean models implemented in the last 15 years for the Mediterranean Sea is able to fully simulate the Strait dynamics. The main limiting factors are the coarse horizontal resolution adopted at the Strait of Gibraltar and the omission of tidal forcing. Our study wants to overcome these limits, laying the foundations on the understanding of the tidal contribution to the ocean dynamic processes in the Mediterranean basin. To this purpose, many efforts have been done in order to improve the accuracy of modelled tidal waves, through an accurate calibration process.

It has been demonstrated that tides strongly affect the hydrological properties of the Atlantic inflow (Sannino, Bargagli, and Artale (2004), Sannino et al. (2009) and Sannino, Pratt, and Carillo (2009)). Moreover recently, several studies have deepen on the effects of tides in the whole basin, such as the ones of Naranjo et al. (2014), Harzallah, Alioua, and Li (2014) and Sannino et al. (2014).

The originality of this work, respect to the mentioned papers, consists in the set up of a modelling chain, used to downscale the FES2014 tidal currents to the Med Sea model lateral open boundary which allows to reduce the errors on tidal representation. The methodology used in this work consists on the implementation of a barotropic equivalent tidal model of the Mediterranean Sea. Once a satisfying tidal barotropic solution is achieved, the results of this implementation are added to a pre-operational forecasting model of the Mediterranean Sea. This allows to study the interactions of tides with the complex dynamics of the Mediterranean Sea with an horizontal resolution never achieved so far.

Consequently three main parts compose this work, the first one is the implementation of tides in a barotropic-equivalent model. Several sensitivity tests on the horizontal resolution, on the bathymetry, on the open lateral boundary scheme and data and on the bottom friction parameterization are performed. This allows an accurate calibration of tidal waves, with a progressive reduction of the errors (Chapter 2). The second and the third parts can be found in Chapter 3 and are the prescription of tides in a realistic and stratified configuration of the Mediterranean Sea and the comparison with the simplified one. Finally an evaluation of the effects of tides in the Mediterranean Sea is given, in terms of transports, salinity, temperature and currents. The conclusions of this work and some hints for future research are given in Chapter 4.

Chapter 2

Modelling the barotropic tides in the Mediterranean Sea

2.1   Introduction

Thanks to the availability of progressive enhanced computational power, current ocean models are able to solve physical processes previously neglected or parameterised. This increased resolution is a crucial factor for modelling tides in a regional sea, like the Mediterranean.

Tides in the Mediterranean Sea are produced by the direct action of the equilibrium tide and the Atlantic tidal wave that can penetrate through the Strait of Gibraltar (Pugh, 1996). Their propagation is strongly affected by its complex bathymetry. This semi-enclosed basin is connected to the Atlantic Ocean through the Strait of Gibraltar and internally is divided into the Eastern and the Western basins, separated by the Straits of Sicily and Messina. The Adriatic Sea and the Aegean Sea are connected to the Eastern basin respectively through the Straits of Otranto and Crete. Many islands, sills and narrow shelves make this configuration even more complex. On the other hand, the Dardanelles and the Suez Canal, connecting respectively the Aegean Sea with the Marmara Sea and the Mediterranean Sea with the Red Sea, can be ignored for tidal simulation studies, since they are are too narrow (Fig. 2.1).

Modelling tides in a marginal sea as the Mediterranean requires enough horizontal resolution to resolve properly the bathymetry and the straits. With respect to the ocean tides, the tidal ranges in the Mediterranean Sea is quite small, of on the order of 20 - 40 cm. Besides the Alboran Sea in which the incoming Atlantic tidal wave penetrates directly, the most tidal affected areas in the Mediterranean basin are the shallow water North Adriatic Sea and the Gulf of Gabès, where tidal amplitudes can reach 1 meter during spring tides.
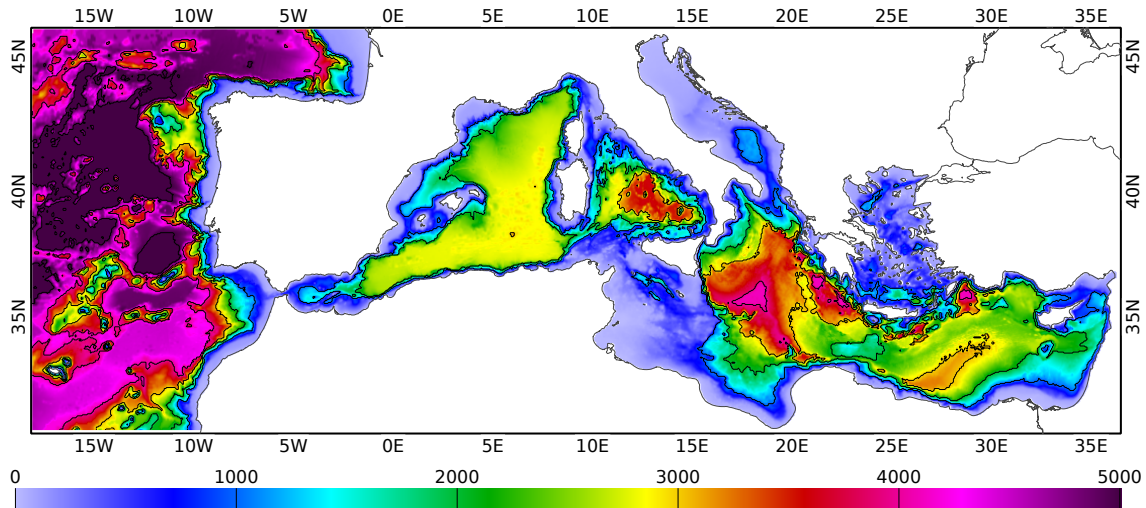
FIGURE 2.1: Model bathymetry and domain (m)

So far, many studies have focused on the role of tidal exchanges through the Strait of Gibraltar, the most recent one are: Sannino, Bargagli, and Artale (2004), Sannino et al. (2009) and Sannino, Pratt, and Carillo (2009)). Furthermore, other studies have addressed to the role of tides in the Adriatic Sea such as the Cushman-Roisin et al. (2013) and Guarnieri et al. (2013), Sammari, Koutitonsky, and Moussa (2006) in the Gulf of Gabès and Tsimplis (1994) in the Ionian and Aegean Sea. All these studies are a huge support to the understanding of the complex tidal pattern in some crucial areas of the Mediterranean Sea.

Nevertheless the aim of the first part of this work is to produce a simulation of the tidal characteristics of the main two semidiurnal (M2 and S2) and diurnal (O1 and K1) tidal components in the whole Mediterranean Sea. Brief considerations of minor tidal components such as K2, N2, P1 and Q1 are also given. The first work reproducing tides with a two dimensional hydrodynamic model was done in 1995 by Tsimplis, Proctor, and Flather (1995), with a resolution of $1/12° \times 1/12°$, forced by the equilibrium tide and by the incoming tide at the Strait of Gibraltar. The result of their work shows that the Atlantic tidal contribution is of equal importance to the direct tidal forcing in the Mediterranean. These results still remain the most complete reference for the main tidal components in the Mediterranean Sea. We will refer to this model as **T-mod** hereinafter.

The other paper dealing with the tidal propagation in the Mediterranean Sea are based on different modelling approaches. In 1995 Lozano and Candela make a study of the semidiurnal lunar M2 tidal component, based on a spectral approximation (Lozano and Candela, 1995). More recently Arabelos et al. (2011) published a study based on the assessment of a barotropic ocean tide model which assimilates tide-gauges and Topex/Poseidon data (**A-mod** hereinafter),

for eight diurnal and semidiurnal tidal constituents.

The most recent work about tides in the Mediterranean Sea is the one of Sannino et al. published in 2015. The authors investigate the importance of tides in determining the main features of the Mediterranean circulation. For this purpose they use a $1/16°$ of horizontal resolution model, with higher resolution at the Strait of Gibraltar. We refer to this model as **S-mod** hereinafter.

Our work can be conceived as the revisited study of the barotropic tides in the Mediterranean Sea, following Tsimplis approach, and using a doubled the resolution. In addition the model used is a version of the NEMO code used as a barotropic-like mode in order to check its performance and develop a methodology to compare NEMO with an existing global ocean tidal model. Our analysis uses a total of 8 tidal components which will be described, one by one, in section 2.3.4.

2.2 Modelling

2.2.1 Mediterranean barotropic model

The numerical model used in this work is based on the NEMO v3.6 ocean general circulation model (Madec, 2008). In figure 2.1 the model domain is shown. It includes the Mediterranean Sea and extends into the Atlantic Ocean with an open lateral boundary composed by three segments. This part is called the Atlantic box and it is necessary in order to simulate the exchange of water masses at the Gibraltar Strait properly, as shown by Tonani et al., 2008.

In the present work, the vertical discretisation used in NEMO is based on geopotential coordinates with partial bottom cells (Bernard et al., 2006). In particular, the z^* vertical coordinate system is used (Adcroft and Campin, 2004).

$$z^* = H\left(x, y\right) \frac{z + \eta\left(x, y, t\right)}{H\left(x, y\right) + \eta\left(x, y, t\right)} \tag{2.1}$$

where, z is the standard vertical coordinate, $\eta\left(x, y, t\right)$ is the sea surface height and $H\left(x, y\right)$ is the total ocean depth at rest. This formulation allows vertical thickness dz to be rescaled at each model time step, accounting for the varying fluid height. The model solves for the non-linear free surface equation and in order to make it equivalent to a barotropic one, constant T and s

initial values are used while surface and lateral boundary conditions are imposed at each time step. Normally the barotropic sea level equations are so written:

$$
\begin{cases}
\frac{\partial \vec{u_b}}{\partial t} + \vec{u_b} \cdot \vec{\nabla} \vec{u_b} - f\hat{k} \times \vec{u_b} = -g\vec{\nabla}\left(\eta + \Phi_{tide}\right) - g\vec{\nabla}[\int_{-H}^{0}\left(\frac{\rho-\rho_0}{\rho_0}\right) + \int_{-H}^{0} z\left(\frac{\rho-\rho_0}{\rho_0}\right)] + C_d \mid \vec{u_b} \mid \vec{u_b} \\
\frac{\partial \eta}{\partial t} + \vec{\nabla} \cdot (H\vec{u_b}) = 0
\end{cases}
$$

(2.2)

where $\vec{u_b}$ is the depth-average current vector, t is the time, $\hat{k}$ is a unit vector that indicates the vertical direction, $f = 2\Omega \sin(\phi)$ is the Coriolis parameter (where ϕ is the latitude and Ω is the Earth's rotation rate), g is the gravitational acceleration, H is the still water depth, η is the surface elevation Φ_{tide} is the equilibrium tide, ρ is the density and $C_d \mid \vec{u_b} \mid \vec{u_b}$ is the quadratic bottom friction.

If constant T and s are prescribed, it results that the density ρ is constant and the second term of the right hand side of the first equation 2.2 is zero, *i. t.* we recover the barotropic model with an equilibrium tidal potential. A three-months long simulation has been performed, neglecting the tidal potential in the equation 2.2, in order to assess the fact that T and s remain constants. In particular, the temperature and salinity have been set constant on the entire domain, respectively to the value of 15°C and 38 PSU.

In this study, a non-linear quadratic bottom friction parameterisation is applied with a logarithmic formulation of the Drag coefficient:

$$
Cd = max\left[Cd_{min'}\left\{k^{-1}ln\left(\frac{dz_b}{2z_{0b}}\right)\right\}^{-2}\right]
$$

(2.3)

where $k = 0.4$ is the Von Karman constant, $Cd_{min'} = 2.5 \times 10^{-3}$ is the minimum drag coefficient, $z_{0b} = 3.5 \times 10^{-3}$ is the bottom roughness and dz_b is the bottom cell thickness. The same formulation and coefficients are used by Maraldi et al. (2013), which describes the design and validation of a high-resolution ocean model with tides, over the Iberian Biscay Irish (IBI) area.

The turbulent mixing scheme used is the Richardson Number Dependent (Pacanowski and Philander, 1981) and the no slip condition is used as lateral boundary condition at the coastline, with no normal gradient for η and with the tangential velocity which decreases linearly from the closest ocean velocity grid point to the coastline.

The tidal forcing deriving from the incoming Atlantic tidal wave is considered, forcing the model by tidal elevation and velocity at the three open boundary segments. For this purpose the Flather boundary scheme (Flather, 1976) is used, as recommended for regional tidal simulations by (Carter and Merrifield, 2007) and reconsidered by Oddo and Pinardi (2008).

$$V = V^{tide} - \frac{\sqrt{gH}}{H} \left(\eta - \eta^{tide} \right) \tag{2.4}$$

In Flather condition (equation 2.4), η^{tide} is the tidal elevation and V^{tide} is the tidal velocity at the open boundary, V is the barotropic velocity normal to the boundary and η is the total model surface elevation. In the Mediterranean Sea, tidal harmonics that reach important amplitude values are the two semidiurnal components M2 and S2, the diurnal components K1 and to a lesser extent O1. Nevertheless a set of height harmonics is considered in the present work. They have been progressively introduced decreasing, if necessary, the external time step of integration in order to ensure the model stability, according to the CFL condition.

The model implementation considers an uniform horizontal resolution of $1/24° \times 1/24°$ which corresponds to 3.2 - 4 km in longitude and 4.6 km in latitude and it has 141 unevenly spaced vertical levels.

The bathymetry used is derived from the 30 $arc-second$ resolution GEBCO dataset [1], linearly interpolated on the $1/24°$ grid and smoothed using a fourth order Shapiro filter applied twice, in order to remove small scale grid noise. The topography is manually modified in critical areas such as the islands along the Eastern Adriatic coasts, Gibraltar and Messina Straits.

As a first approximation, the barotropic-equivalent experiments have been performed considering only the tidal forcing due to the gravitational potential, ignoring the effects of the incoming Atlantic tidal wave. This closed basin approximation gives a tidal pattern that is closed to the one described by Tsimplis, Proctor, and Flather (1995), but with a strong reduction of tidal amplitudes in the Western the basin and several discrepancies in the Eastern basin, since the incoming Atlantic tide has non-negligible effects in the Levantine Sea, in the Ionian Sea hence in the Adriatic Sea. For sake of brevity those results are omitted in this work.

In this study, the barotropic part of the dynamical equations is integrated explicitly with a short time steps of 2 s (called external or barotropic time step) while the depth varying variables, that evolve more slowly are solved with a time step of 180 s (called internal or baroclinic time step).

---

[1] http://www.gebco.net/data_and_products/gridded_bathymetry_data/gebco_30_second_grid/

This combination of internal and external time steps ensures the stability of the model with the following tidal components: M2, S2, N2, K2, K1,O1, P1, Q1.

T-UGO model is a 2D and tridimensional model [2] based on unstructured meshes which has an embedded spectral solver for tides. More precisely a frequency domain tidal dynamics solver is nested inside T-UGO model time sequential solver, so that spectral simulations can be performed. The main advantages of using the embedded spectral solver for tides are the easy implementation and the low computational coast, compared to time-step modelling.

Another powerful capability of T-UGOm is the downscaling of global tidal data of currents at the open boundaries of regional configurations. In practice, T-UGO can be run with the same bathymetry of the regional model, forced only by tidal elevations of a global tidal model. Then the simulated TUGO-m tidal currents are extracted at the boundary and used to force the regional nested model. In section 2.3.1 such application of T-UGO model is widely discussed. T-UGOm momentum and continuity equations are identical to the MOG2D generalised wave equation solver that has been derived from Lynch and Gray, 1979. The quasi-linearised, complex shallow water spectral tidal equations, for every astronomical tidal constituent (Eq. 2.6) can be obtained applying the equations 2.5 to the equations 2.2.

$$
\begin{aligned}
\vec{u} &= Re\big\{\vec{u}e^{i\omega t}\big\} \\
\eta &= Re\big\{\alpha e^{i\omega t}\big\}
\end{aligned}
\tag{2.5}
$$

$$
\begin{cases}
j\omega\vec{u} + \vec{f} \times \vec{u} = -g\nabla \cdot (\alpha) + g\nabla\Pi - \vec{D}\vec{u} \\
j\omega\alpha + \nabla \cdot H\vec{u} = 0
\end{cases}
\tag{2.6}
$$

where $j = \sqrt{-1}$, ω is the tidal frequency in rad/s, α is the surface elevation, Π is ocean tidal amplitude potential, $\vec{D}$ the drag tensor, $\vec{f} = 2\Omega\sin\theta\hat{k}$ is the Earth rotation vector and g is the gravity constant. The drag tensor takes account both the bottom drag contribution and of the wave drag energy dissipation (Lyard et al., 2006).

T-UGOm numerical scheme is based on finite elements, with a triangle or quadrangle mesh. The latter has been implemented in order to make TUGO-m (model) solutions comparable to the ones of structured model grids, such as NEMO.

In regional configurations studies, TUGO-m requires the bathymetry and the tidal elevation amplitude and phase as lateral boundary data. These harmonics are extracted from the global

---

[2] http://sirocco.omp.obs-mip.fr/ocean_models/tugo

tidal model FES2014. In the present study, the vertical viscosity coefficient is the same of NEMO $(1.2 \times 10^{-6} m^2 s^{-1})$ and a quadratic bottom friction coefficient is used, with the dimensionless friction coefficient Cd taken as 2.5×10^{-3}. As for the NEMO barotropic-equivalent experiment, the atmospheric pressure forcing is neglected.

2.2.2 Global Ocean Tidal models

The Mediterranean Sea model has been nested into a global tidal model which we have chosen to be FES2014. FES2014 was produced by Noveltis, Legos and CLS Space Oceanography Division and distributed by Aviso, with support from Cnes [3]. FES2014 is the last version of the Finite Elements Solution tidal model, the previous ones being FES99 (Lefevre et al., 2002), FES2004, (Lyard et al., 2006) and FES2012. FES2014 is based on tidal barotropic equations of T-UGO model with an unstructured triangular grid and a spectral configuration. These solutions are improved by assimilating long-term altimetry data and tidal gauges through a representer assimilation method, described in Lyard et al. (2006).

While in the T-UGOm model, the Self-Attraction and Loading effect can be optionally accounted for, it is worth remembering that FES2014 considers ocean tides caused by the attraction of the moving water masses and also of the deformation of the crust due to the water load. FES2014 tidal products are the amplitude and the phase of tidal elevations, tidal currents and tidal loads, distributed globally on $1/16° \times 1/16°$ of resolution grid, for 34 tidal constituents. In addition to FES2014, TPXO-8 has been used as an alternative tidal global model. TPXO-8 is the current version of a global model of ocean tides, which bests-fits, in a least-square sense, the Laplace tidal equations and along track averaged data from TOPEX/Poseidon and Jason, using OTIS (Oregon State Univercity Tidal Inversion Software). which is a tidal inversion software. A more detailed description of TPXO model is given by Egbert, Bennett, and Foreman (1994) and Egbert and Erofeeva (2002).

Both FES2014 and TPXO models are altimetry-constrained models but they mainly differ for the numerical method used to solve the partial differential equations. TPXO is a finite difference model while FES is a finite element model.

---

[3]http://www.aviso.altimetry.fr/

2.3   Sensitivity tests and validation

The aim of this section is to show and discuss the results of several sensitivity tests that have been done in order to achieve an accurate tidal representation in the Mediterranean basin.

The assessment of NEMO barotropic experiments is performed considering the tidal amplitude and phase estimated through the harmonic analysis of the hourly time series of the sea surface elevations, simulated at each sea grid point of the domain. Such analysis has been performed with the TUGO-m Tidal ToolBox (Allain, 2016), based on the work of Schureman (1940). TUGO-m Tidal ToolBox is developed and maintained by the SIROCCO national service (CNRS/INSU). SIROCCO is funded by INSU and Observatoire Midi-Pyrénées/Université Paul Sabatier and receives project support from CNES, SHOM, IFREMER and ANR.

The length of the time series needed to distinguish the tidal waves with the harmonic analysis is based on the Rayleigh criterion for separation and it depends on the number of tidal waves implemented. Typically 30 days of simulation are sufficient to separate six tidal components: M2, S2, N2, K1, O1, Q1 and six months are needed to distinguish the latter with the addiction of K2 and P1 tidal constituents. In both cases, an adequate spin-up period of several days of simulation should be considered.

The capability of NEMO to model tidal waves in the Mediterranean Sea is assessed through a comparison with the observations. In particular, the accuracy of the model in coastal areas is estimated through the comparison of tidal harmonics, with the ones derived from the tide gauges time series. Conversely, when the interest is in a basin scale, the harmonics derived from satellite data are used, namely the CTOH tidal constants described by Roblou et al., 2011. More details on the two validation dataset can be found on Appendix A and B.

One of the main issues in assessing tides in the Mediterranean Sea is the lack of an adequate spatial coverage of tidal gauges data. In particular, few data are available on the North African coast and in the Levantine. For this reason a comparison of NEMO barotropic-equivalent solution with a global tidal altimetry constrained model is recommended (Stammer et al., 2014).

2.3.1   Sensitivity to the open lateral boundary data

The important role of the Atlantic tidal wave in the Mediterranean Sea, has been already discussed in section 2.1. Here, an overview of tidal propagation in the North Atlantic Ocean is

given. The amplitude and phase of the principal M2 lunar tidal component, from FES2014 are shown in figure 2.2.
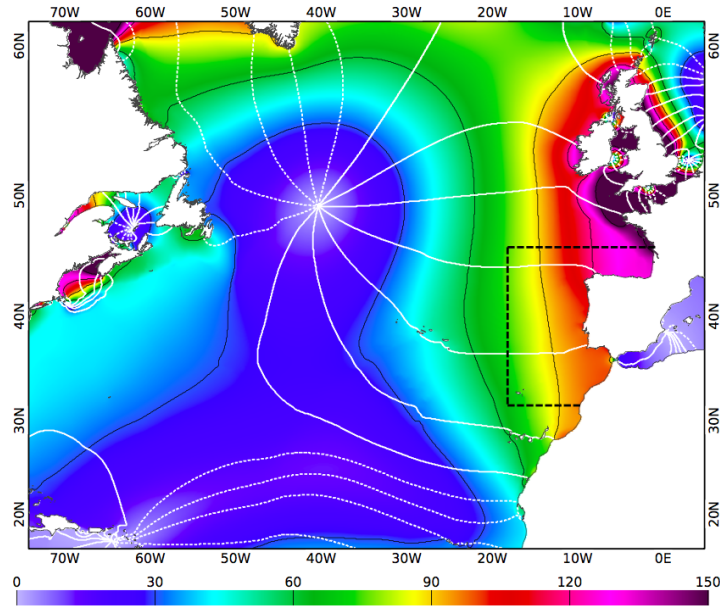
FIGURE 2.2: M2 tidal constituent in the North Atlantic Ocean from FES2014 global tidal model. The black solid lines represent the corange lines (*cm*) and the white solid and dashed lines are positives and negatives the cotidal lines (°). The black dashed lines define the Atlantic box of the Mediterranean Sea domain.

In the North Atlantic Ocean the M2 tidal wave propagates cyclonically around the amphidromic point. This is placed at about 40 °W of longitude and 48.5 °N of latitude. In the eastern side of the North Atlantic, tidal amplitude increases progressively from the amphidrome toward the North African and European coasts, reaching huge values especially on the continental shelf of the Celtic Sea and the Bay of Biscay. Here tidal amplitudes have typical amplitudes of 1.5 *m* with tidal current of about 20 *cm/s*, with local accelerations at coasts (Pairaud et al., 2008).

It is evident from figure 2.2 that the northern segment of the Atlantic box of the Mediterranean Sea model crosses both Abyssal Plain and the Shelf of the Bay of Biscay. This area, characterised by a huge bathymetry gradient causes several modelling issues. Notably the high tidal velocity at the boundary of the model can be responsible of instability problems and requires a careful calibration of the time step of integration.

It should be noted that at the entrance of the Strait of Gibraltar, the Atlantic tidal amplitude due to the M2 tidal component, reaches a value of about 60 *cm* and it reduces at the entrance of the Mediterranean basin of 50 %.

The strong transition between the Atlantic and the Mediterranean at the Strait of Gibraltar is

	Tidal model	RMS_{misfit} (cm) M2 tidal component
EXP1	TPXO-8	2,6
EXP2	FES2014	3,3
EXP3	FES2014 and T-UGOm	1,8

TABLE 2.1: RMS_{misfit} (cm) calculated respect to the satellite altimetry in the Atlantic box, for the M2 tidal component. EXP1 is forced with tidal elevation and currents from TPXO-8, EXP2 is forced with tidal elevation and currents from FES2014 and EXP3 is forced with tidal elevation from FES2014 and tidal currents calculated by T-UGOm.

well described by Candela (1991). He says that the North Atlantic in the vicinity of the strait can reach tidal ranges of about 2 m, and about 1 m tidal amplitudes on the Mediterranean side, during spring tide. This high contrast together with the particular strait's topography, determines the complicated tidal dynamics of the strait.

In this work, two sensitivity tests have been done, forcing the Mediterranean barotropic-equivalent model, at its open boundary with the tidal elevations and currents extracted from the global tidal models TPXO-8 (EXP1) and FES2014 (EXP2). A third experiment has been done using FES2014 elevations and T-UGOm downscaled currents (EXP3). More precisely, a simulation with T-UGOm is performed on the same configuration of NEMO implementation in the Med, forced at the open boundary only by tidal elevations from FES2014.

These three sensitivity experiments last 30 days and are performed considering the main semidiurnal and diurnal tidal components: M2, S2, K1, O1. The harmonics obtained have been validated with the along track CTOH tidal constants in the Atlantic part of the domain and separately in the Mediterranean basin. The $RMS_{misfits}$ calculated for the M2 tidal component and for the three experiments, in the Atlantic portion of the domain, are shown in table 2.1.

$$RMS_{misfit} = \left(\frac{1}{2N} \sum_N \left[A_0 \cos\left(\phi_0\right) - A_m \cos\left(\phi_m\right) \right]^2 + \left[A_0 \sin\left(\phi_0\right) - A_m \sin\left(\phi_m\right) \right]^2 \right)^{\frac{1}{2}} \quad (2.7)$$

In (2.7) equation, A_0 and ϕ_0 are the observed amplitude and phase and A_m and ϕ_m are the modelled ones. From the three sensitivity tests it results that the RMS_{misfit} calculated in the Atlantic box is reduced in case the model is forced at its open lateral boundary with elevations from FES2014 and the tidal currents calculated with the T-UGOm model, in the Atlantic box (EXP3). This reduction is of 50% respect the EXP2 which differs only for the tidal current forcing. For this reason, hereinafter all the experiments carried out with the Mediterranean

Sea model configuration, are forced with FES2014 tidal elevations and T-UGOm downscaled currents.

2.3.2 Sensitivity to the horizontal resolution and bathymetry

The horizontal resolution is a crucial factor in modelling the Mediterranean Sea tidal response, since the accurate solving of the straits dynamics is of primary importance. To demonstrate the importance of the horizontal resolution, the tides modelled with the same configuration but with two different horizontal resolutions are compared. More precisely the comparison of tidal harmonics calculated with the current NEMO barotropic-equivalent tidal model, at $1/24° \times 1/24°$ of resolution ($NEMO24$ hereinafter) and an analogous model at $1/16° \times 1/16°$ of resolution (NEMO16 hereinafter) is shown. These two configurations differ also for the bathymetry and for the representation of the coastline.

In the overall basin, the tidal harmonics calculated for both configurations have been validated respect to the CTOH altimetry data. For the M2 tidal component, the RMS_{misfit} for the lower resolution configuration is of 2 cm and it is reduced of the 30% for $NEMO24$. Moreover, the comparison of the two configuration is performed locally in the most tidally affected areas. In general $NEMO24$ performs better than NEMO16, nevertheless an opposite trend is found in the Alboran Sea.

Figure 2.3 shows the maps of the vectorial differences d, or the M2 elevation, between the harmonics obtained from the two different resolution NEMO barotropic experiments and FES2014 with the equation 2.8, defined by Foreman et al. (1993).

$$d = \left[(A_N \cos \phi_N - A_F \cos \phi_F)^2 + (A_N \sin \phi_N - A_F \sin \phi_F)^2\right]^{\frac{1}{2}} \qquad (2.8)$$

In the Atlantic, the differences with FES2014 is of 2 - 4 cm and it is lower in $NEMO24$ both in the open ocean and in coastal areas, but once the tidal wave overpasses the Gibraltar Strait, in the Alboran Sea, NEMO16 seems to perform better.

Sánchez-Garrido et al. (2011) discuss the narrow channel of the Gibraltar Strait characterized by a minimum width of 14 km and an irregular bottom topography that include a system of submarine sills. The main ones are the Camarinal and the Espartel sills that are difficult to resolve properly with a horizontal resolution of about 4 km.

(a) NEMO16 difference with FES2014   (b) *NEMO*24 difference with FES2014
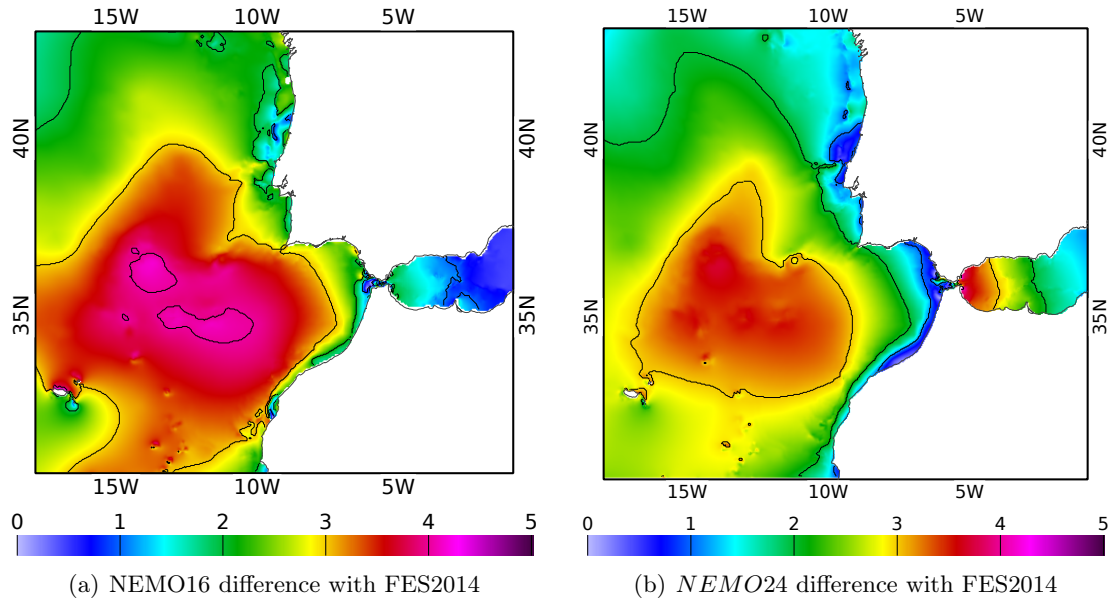
FIGURE 2.3: Complex amplitude error d (cm) of NEMO barotropic experiments respect to FES2014, for M2 tidal component at the Strait of Gibraltar

The fact that $NEMO$24 underestimates the tidal amplitude in the Alboran Sea can be due to the fact that with the current resolution, this system of sills, can be an obstruction to the propagation of tides. For what concerns NEMO16, the lower discrepancy with FES can be attributed to the fact that a less realistic bathymetry can compensate for the underestimation at the Alboran Sea. In fact, at 1/16 ° of resolution, the bathymetry in the Strait is more smoothed and the coastline in the Strait is roughly represented, the Moroccan promontory of the Gibraltar Strait has been neglected and modelled as sea. This can be appreciated from the panel (b) of figure 2.5.

In order to reduce the tidal amplitude discrepancy at the Alboran Sea in $NEMO$24, several sensitivity test have been done, with some slightly and manually modified bathymetry at the Gibraltar Strait. Finally the bathymetry that allows the better representation of tides at the Alboran Sea can be seen in the right panel (b) of figure 2.4, in which both the system of sills are reduced and smoothed. Hereinafter we refer to the experiment performed with this bathymetry as $NEMO$24*.

In figure 2.5, the amplitude and the phase relatives to the M2 tidal component simulated by the three configurations (NEMO16, $NEMO$24 and $NEMO$24*) in the Alboran and in the Balearic Sea are compared to the FES2014 solution.

With regard to the phase, it is evident that the amphidromic point simulated with $NEMO$24 (with both bathymetries) is placed near the Spanish coast like in FES2014, while in NEMO16 it

(a) *NEMO*24 bathymetry   (b) *NEMO*24* bathymetry
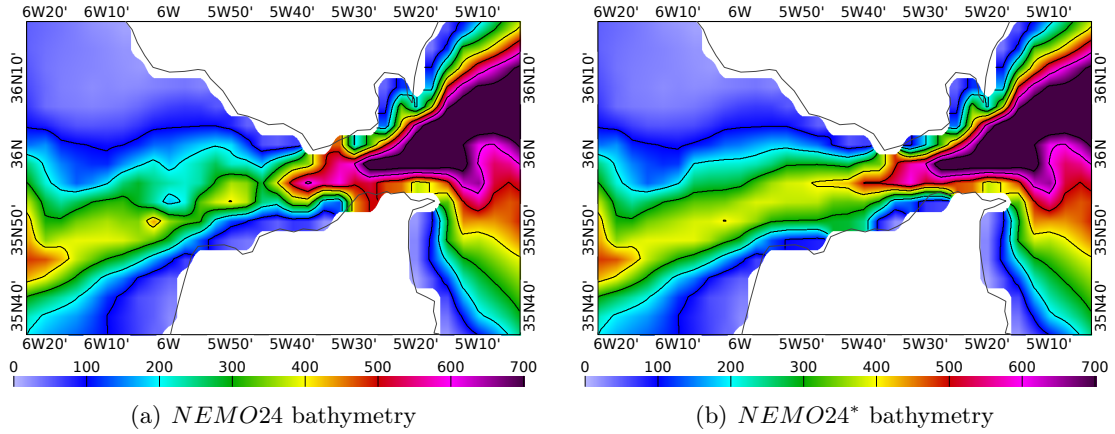
FIGURE 2.4: Model bathymetry original (a) and modified (b), at the Strait of Gibraltar (m)

M2 tidal component (cm)						
	lon	*lat*	Obs Amp	NEMO16 Amplitude	*NEMO*24 Amplitude	*NEMO*24* Amplitude
Algeciras	$5°24'00''W$	$36°10'48''N$	32	28	27	30
Ceuta	$5°19'01''W$	$35°54'00''N$	30	29	28	30

TABLE 2.2: Observed and modelled amplitude (cm) in the tide gauge stations of Algeciras and Ceuta for the three experiments: NEMO16, *NEMO*24 and *NEMO*24* with the modified bathymetry at the Strait of Gibraltar.

is shifted southeast. A similar pattern of NEMO16, for this amphidromic point, is found in **T-mod**, at $1/12°$ of resolution. This is the demonstration of the fact that an horizontal resolution of 3 - 4 km is necessary to solve the incoming tidal wave from Gibraltar.

The analysis of tidal amplitudes for the four configurations, in the Alboran Sea deserves further considerations. Both the NEMO16 and the *NEMO*24 underestimate the M2 tidal amplitude of few centimetres nearby the Strait of Gibraltar, especially *NEMO*24 but the improvement achieved with the modified bathymetry at Gibraltar can be appreciated in the left bottom panel of figure 2.3. The improvement of *NEMO*24* respect to *NEMO*24, is evident from the comparison with FES2014 and it is confirmed by the harmonics measured at two Spanish tide gauges of Algeciras and Ceuta, both placed at the entrance of Strait of Gibraltar, with the latter sit in the African coast (figure B.1).

The observed and modelled amplitudes for the three barotropic experiments with NEMO16, *NEMO*24 and NEMO24* are listed in table 2.2. In light of the improvement achieved with the bathymetry in which the Camarinal and the Espartal Sill have been reduced and smoothed, the results shown in section 2.3.4 are referred to the experiments performed with this locally modified bathymetry.

(a) FES2014 amplitude and phase

(b) NEMO16 amplitude and phase

(c) $NEMO24$ amplitude and phase

(d) $NEMO24^*$ amplitude and phase
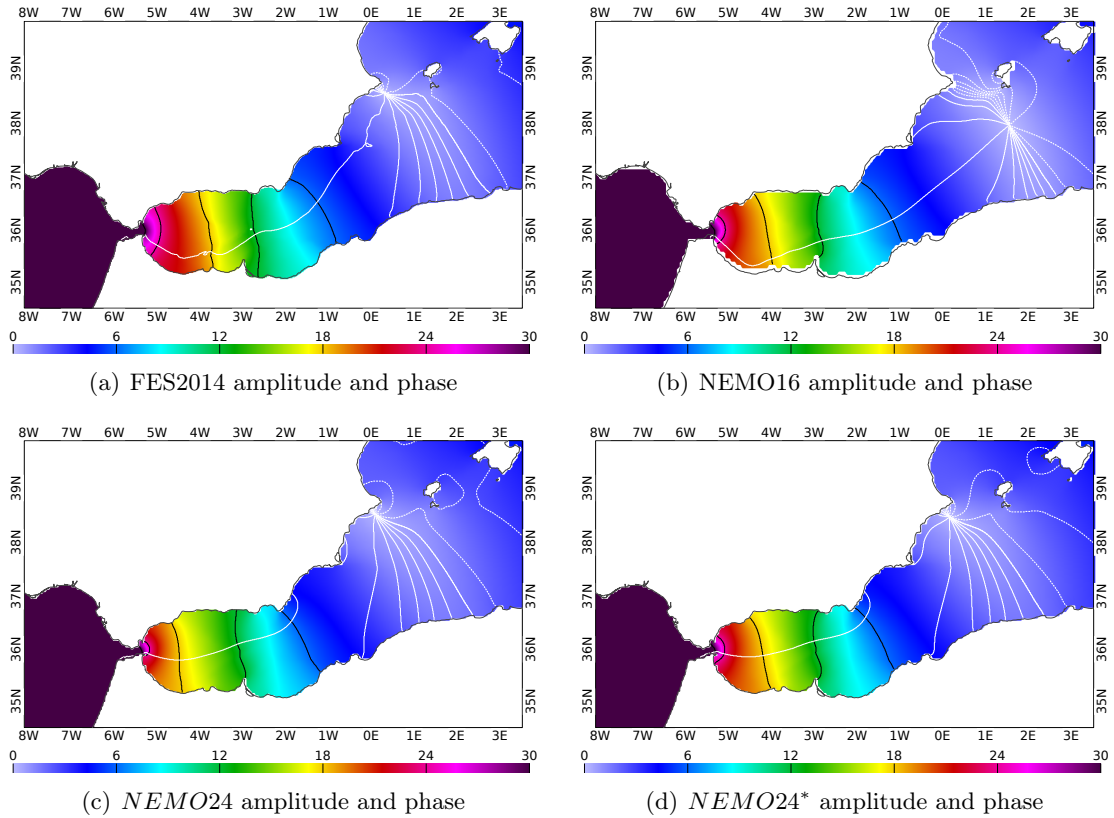
FIGURE 2.5: M2 elevation amplitude in cm (colours and black contours, interval $= 6$ cm) and phase in degrees (white contours for phase lag, interval $= 20°$) at the Alboran Sea.

It worth saying that another sensitivity test is carried out with a GEBCO unsmoothed bathymetry. The result of this test is an improvement of the $NEMO24$ representation of the diurnal constituent and a worsening of the semidiurnal one. For example the $RMS_{misfits}$ calculated against the satellite altimetry data decreased from 1.3 cm to 1.2 cm for the K1 constituent and from 0.7 cm to 0.5 cm for O1. Nevertheless, since the diurnal tidal constituents are the dominant ones, we prefer to use the GEBCO smoothed bathymetry.

2.3.3   Sensitivity to dissipation parameterization

One of the important differences between $NEMO24^*$ and FES2014 is that in this latter, the dissipation due to the internal wave drag is parametrised. For this reason, many experiments have been carried out in order to tune the bottom friction coefficient over all the domain and reduce the error respect the FES2014 solution and the tide gauges.

Figure 2.6 shows the complex amplitude error of $NEMO24^*$ respect to FES2014, for the M2 and S2 tidal harmonics. In $NEMO24^*$ the minimum drag coefficient is $Cd_{min'} = 2.5 \times 10^{-3}$ and the

bottom roughness is $z_{0b} = 3.5 \times 10^{-3}$. For both tidal constituents, there are high discrepancies in the Gulf of Gabès and in the North Adriatic.

(a) M2 tidal component

(b) S2 tidal component
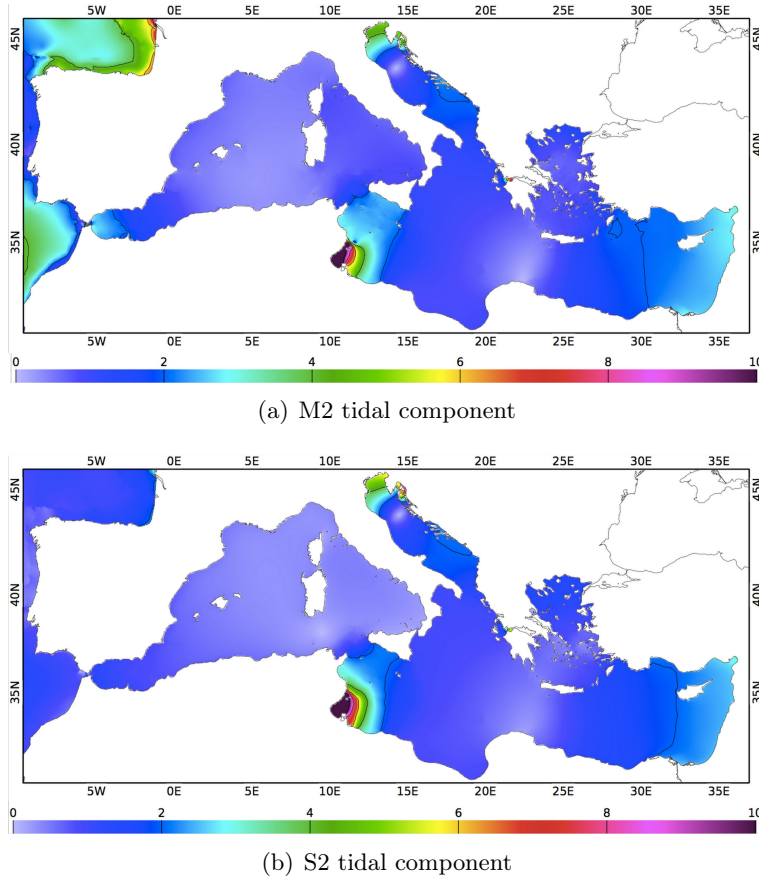
FIGURE 2.6: Complex amplitude error d (cm) of $NEMO24$ respect to FES2014 for M2 and S2 elevation in the Mediterranean Sea

In order to reduce the errors in the two shallow water areas, several roughness length values have been tested in the equation 2.3. It results that enhancing the bottom roughness (for example $z_{0b} = 1 \times 10^{-2} m$), the discrepancies with FES2014 are reduced in the North Adriatic and in the Gulf of Gabès, suggesting the idea that some physics is missing in $NEMO24^{*}$ experiment. On the other hand, increasing the roughness length over all the domain deteriorates the tidal solution in its Atlantic part and consequently in the Alboran Sea, partially canceling the improvements achieved modifying the bathymetry at the Strait of Gibraltar.

The solution that has given more promising result is achieved by locally increasing of the bottom friction only in the two shallow water areas, shown in figure 2.7, by a factor 5.

The sensitivity test with the locally enhanced bottom friction have been done for the semidiurnal M2 and S2 tidal components, giving impressing results that can be appreciated comparing figure 2.6 respectively with panels (b) of figures 2.8 and 2.9.

(a) Gulf of Gabès   (b) North Adriatic
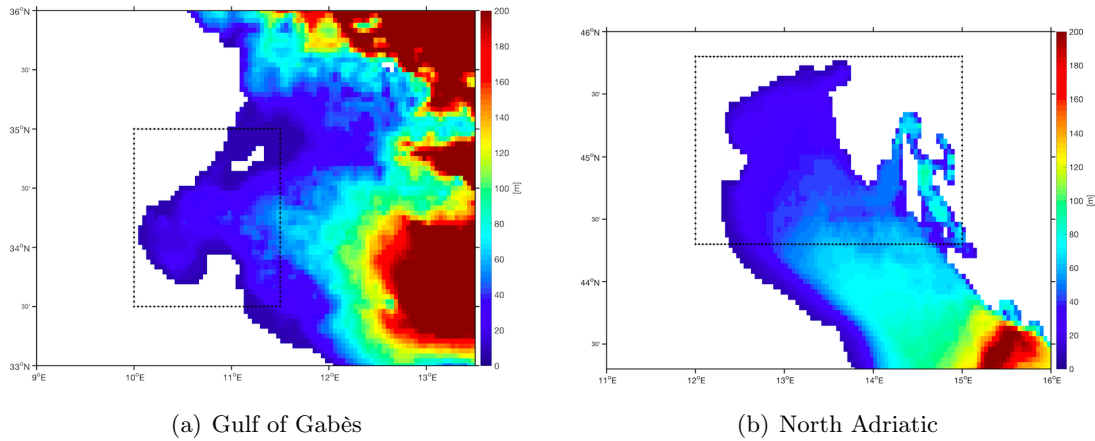
FIGURE 2.7: $NEMO24$ bathymetry, increased bottom friction boxes.

In general the reduction of the error is particular important in the Tunisian Gulf while the diurnal constituents are less sensitive to this parameterisation. The observed tidal amplitude of the city of Gabès, extracted from the paper of Sammari, Koutitonsky, and Moussa (2006), are respectively 51 *cm* and 36 *cm* for the M2 and S2 tidal waves and can be considered as reference values. At this tide gauge site, the effect of the increased bottom friction is the lowering of the tidal amplitude modelled by $NEMO24$ from 58 *cm* to 52 *cm*. For the S2 components the reduction of the error is even more strong, since the modelled amplitude decreases from 50 *cm* to 37 *cm*, when a further dissipation is taken into account. The results shown in next section take account of these corrections for the two shallow water areas.

2.3.4   Mediterranean tides

In this section, the main harmonics, derived with the harmonic analysis for the barotropic model $NEMO24^{*}$, in the Mediterranean Sea are discussed, together with their validation with both the control tide gauge dataset and with the altimetry data. The experiment analysed here takes advantages of all the results of the sensitivity tests performed in section 2.3. The so obtained harmonics have been compared with FES2014 solutions and some discrepancy have been found in the most tidally affected areas of the basin such as the North Adriatic and the Gulf of Gabès. In order to distinguish heigh tidal components, a simulation of seven months has been done and only the last six are harmonically analysed. The amplitudes and phases for the semidiurnal (M2 and S2) and diurnal (K1, O1) tidal waves are shown, compared to the literature tidal solutions of **T-mod** and **A-mod** models and to the FES2014 solutions. Some comments on the secondary tidal components: N2, K2, P1 and Q1 are also added.

	RMS_{mifsit} (cm) respect to the CTOH altimetry data				RMS_{mifsit} (cm) respect to the tide gauges			
	M2	**S2**	**K1**	**O1**	**M2**	**S2**	**K1**	**O1**
*NEMO*24	1.1	0.8	1.3	0.7	2.2	1.0	1.7	0.9

TABLE 2.3: Validation of $NEMO24^*$ in the Mediterranean basin respect to the CTOH altimetry data and to all the tide gauge sites.

In table 2.3 the RMS_{mifsit} errors (2.7) calculated in the Mediterranean basin are listed for the main four tidal waves and in general, there is a good coherence between the results obtained with the two validation systems. Even if we can notice that the RMS_{mifsit} calculated respect to the tide gauge data are greater than the ones calculated respect to the satellite data. For the M2 tidal component a doubled error is found. This trend can be attributed to the fact that the validation against the tide gauge harmonics only refer to the coastal areas, characterized by the greater tidal amplitudes and so by more significative discrepancies. Moreover, due to the inhomogeneity of the tide gauge dataset, the RMS_{mifsit} referred to the CTOH harmonics gives a more general information.

It is surprising that the RMS_{misfit} error associated to the K1 tidal component is greater than the M2 one but this can be justified by the fact that in this work the calibration has been done mainly on the semidiurnal tidal components, whose magnitudes are the dominating ones. To have an idea of which is the spatial distribution of these errors, the observed and modelled amplitudes (A) in *cm* and phases (ϕ) in degrees, for the control set of 61 tide gauges, is given in Table 2.4

In general the agreement is good for both amplitudes and phases, the only two stations that have great discrepancies are the one of Messina and Reggio Calabria. We argue that the current resolution of 4 *km* is not sufficient to resolve well the tidal dynamics in the Messina Strait, since the minimum distance between the Sicily and the Italian peninsula is of about 3 *km*.

TABLE 2.4: Observed (obs) and modelled (mod) amplitudes (A) in *cm* and phases
(φ) in degrees for the control set of 61 tide gauges. Modelled harmonics refer to
the experiment *NEMO*24*

No	Station	longitude	latitude	M2(obs/mod)		S2(obs/mod)		K1(obs/mod)		O1(obs/mod)	
				A(cm)	φ(deg)	A(cm)	φ(deg)	A(cm)	φ(deg)	A(cm)	φ(deg)
1	Ajaccio	8°45'36.00"	41°55'12.00"	7.3/7.5	212/228	3.1/3.0	230/241	3.6/4.9	182/206	1.5/2.9	100/125
2	Alcudia	3°08'24.00"	39°49'48.00"	4.6/4.8	206/228	1.7/1.8	225/244	3.6/4.6	158/197	2.2/3.5	98/120
3	Algeciras	-5°24'00.00"	36°10'48.00"	32.0/29.7	37/51	11.6/11.0	64/74	2.5/2.3	116/172	0.8/2.1	161/139
4	Almeria	-2°28'48.00"	36°49'48.00"	9.5/8.7	38/51	3.9/3.5	66/73	3.5/4.0	146/186	2.2/3.5	114/124
5	Ancona	13°30'00.00"	43°37'12.00"	6.7/5.7	289/293	3.6/3.2	303/300	12.9/15.4	65/72	4.2/4.9	53/43
6	Barcelona	2°09'36.00"	41°20'24.00"	4.5/4.7	200/225	1.5/1.7	217/239	3.5/4.4	160/195	2.3/3.6	97/119
7	Bari	16°51'36.00"	41°08'24.00"	9.7/8.7	60/71	6.0/6.0	67/73	5.2/5.6	43/54	1.9/2.1	25/20
8	Cagliari	9°06'36.00"	39°12'36.00"	8.4/8.4	220/238	3.0/3.1	245/259	2.9/4.0	174/202	1.5/2.6	100/122
9	Carloforte	8°18'36.00"	39°09'00.00"	7.0/6.6	218/ 233	2.8/2.7	237/248	3.9/4.9	176/203	1.8/3.0	103//125
10	Catania	15°05'24.00"	37°29'24.00"	6.5/5.8	47/53	3.4/3.2	53/53	1.7/2.2	36/51	1.2/1.1	28/28
11	Centuri	9°21'00.00"	42°57'36.00"	8.4/8.2	210/228	3.3/3.3	227/239	3.5/4.9	184/208	1.5/2.8	105/126
12	Ceuta	354°40'58.80"	35°54'00.00"	30.0/30.0	49/60	11.3/11.2	77/84	3.7/2.8	143/152	2.0/1.7	102/104
13	Civitavecchia	11°47'24.00"	42°05'24.00"	10.0/10.8	228/231	3.6/3.9	247/250	2.4/4.0	189/205	1.1/2.2	104/122
14	Crotone	17°08'24.00"	39°04'48.00"	6.3/5.4	51/59	3.3/3.0	56/58	2.0/2.2	34/45	0.9/1.1	27/13
15	Dubrovnik	18°03'46.80"	42°39'28.80"	8.5/8.5	91/74	5.5/5.9	104/74	4.9/5.9	51/44	1.7/2.2	36/11
16	Formentera	1°25'12.00"	38°43'48.00"	1.4/1.5	167/209	0.6/0.6	170/223	3.8/4.4	156/193	2.2/3.5	102/120
17	Fos Sur Mer	4°53'24.00"	43°24'00.00"	6.3/6.6	202/223	2.4/2.5	216/236	3.5/4.6	171/200	1.8/3.3	99/120
18	Gandia	-0°09'00.00"	38°59'24.00"	1.6/2.1	190/230	0.5/0.6	177/246	3.1/4.5	152/191	2.5/3.8	100/120
19	Genova	8°55'12.00"	44°24'36.00"	8.6 /8.3	207/226	3.3/3.2	224/237	3.5/4.8	179/206	1.6/2.9	103/124
20	Girne	33°19'48.00"	35°20'24.00"	8.2/8.6	248/230	4.9/5.3	265/239	2.4/1.9	283/293	1.6/2.2	267/268
21	Hadera	34°52'01.20"	32°28'01.20"	11.2/10.0	235/231	6.5/6.1	249/239	2.6/1.8	270/278	2.0/2.3	247/258
22	Ibiza	1°27'00.00"	38°54'36.00"	1.8/2.0	202/232.1	0.7/0.7	208/248	3.8/4.4	158/195	2.3/3.6	102/121
23	Imperia	8°01'12.00"	43°52'48.00"	7.8/7.8	217/226	3.0/3.1	234/238	3.4/4.8	181/205	1.7/2.9	106/123
24	Katakolo	21°18'54.00"	37°39'00.00"	3.3/3.4	74/47	1.6/2.0	83/43	1.3/1.7	14/17	0.5/0.9	357/333
25	La Figueirette	6°55'48.00"	43°28'48.00"	7.3/7.4	205/225	2.8/2.9	222/238	3.5/4.7	175/203	1.7/3.1	98/122
26	Lampedusa	12°36'00.00"	35°30'00.00"	7.6/8.0	28/32	5.1/5.7	43/45	0.6/1.5	356/352	0.8/0.2	75/164
27	Livorno	10°17'24.00"	43°32'24.00"	9.7/9.0	215/230	3.6/3.5	231/242	3.6/5.2	176/204	1.7/2.9	102/123
28	Mahon	4°16'12.00"	39°53'24.00"	5.1/5.2	211/230	2.0/2.0	228/247	3.7/4.6	162/199	2.1/3.3	102/121
29	Malaga	-4°24'36.00"	36°42'36.00"	18.6/17.3	37/52.0	7.1/6.7	62/75	3.2/3.4	139/179	1.9/3.0	119/126
30	Marseille	5°21'00.00"	43°16'48.00"	6.8/6.7	205/224	2.5/2.6	222/236	3.7/4.6	172/201	1.9/3.2	96.8/120
31	Melilla	-2°55'48.00"	35°17'24.00"	12.5/11.3	54/73	5.0/4.3	78/93	3.5/4.3	135/175	2.0/3.4	113/111
32	Messina	15°33'36.00"	38°11'24.00"	4.8/1.6	341/61	2.6/1.4	7/44	0.6/1.1	265/79	1.0/0.8	45/43
33	Monaco	7°25'12.00"	43°43'48.00"	7.3/7.6	206/225	3.1/3.0	222/238	3.5/4.7	177/204	1.6/3.0	101/122
34	Motril	-3°31'12.00"	36°43'12.00"	15.4/14.2	35/52	6.1/5.5	62/74	3.3/3.6	142/183	1.9/3.2	116/125
35	Napoli	14°16'12.00"	40°48'36.00"	11.6/11.4	219/233	4.2/4.3	240/251	2.7/4.2	195/210	0.9/2.0	106/129
36	Nice	7°16'48.00"	43°41'24.00"	7.5/7.5	207/225	2.9/2.9	226/238	3.5/4.7	177/204	1.8/3.0	102/122
37	Ortona	14°24'36.00"	42°21'00.00"	6.7/6.2	49/64	4.7/4.8	58/69	8.8/10.5	60/68	3.0/3.5	49/38
38	Otranto	18°29'24.00"	40°09'00.00"	7.0/6.0	59/68	4.0/3.8	67/70	2.3/3.1	56/59	1.0/1.3	42/18
39	Palermo	13°22'12.00"	38°07'12.00"	11.1/10.9	221/235	4.1/4.1	243/256	2.8/4.2	189/207	1.0/2.2	112/129
40	Palinuro	15°16'12.00"	40°01'48.00"	12.2/11.7	218/234	4.5/4.4	238/252	2.9/4.3	194/211	0.8/1.9	115/132
41	Palma De Mallorca	2°37'48.00"	39°33'36.00"	2.8/3.0	196/221	1.1/1.1	210/237	3.7/4.4	159/195	2.2/3.4	100/120
42	Porto Empedocle	13°31'12.00"	37°16'48.00"	4.8/4.1	59/54	3.5/3.6	56/51	1.8/1.7	83/95	1.2/1.2	62/63
43	Portomaso	14°29'24.00"	35°55'12.00"	6.3/5.9	54/43	3.9/3.9	63/48	1.0/1.9	30/18	0.8/0.2	66/24
44	Portotorres	8°24'00.00"	40°50'24.00"	7.3/7.4	228/229	2.8/3.0	248/243	3.6/4.9	188/206	1.6/3.0	114/125
45	Port Vendres	3°06'36.00"	42°31'12.00"	5.7/5.9	203/224	1.9/2.2	222/238	3.5/4.5	165/197	2.2/3.4	97/119
46	Ravenna	12°16'30.00"	44°29'31.20"	16.9/15.7	264/268	9.8/10.3	271/270	15.9/19.1	63/69	5.0/6.0	54/42
47	Reggio Calabria	15°38'24.00"	38°07'12.00"	7.5/3.7	270/68	4.5/2.2	269/61	9.6/1.9	58/66	3.3/1.1	50/32
48	Rhodes	28°13'58.80"	36°26'49.20"	4.2/5.0	259/239	2.4/3.4	276/249	1.7/1.6	301/322	1.0/1.7	284/282
49	Sagunto	-0°12'00.00"	39°37'48.00"	1.9/2.3	183/224	0.5/0.7	182/239	3.7/4.4	151/191	2.5/3.8	102/119
50	Salerno	14°45'36.00"	40°40'12.00"	11.8/11.6	217/233	4.4/4.3	238/252	2.8/4.2	192/210	0.9/2.0	111/130
51	Senetosa	8°48'46.80"	41°33'00.00"	7.2/7.5	228/229	2.7/3.0	251/242	3.5/4.9	193/206	1.6/2.9	113/125
52	Sete	3°42'00.00"	43°24'00.00"	5.9/6.5	194/222	1.6/2.4	197/235	4.3/4.5	140/198	2.0/3.4	91/119
53	Solenzara	9°24'00.00"	41°51'36.00"	9.7/10.0	214/231	3.9/3.6	241/251	2.6/3.8	180/205	1.3/2.4	94/121
54	Taranto	17°13'12.00"	40°28'12.00"	6.7/5.6	55/63	3.5/3.1	59/61	2.1/2.3	31/43	0.9/1.2	23/11
55	Tasucu	33°49'48.00"	36°16'48.00"	9.8/9.3	240/230	5.9/5.7	251/240	2.3/2.1	286/293	1.8/2.3	265/269
56	Touloun	5°54'36.00"	43°07'48.00"	6.5/6.8	209/225	2.6/2.6	231/238	3.6/4.6	180/202	1.8/3.2	101/121
57	Trieste	13°45'00.00"	45°39'00.00"	26.5/24.1	233/249	15.9/16.3	240/251	17.7/20.8	49/61	5.3/6.5	39/34
58	Valencia	-0°18'36.00"	39°26'24.00"	0.9/2.2	108/224	0.5/0.7	105/240	17.7/20.8	49/61	2.3/3.8	102/119
59	Venezia	12°25'12.00"	45°24'36.00"	23.5/21.4	248/257	14.1/14.4	255/259	17.6/20.5	57/65	5.4/6.4	45/39

TABLE 2.4: Observed (obs) and modelled (mod) amplitudes (A) in *cm* and phases
(φ) in degrees for the control set of 61 tide gauges. Modelled harmonics refer to
the experiment *NEMO*24*

No	Station	longitude	latitude	M2(obs/mod)		S2(obs/mod)		K1(obs/mod)		O1(obs/mod)	
				A(*cm*)	φ(*deg*)	A(*cm*)	φ(*deg*)	A(*cm*)	φ(*deg*)	A(*cm*)	φ(*deg*)
60	Vieste	16°10'48.00"	41°52'48.00"	9.5/8.6	57/68	6.0/6.0	66/71	5.2/5.9	67/74	1.9/2.1	39/38
61	Zadar	15°14'06.00"	44°07'22.80"	5.0/7.6	215/194	2.8/4.8	220/186	11.8/15.4	53/47	3.5/4.9	42/18

In general the amplitude of the M2 tidal wave is less than 10 *cm* over all the basin, showing local
amplifications in the Alboran Sea, in the North Adriatic Sea and in the Gulf of Gabès. This
tidal pattern is well reproduced by the *NEMO*24* model it is in a good agreement with both
the results of other papers dealing with tides in the Mediterranean Sea, for what concerns both
amplitude and phase.
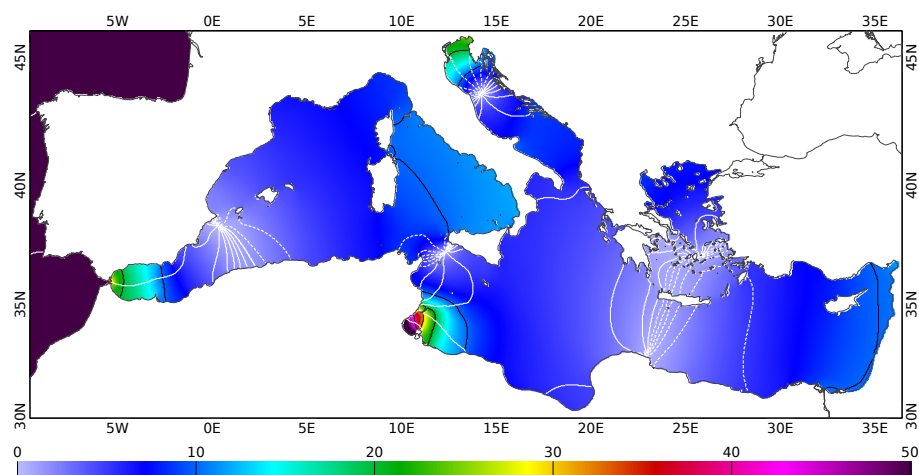
(a) *NEMO*24* M2 elevation amplitude in *cm* (black contours, interval = 10 *cm*) and
phase in degrees (white solid contours for positive phases and white dashed contours
for negative phases, interval = 20°)
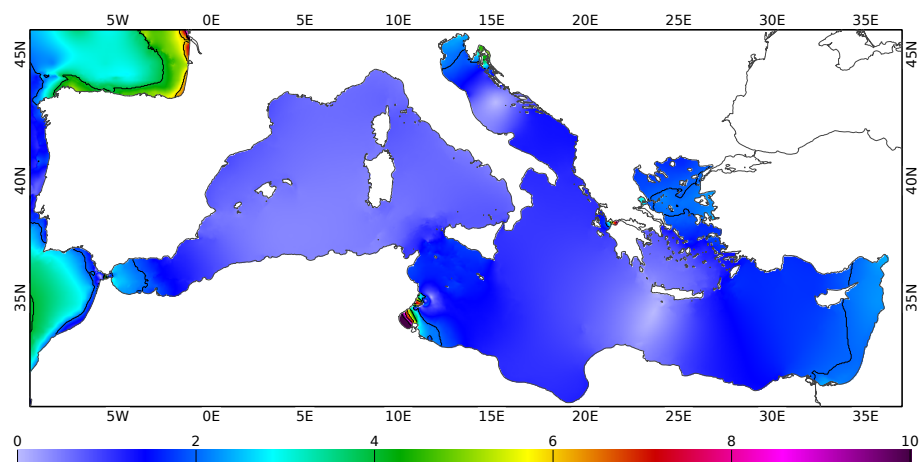
(b) Complex amplitude error *d* (*cm*) of *NEMO*24* respect to FES2014 for M2 ele-
vation in the Mediterranean Sea

FIGURE 2.8: M2 tidal component in the Mediterranean Sea

The amphidromic points modelled by $NEMO24^*$ are basically four: the first one is placed in the Western basin and it has been already commented in section 2.3. The other zero amplitude points, placed in the Strait of Sicily, in the Adriatic Sea and the degenerate amphidromic point is placed between the North coast of Africa and Crete are in a good agreement with literature results (Fig. 2.8). In the panel (b) of figure 2.8 the complex amplitude error d respect to the FES2014 solution is represented, showing relevatnt discrepancies only in the Tunisian shelf. From the comparison with the control coastal observations dataset, shown in panels (a) and (b) of figure 2.12, it is evident that, the agreement for the tidal amplitudes is good, with a slight tendency of $NEMO24^*$ to underestimate the semidiurnal tidal amplitudes. The sites that show the higher discrepancies are the one of Messina (32) and Reggio Calabria (47), that have been already discussed and the tide gauge of Zadar (61), where $NEMO24^*$ overestimates the tidal amplitude. This is due to the the fact that tide gauge is placed in the Croatian coast, near a complex system of small islands, difficult to model with the current resolution. The two tide gauges placed in the Strait of Messina, show great discrepancies also for what concerns the phase lag, together with the tide gauge of Valencia (59). Other smaller discrepancies characterize the sites of Formentera (16), Dubrovnik (15), and Katakolo (24).

The S2 main semidiurnal solar tidal components propagates in the Mediterranean Sea like the lunar one, in fact the phase lines converge at about the same positions. Also for the S2 tidal component a good agreement is found with the results of the tidal models **T-mod** and **A-mod**. For what concerns the complex amplitude error d, the agreement with FES2014 is very good, the panel (b) of figure 2.9 shows differences lower than 2 cm in the all the domain, some discrepancies are found only in the Gulf of Gabès.

From the panels (c) and (d) of the figure 2.12, it is possible to deduce that there is a perfect correspondence between modelled and observed amplitudes with the same discrepancies found at the sites of Messina (32) and Reggio Calabria (47) and Zadar (61). For the same reason discussed for the component M2. Beside these three critical sites, some delay of advance of phase are found in the sites of Valencia (58), Formentera (16), Sagunto (49) and Gandia (18). The discrepancies associated to these Spanish sites can be attributed to the proximity of the western amphidromic point, around which some delay of propagation are more probable than in other sites.

The K1 wave is the lunisolar diurnal constituent. This constituent together with O1, express the effect of the Moon's declination. The diurnal components, K1 and O1 have a completely different pattern respect to the semidiurnal ones, the Adriatic Sea being the only area characterised by important tidal amplitude values and having only one amphidromic node. K1 tidal harmonic

(a) $NEMO24^*$ S2 elevation amplitude in cm (black contours, interval $= 10\ cm$) and phase in degrees (white solid contours for positive phases and white dashed contours for negative phases, interval $= 20°$)

(b) Complex amplitude error d (cm) of $NEMO24^*$ respect to FES2014 for S2 elevation in the Mediterranean Sea
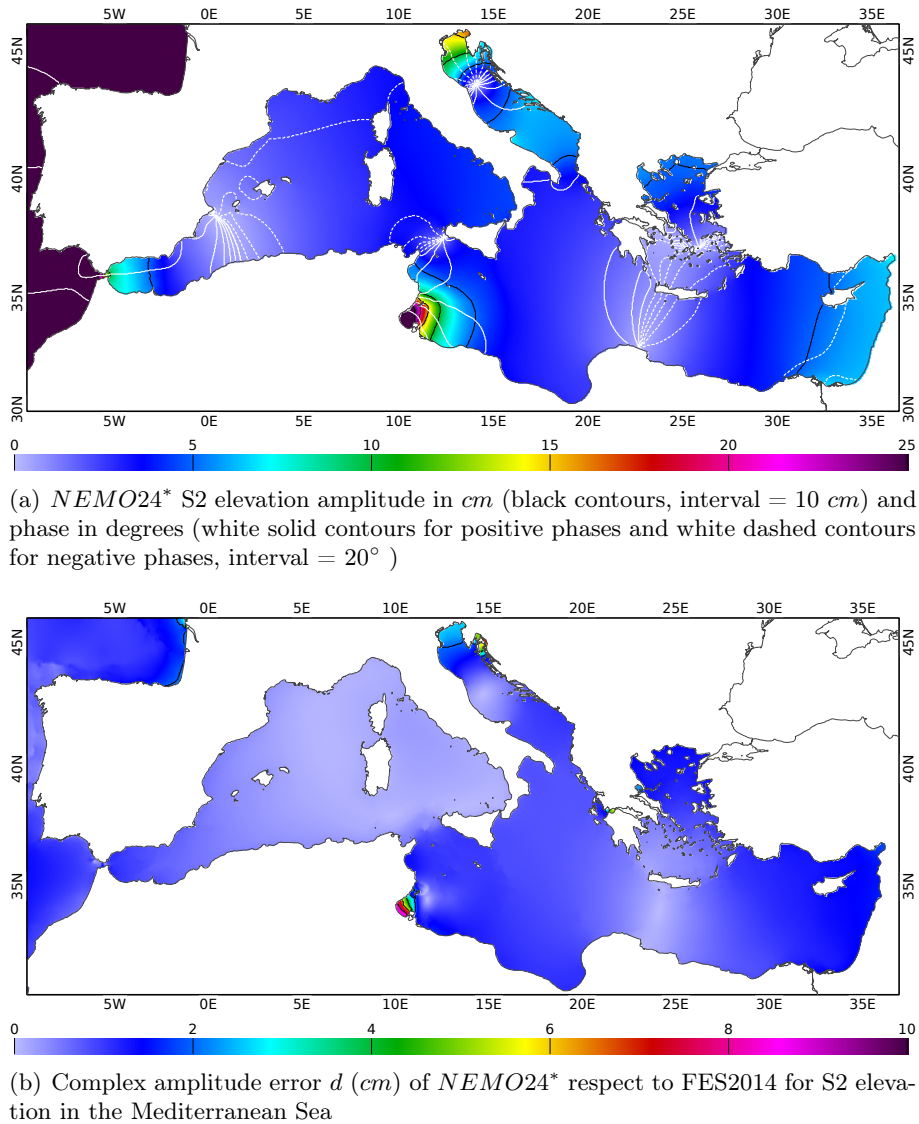
FIGURE 2.9: S2 tidal component in the Mediterranean Sea

modelled by $NEMO24^*$ reaches amplitudes of 20 cm in the North Adriatic Sea and unlike the semidiurnal case, tends to overestimate the tidal amplitudes in this area (panel (b) of figure 2.10). This trend is found mostly at all tide gauges site where tidal amplitudes higher than 8 cm are recorded, and it can be observed in panels (e) and (f) of figure (2.12). A similar feature is found also in **T-mod** where there an overestimation of several cm is associated to this tidal component in the North Adriatic Sea. With the exception of the tide gauges of Messina (32) and Reggio Calabria (47), the observed and the modelled phases are in a good agreement.

Respect to the previous three tidal waves, classified as main tidal constituent, the O1 tidal component is characterised by very low amplitudes values, reaching 6 - 7 cm only in the North Adriatic Sea. In fact in figure 2.11, this component is represented with a scale of 20% respect to the M2 tidal component. In $NEMO24^*$, the amphidromic point placed near the African coast,
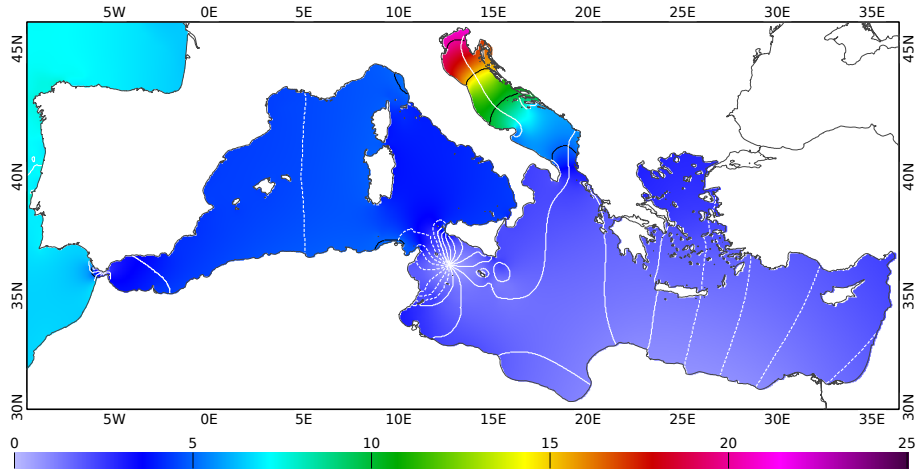
(a) $NEMO24^*$ K1 elevation amplitude in cm (black contours, interval $= 5\ cm$) and phase in degrees (white solid contours for positive phases and white dashed contours for negative phases, interval $= 20°$)
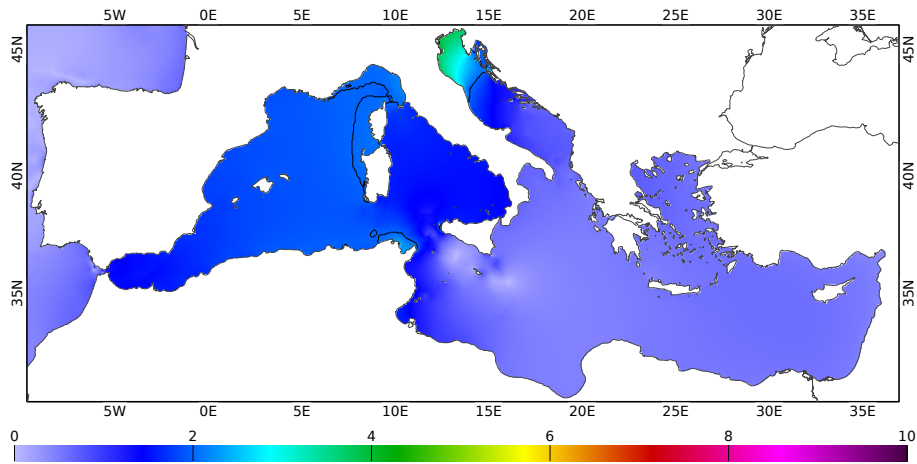
(b) Complex amplitude error d (cm) of $NEMO24^*$ respect to FES2014 for K1 elevation in the Mediterranean Sea

FIGURE 2.10: K1 tidal component in the Mediterranean Sea

is slightly shifted eastward, respect to the **T-mod** and the **A-mod**. We think that this shifting may be due to the inaccuracy of the bathymetry in the eastern basin, since the node is placed at the same position of the two models **T-mod** and the **A-mod**, when the unsmoothed bathymetry is used. Consequently the differences between $NEMO24^*$ and FES2014 (panel (b) of figure 2.11), represented with an halved scale, respect to the other components, show some discrepancies in the Eastern basin (1.5 cm) and in the North Adriatic (2 cm).

From the figure 2.12, the O1 modelled tidal amplitudes show a greater dispersion respect to the other components, mostly for what concerns the amplitudes. $NEMO24^*$ tends to overestimates the amplitudes in the majority of sites. With the exception of the site of Lampedusa (26), the phases are in a good agreement.

(a) $NEMO24$ O1 elevation amplitude in cm (black contours, interval $= 2$ cm) and phase in degrees (white solid contours for positive phases and white dashed contours for negative phases, interval $= 20°$)

(b) Complex amplitude error d (cm) of $NEMO24$ respect to FES2014 for O1 elevation in the Mediterranean Sea
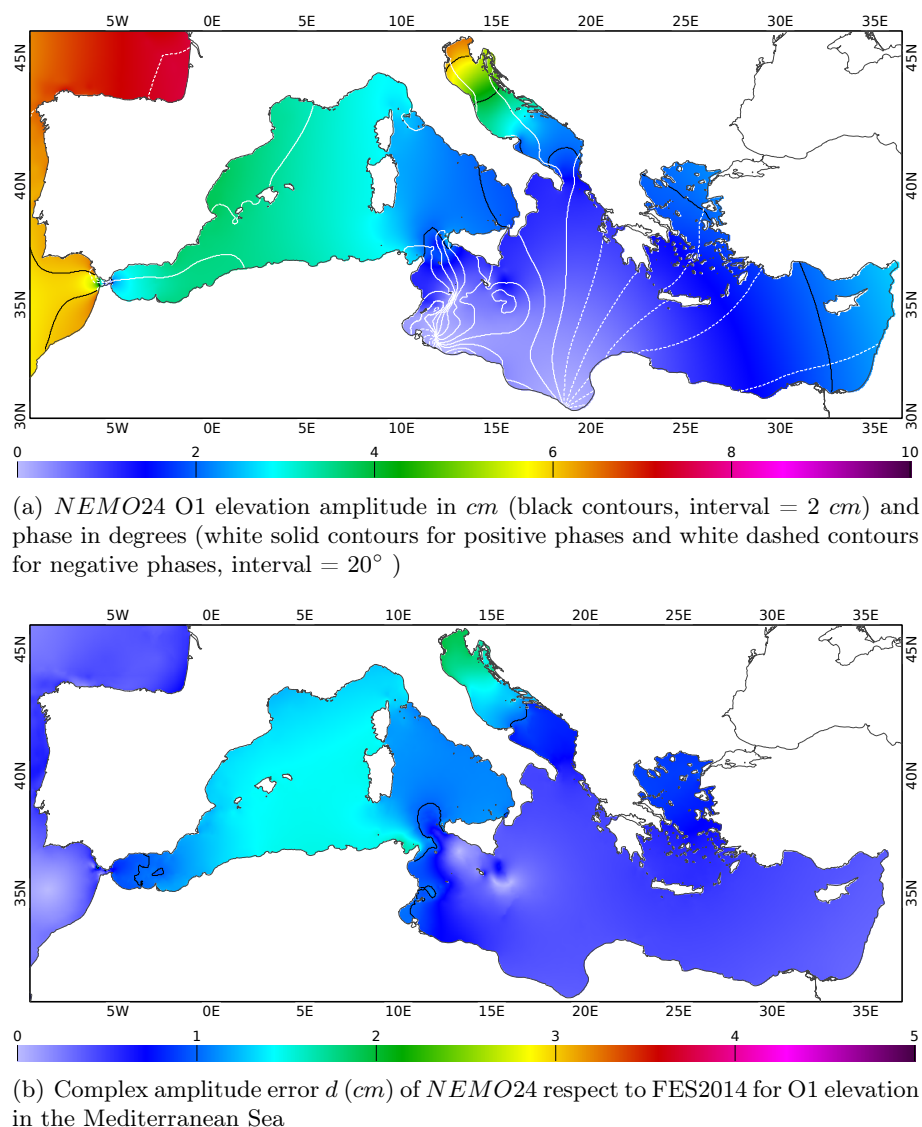
FIGURE 2.11: O1 tidal component in the Mediterranean Sea

The K2, N2, P1 and Q1 tidal constituents also have a signature in the Mediterranean Sea, although with reduced intensity. Actually the effect of the semidiurnal K2, N2 has similar ranges and even local higher amplitudes than O1 tidal constituent, that in this study has been classified among the main tidal constituents following the classification of Tsimplis, Proctor, and Flather (1995). M2, S2, K1 and O1 are the standard tides considered in the majority of tidal studies but the character of the Mediterranean Sea is mainly semidiurnal.

K2 and N2 tidal components reach important tidal amplitudes in the Gulf of Gabès, but beside the results of the work of Arabelos et al. (2011), we do not know much about these four tidal waves and we think that they deserve more attention.

K2 is a lunisolar tidal constituent that modulates the amplitude and the frequency of M2 and

S2 for the declinational effect of the Moon and the Sun respectively. It has a similar pattern than the M2 and S2 tidal constituents, showing the same amplification at the Gulf of Gabès and in the North Adriatic Sea, although the amplitudes are reduced. Unlike M2 and S2, the tidal amplitudes modelled and measured at the Alboran Sea are low, pointing out that this wave is less affected by the incoming Atlantic wave. On the other hand, the amphidromic nodes are exactly the same found in M2 and S2. The overall agreement with FES2014 is very good, with a difference of few centimetres only in the Tunisian shelf.

The N2 tidal component, is the larger lunar elliptic semidiurnal constituent that, together with L2 (the smaller one), modulates the amplitude and the frequency of M2 and the effect of the variation in the Moon's orbital speed, due to its elliptical orbit. N2 shows the same pattern of K2 with a sligthly reduction of the tidal amplitudes in the Mediterranean Sea basin, mostly in the tidal affected areas. Unlike N2, in this case the Atlantic tidal wave has a moderate signature in the Alboran Sea. The agreement with FES2014 for this component in the Mediterranean sea is perfect, with difference of orders of millimetres.

The P1 tidal constituent is a solar diurnal constituent, that together with K1, expresses the effect of the Sun's declination. In fact its pattern is very similar to the one of K1, with tidal amplitudes of several centimetres, reached only in the Adriatic Sea and with the only amphidrom node placed in the Strait of Sicily. The overall agreement with FES2014 is very good, with a slightly overestimation of 1 cm in the North Adriatic, consistently with what is found for the K1 tidal constituent.

Q1 is the larger lunar elliptic diurnal constituent that together with M1, which is the smaller lunar elliptic diurnal constituent, modulates the amplitude of the frequency of the declinational component O1. Among the height tidal harmonic considered in the present work, Q1 is the tidal wave who has the smallest amplitude in the Mediterranean basin, with maximum values of about 1 cm reached in the North Adriatic. It has a similar pattern than the O1 tidal constituent, even if the phase lines converge slightly northward, near the island of Crete. This is true both for $NEMO24^*$ and FES2014, with which the agreement is perfect.
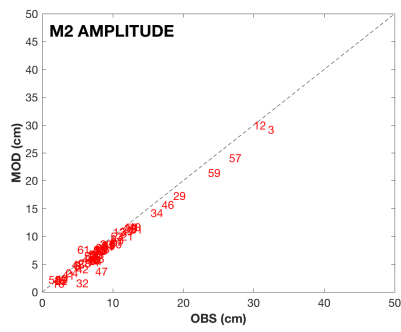
(a) M2 tidal elevation amplitude
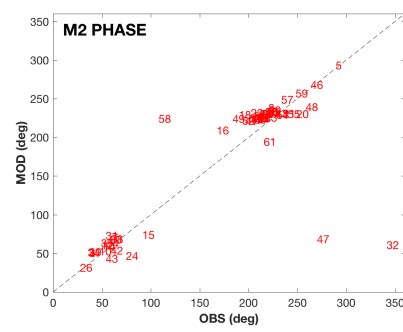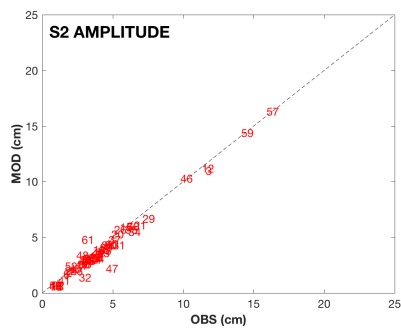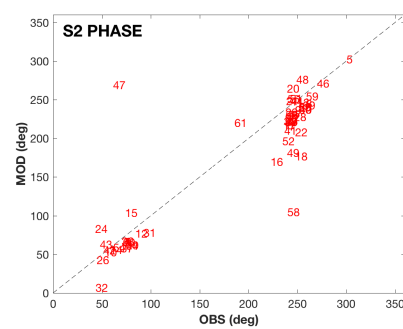
(b) M2 tidal elevation phase

(c) S2 tidal elevation amplitude

(d) S2 tidal elevation phase
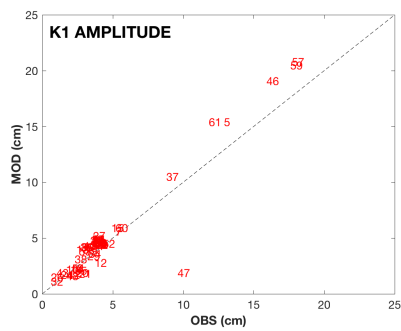
(e) K1 tidal elevation amplitude
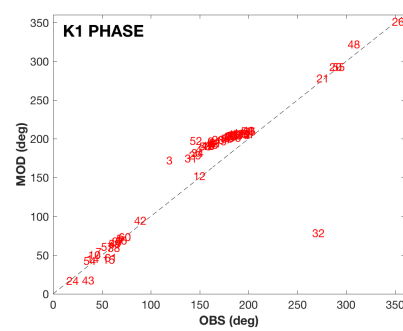
(f) K1 tidal elevation phase
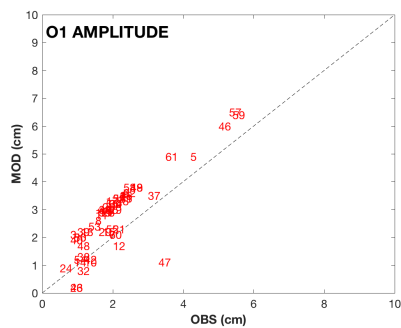
(g) O1 tidal elevation amplitude
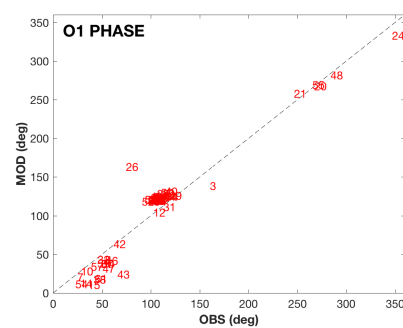
(h) O1 tidal elevation phase

FIGURE 2.12: Validation of the amplitudes and phases of the M2 (a) and (b), S2 (c) and (d), K1 (d) and (e) and O1(f) and (h) tidal constituent. The observed data are on the x axis and the modelled ones on the y axis (*cm*). The number associated to each tide gauge site can be referred to table 2.4

2.4   Summary and conclusions

In this work, we have revisited the tidal simulation with a $NEMO$ barotropic-equivalent model. Tides are due to both the Atlantic tidal wave entering the Strait of Gibraltar and the equilibrium tidal forcing. Besides NEMO that is the main model used in this work, also the main features of the unstructured grid T-UGO model are described. Thanks to its embedded spectral solver, this model allows to perform fast sensitivity tests. Another application of T-UGO is the downscaling of the boundary tidal currents from FES2014 model to a regional simulation. Moreover the elevations of FES2014 global tidal solutions are used to force the model at its open lateral boundary. One of the key factor that influences the accuracy of modelled tides is a satisfying horizontal resolution that allows to solve well the straits, the complex shorelines and the small islands. Other factors influencing the modelling of tides in a configuration of the Mediterranean Sea are the lateral boundary conditions and data, used to force the model. In this work, a downscaling of the tidal currents at the open lateral boundary has allowed to reduce the error in the Atlantic box, and consequently in all the domain.

Tides are also very sensitive to the parameterization of the bottom friction. In this work a logaritimic formulation is used, and a lot of test have been done, with different roughness length and drag coefficients, evidencing the necessity to add locally, in the shallow water areas (namely the North Adriatic and the Gulf of Gabès), further dissipation effects. Enhancing of the bottom friction in the shallow water areas has allowed to improve impressively the accuracy of tides, especially in the Gulf of Gabès. This suggest the necessity to locally parameterize the dissipation effects due to tides in the Mediterranean Sea, and also the fact that, for its complex geometrical and bathymetric feature, the Mediterranean Sea deserves local calibration and adjustments. On the other hand, semidiurnal and diurnal tides have very different patterns, for their astronomical nature, so the calibration of a specific wave doesn't imply the improvements of other waves. Due to the semidiurnal character of tides in the Mediterranean Sea, in this work the main adjustments have to be done in order to improve the M2 and the S2 tidal components, characterized by the higher tidal ranges are associated. An interesting finding of this work is the non negligible effect of the K2 and the N2 tidal components, that have local higher amplitudes respect to the O1 diurnal tidal component in the Mediterranean Sea.

The results obtained for the modelled main height tidal components are widely discussed in section 2.3.4. An overview on the basin scale $RMS_{misfits}$ calculated respect to both the satellite

altimetry data and the tide gauges is given in table 2.3. These errors for the main lunar semidurnal component M2 are respectively 1.1 *cm* and 2.2 *cm*, evidencing the fact that the main errors are associated to tidal modelling in coastal area.

A more detailed analysis of coastal representation of tides, is given by the comparison between the amplitude and phase with the harmonics calculated at the control dataset of tide gauges.

With the exception the sites of Messina and Reggio Calabria which have the main discrepancies in terms of both amplitude and phase, an overall agreement between the observations and the $NEMO24^*$ modelled values is found. Moreover the agreement is also good respect FES2014 and satellite data. The general tendency of $NEMO24^*$ is a slight underestimation of the semidiurnal tidal constituents and an overestimation of the diurnal one.

Unfortunately, tide gauges used for the validation of modelled results, are not uniformly distributed on the Mediterranean coast. There is a lack of data, especially in the African and in the Eastern basin coasts. This problem, was already pointed out by Tsimplis, Proctor, and Flather (1995) and still remain unresolved. The great improvement respect to twenty years ago, is the fact that the satellite altimetry offers a new great opportunity to validate the modelled tidal waves, together with the fact that tide gauges provide more accurate records.

Chapter 3

Effects of baroclinic tides on the Mediterranean Sea General circulation

3.1   Introduction

In this chapter we want to investigate the role of tides in the Mediterranean Sea and their interaction with its complex geometry and large scale dynamics, trying to capture the way in which the barotropic tides, by the interaction with the Strait and the topography, generate internal tidal waves which enhance the vertical mixing. To this purpose, a baroclinic tidal model which accounts for the stratification and the atmospheric forcing is needed. The barotropic tidal model, discussed in the Chapter 2 is able to reproduce the tidal structures in the Mediterranean Sea, in particular the semidiurnal components, which dominate the tidal propagation in the basin. The baroclinic model used to simulate the Mediterranean Sea, is based on the implementation Mediterranean Monitoring Forecasting Center (Med - MFC), which aims is to provide regular and systematic informations about the physical state of the ocean and marine ecosystems for the Mediterranean Sea, in the frame of the Copernicus Marine Environment Monitoring Service (CMEMS) [1]. The scientific and numerical basis of the Med-MFC current system can be found on the work of Pinardi et al. (2003), which describe a model with a resolution of 1/8 ° and 31 vertical levels, developed for a forecasting purpose, in the Mediterranean Sea and on the work of Pinardi and Coppini (2010). More recent versions of this model, with a doubled horizontal resolution and with 72 unevenly spaced vertical levels, are described by Tonani et al. (2014) and Oddo et al. (2014).

Currently, the physical component of the current Med-MFC system is provided by means of a configuration of NEMO that has an horizontal resolution of $1/24° \times 1/24°$ (which correspond

---

[1]http://marine.copernicus.eu/mediterranean-monitoring-forecasting-centre-med-mfc/

to about 4 *km*) and 141 unevenly spaced vertical levels (Clementi *et al.*, 2017). The increased resolution, together with some modelling refinements (such as the non-linear free surface formulation, implemented in NEMO by Levier et al. (2007)), lay the foundations for an accurate modelling of tides in the Mediterranean basin. In fact, due to the important Atlantic component of tides in the Mediterranean Sea, a minimum resolution is needed in order to properly resolve the Strait of Gibraltar and all the complex bathymetric features that characterize the Mediterranean Sea and its sub-basins, which are determinant in modelling tides. Despite the fact that in the Mediterranean Sea, the tidal signal is generally superimposed to atmospheric-induced and steric sea level variations, a more accurate determination of the tidal excursion has recently been urged (Sannino et al., 2015). The implementation of tides in a baroclinic model of Med-MFC, discussed in this chapter, relies on the results of the sensitivity tests performed with the barotropic-equivalent model, discussed in chapter 2.

In this work, the interest on the baroclinic tides is twofold: first we want to test the consistency of the barotropic signal of tides in a baroclinic model of the Mediterranean Sea. On the other hand, we are interested in studying the impact of tides in the Mediterranean Sea temperature and salinity profiles, transport at Gibraltar Strait, surface and intermediate currents. In the first part of this chapter, the results of a baroclinic simulation with four tidal components is shown, assessed and compared to the barotropic model results, followed by a preliminary evaluation of the effects of tides on the large scale circulation of the Mediterranean Sea. The study concerns a one-year long experiment, which can be considered an assessment of the coupled dynamics of tides and turbulence currents for the short time scales, i.e., from the mesoscales to the seasons.

3.2   Mediterranean tides

In this section a description of the tidal baroclinic model used in the study is given together with the results in terms of tidal harmonics and their validation.

As for the barotropic simulations, the hydrodynamic NEMO model (version 3.6) is used. It solves the primitive equations, with the Boussinesq, hydrostatic and the incompressible approximations. For sake of brevity, in this section we focus only on the differences between the baroclinic and the barotropic model settings, discussed in the previous chapter. In the baroclinic model the GEBCO interpolated bathymetry is used without the modifications at the Gibraltar Strait. Currently this bathymetry assures better results at Gibraltar Strait, in term of transport, for the experiment without tidal waves, with respect to the modified one (Clementi *et al.*, 2017).

Hence further sensitivity tests are needed in order to adapt the Gibraltar Strait's bathymetry to both a reliable representation of the Atlantic tides entering the Alboran Sea and to the right baroclinic transport values at Gibraltar. At the moment, we privilege the accuracy of baroclinic transport and we refer to future research for more sensitivity on the bathymetry at this Strait. As for the barotropic experiment, a quadratic bottom drag coefficient with a logarithmic drag coefficient formulation has been used at the bottom, but with a roughness length of 1 *cm*. Finally the enhancement of the bottom friction in the shallow water areas is neglected in the baroclinic experiment, since it has been added in the barotropic experiment under the assumption that some physics was missing in the simplified two-dimensional model.

The main two fundamentals factors that distinguish the baroclinic experiment from the barotropic one is the fact that the former is forced by the atmospheric surface atmospheric pressure, heat and water air-sea fluxes and nested in a numerical global ocean model. In particular the model interactively computes air-surface fluxes of momentum, water, and heat. The implemented bulk formulae are described by Pettenuzzo, Large, and Pinardi, 2010, using the 6-hours, 0.125° horizontal-resolution operational analysis and forecast fields from the European Centre for Medium-Range Weather Forecasts (ECMWF). The hydrodynamic model is nested in the Atlantic, within the daily analysis and forecast CMEMS GLO-MFC product at $1/12° \times 1/12°$ horizontal resolution. A detailed description of other specific features of the model implementation can be found in Oddo et al., 2009 and Oddo et al., 2014. Moreover, tidal elevations and currents are added in the specified lateral boundary condition fields, as described in previous chapter.

The effects of tides in the Mediterranean Sea are studied by the comparison of two identical simulations, that differ only by the tidal forcing. Here we considers both the Atlantic tidal forcing and the equilibrium tide only for the main four tidal components (M2, S2, K1, O1) since they are responsible of almost all the signal in the Mediterranean basin.

Hereinafter we refer to this experiment as $NEMO24_{tide}$, while the non tidal experiment is called simply $NEMO24$. Basically the experiments have been running for two years (namely the 2015 and 2016) and only the simulations during the last year are analysed. In turn, in order to ensure the robustness of the simulations both experiments have been started from a restart of another 2-yr long simulation which has exactly the same settings of $NEMO24$. In order to ensure the stability of the tidal model and to explicitly solve the fast gravity tidal waves, both the internal and the external time steps are reduced in $NEMO24_{tide}$. The internal time step is lowered from 300 *s* to 180 *s* while the external one from 3 *s* to 2 *s*. A third 2-yr long experiment is performed with eight diurnal and semidiurnal tidal components, with a lower internal time step

	RMS_{mifsit} (cm) respect to the CTOH altimetry data				RMS_{mifsit} (cm) respect to the tide gauges			
	M2	**S2**	**K1**	**O1**	**M2**	**S2**	**K1**	**O1**
$NEMO24_{2D}$	1.1	0.8	1.3	0.7	2.2	1.0	1.7	0.9
$NEMO24_{tide}$	1.0	0.8	1.0	0.3	2.1	1.0	0.9	0.3

TABLE 3.1: Results of the validation (RMS_{mifsit} in cm) of both $NEMO24_{2D}$ and $NEMO24_{tide}$ in the Mediterranean, basin respect to the CTOH altimetry data and to all the tide gauge sites.

of 120 s even if the results are not shown in the present study, since they do not differ much by $NEMO24_{tide}$. In this work, the main harmonics deriving from the simulation of baroclinic tides with $NEMO24_{tide}$ are compared with the corresponding results achieved for the barotropic one ($NEMO24_{2D}$ hereinafter). The harmonic analysis is performed on a one year long series of simulated SSH values, for each grid point of the domain. We start this comparison, using the CTOH altimetry data and to all the tide gauges, for both the barotropic and baroclinic configurations. The table 3.1 contains the $RMS_{misfits}$ in cm calculated in the overall basin for the two experiments.

The main result is that $NEMO24_{tide}$ shows a RMS_{mifsit} error reduced with respect to $NEMO24_{2D}$. This is true for both the validation against coastal tide gauge sites and against the CTOH satellite dataset.

We argue that this difference is due to the atmospheric pressure effects that are not adequately subtracted from tide gauges and satellite altimetry because in the Mediterranean pressure effects are very different from inverse barometer effects (Le Traon et al., 1994). This probably makes the baroclinic model closer to the observations. As shown in the scatter plots (3.1), the baroclinic configuration tends to slightly underestimate the semidiurnal M2 and S2 amplitudes and the main difference between modelled and observed phases are relative always to the tide gauge stations, such as Reggio Calabria, Messina and Valencia, already pointed out in the barotropic simulations. These discrepancies have been already commented for the barotropic tides and are attributed to the issue of inaccuracies in the bathymetry at the Strait of Messina.
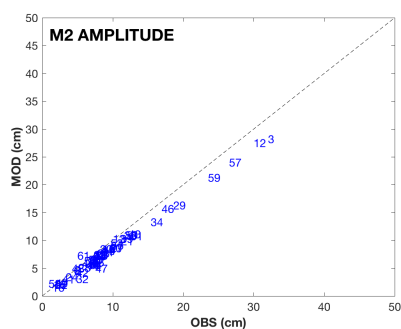
(a) M2 tidal elevation amplitude
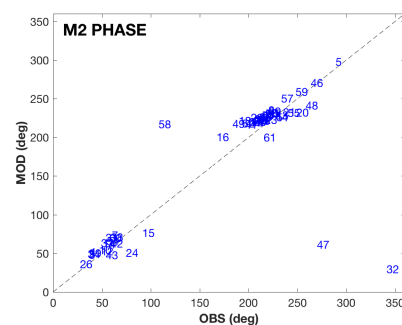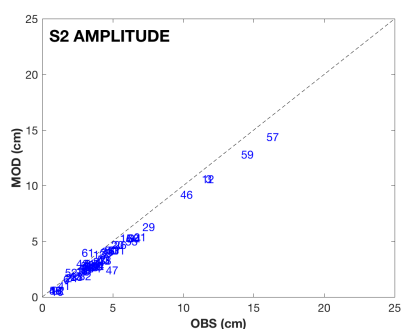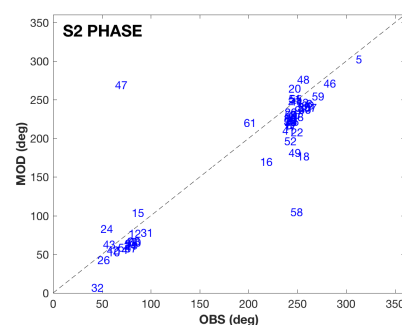
(b) M2 tidal elevation phase

(c) S2 tidal elevation amplitude

(d) S2 tidal elevation phase
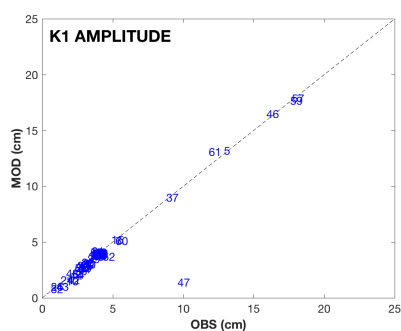
(e) K1 tidal elevation amplitude
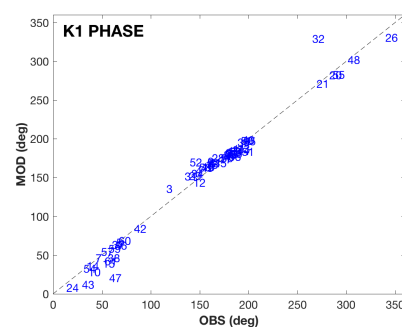
(f) K1 tidal elevation phase
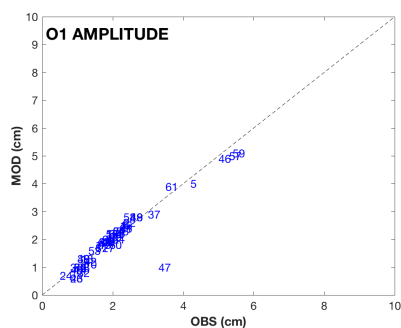
(g) O1 tidal elevation amplitude
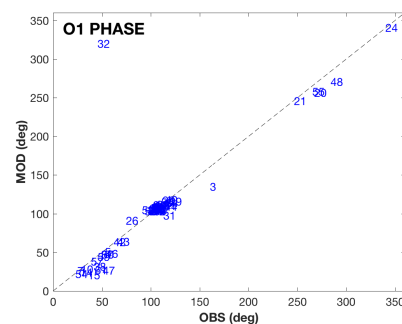
(h) O1 tidal elevation phase

FIGURE 3.1: Validation of the amplitudes and phases of the M2 (a) and (b), S2 (c) and (d), K1 (d) and (e) and O1(f) and (h) tidal constituent calculated from 1 year of simulation of the experiment $NEMO24_{tide}$. The observed data are on the x axis and the modelled ones on the y axis (cm). The number associated to each tide gauge site can be referred to table 3.2

Another possible validation considers the comparison of NEMO24 with FES2014 tidal compo-nents. The results for the main four tidal constituents are shown in fig. 3.2. M2 is again several *cm* different at Gibraltar probably due to the fact that the bathymetry in the baroclinic model has not been modified.

For what concerns the S2 component, the agreement with FES2014 is very good, with some discrepancy found only at the Gulf of Gabès (panel (d) of figure 3.2). The agreement with FES2014 is very good for both K1 and O1 in the overall basin (panel (f) and panel (h) of figure 3.2). Tides in the North Adriatic are no more overestimated, a trend found for both components in the barotropic experiment. A comparison between the modelled and observed amplitudes and phases, for the control dataset of the main four tidal waves is given in table 3.2.

As expected, the tidal pattern obtained for the baroclinic experiment are very similar to the ones obtained for the barotropic one, the main difference resulting in small horizontal scale perturbations to the co-phases lines, especially for the semidiurnal components M2 and S2. Shriver et al. (2012) suggest that such perturbations can be attributed to the presence of internal waves.

TABLE 3.2: Observed (obs) and modelled (mod) amplitudes (A) in *cm* and phases (ϕ) in degrees for the control set of 61 tide gauges.

No	Station	longitude	latitude	M2(obs/mod)		S2(obs/mod)		K1(obs/mod)		O1(obs/mod)	
				A(cm)	$\phi(deg)$	A(cm)	$\phi(deg)$	A(cm)	$\phi(deg)$	A(cm)	$\phi(deg)$
1	Ajaccio	8°45'36.00"	41°55'12.00"	7.3/7.3	212/226	3.1/2.8	230/241	3.6/3.8	182/185	1.5/1.8	100/109
2	Alcudia	3°08'24.00"	39°49'48.00"	4.6/4.76	206/224	1.7/1.7	225/243	3.6/4.0	158/171	2.2/ 2.4	98/104
3	Algeciras	-5°24'00.00"	36°10'48.00"	32.0/29.0	37/48	11.6/10.6	64/73	2.5/2.9	116/136	0.8/1.0	161/135
4	Almeria	-2°28'48.00"	36°49'48.00"	9.5/8.2	38/52	3.9/3.3	66/73	3.5/3.9	146/159	2.2/2.5	114/113
5	Ancona	13°30'00.00"	43°37'12.00"	6.7/5.9	289/298	3.6/3.0	303/310	12.9/13.2	65/66	4.2/4.0	53/51
6	Barcelona	2°09'36.00"	41°20'24.00"	4.5/4.6	200/220	1.5/1.6	217/238	3.5/3.8	160/169	2.3/2.5	97/103
7	Bari	16°51'36.00"	41°08'24.00"	9.7/8.7	60/74	6.0/5.3	67/79	5.2/5.1	43/46	1.9/1.9	25/26
8	Cagliari	9°06'36.00"	39°12'36.00"	8.4/8.0	220/235	3.0/3.0	245/259	2.9/3.1	174/179	1.5/1.7	100/108
9	Carloforte	8°18'36.00"	39°09'00.00"	7.0/6.4	218/230	2.8/2.4	237/247	3.9/4.0	176/182	1.8/1.9	103/111
10	Catania	15°05'24.00"	37°29'24.00"	6.5/5.6	47/54	3.4/2.8	53/56	1.7/1.5	36/28	1.2/1.1	28/28
11	Centuri	9°21'00.00"	42°57'36.00"	8.4/7.9	210/225	3.3/3.0	227/239	3.5/3.9	184/187	1.5/1.7	105/112
12	Ceuta	354°40'58.80"	35°54'00.00"	30.0/27.5	49/53	11.3/10.6	77/77	3.7/3.9	143/144	2.0/2.1	102/103
13	Civitavecchia	11°47'24.00"	42°05'24.00"	10.0/10.3	228/228	3.6/3.8	247/249	2.4/2.8	189/187	1.1/1.3	104/104
14	Crotone	17°08'24.00"	39°04'48.00"	6.3/5.4	51/62	3.3/2.6	56/64	2.0/2.0	34/36	0.9/0.9	27/24
15	Dubrovnik	18°03'46.80"	42°39'28.80"	8.5/8.5	91/77	5.5/5.3	104/80	4.9/5.2	51/39	1.7/1.9	36/21
16	Formentera	1°25'12.00"	38°43'48.00"	1.4/1.5	167/291	0.6/0.5	170/212	3.8/4.0	156/167	2.2/2.5	102/107
17	Fos Sur Mer	4°53'24.00"	43°24'00.00"	6.3/6.5	202/220	2.4/2.3	216/237	3.5/3.8	171/174	1.8/2.2	99/104
18	Gandia	-0°09'00.00"	38°59'24.00"	1.6/2.1	190/222	0.5/0.6	177/203	3.7/4.1	152/164	2.5/2.8	100/104
19	Genova	8°55'12.00"	44°24'36.00"	8.6/8.1	208/223	3.3/3.0	224/236	3.5/3.8	179/184	1.6/1.8	103/104
20	Girne	33°19'48.00"	35°20'24.00"	8.2/8.5	249/232	4.9/4.7	264/241	2.4/2.7	283/282	1.6/1.9	267/257
21	Hadera	34°52'01.20"	32°28'01.20"	11.2/9.9	236/233	6.5/5.4	249/241	2.6/2.6	270/271	2.0/2.0	257/246
22	Ibiza	1°27'00.00"	38°54'36.00"	1.8/2.0	202/226	0.7/0.6	208/244	3.8/4.0	158/169	2.3/2.6	102/107
23	Imperia	8°01'12.00"	43°52'48.00"	7.8/7.7	217/223	3.0/2.8	234/237	3.4/3.8	181/181	1.7/1.9	106/109
24	Katakolo	21°18'54.00"	37°39'00.00"	3.3/3.4	75/51	1.6/1.7	83/49	1.3/1.6	14/2	0.5/0.7	357/341
25	La Figueirette	6°55'48.00"	43°28'48.00"	7.3/7.2	205/222	2.8/2.6	222/237	3.5/3.6	175/179	1.7/2.0	98/107
26	Lampedusa	12°36'00.00"	35°30'00.00"	7.6/7.5	28/36	5.1/4.7	43/46	0.6/1.0	356/331	0.8/0.6	75/91
27	Livorno	10°17'24.00"	43°32'24.00"	9.7/8.7	215/228	3.6/3.2	231/242	3.6/3.8	176/179	1.7/1.7	102/109
28	Mahon	4°16'12.00"	39°53'24.00"	5.1/5.1	211/226	2.0/1.8	228/244	3.7/3.8	162/175	2.1/2.3	102/107
29	Malaga	-4°24'36.00"	36°42'36.00"	18.6/16.3	37/51	7.1/6.3	62/74	3.2/3.5	139/152	1.9/2.1	119/116
30	Marseille	5°21'00.00"	43°16'48.00"	6.8/6.5	205/220	2.5/2.3	222/236	3.5/3.8	172/176	1.9/2.2	119/116
31	Melilla	-2°55'48.00"	35°17'24.00"	12.5/10.8	54/71	5.0/4.2	78/90	3.5/4.2	134/152	2.0/2.3	113/98
32	Messina	15°33'36.00"	38°11'24.00"	4.8/3.1	342/30	2.6/1.9	7/39	0.6/0.8	265/329	1.0/0.8	45/345
33	Monaco	7°25'12.00"	43°43'48.00"	7.3/7.4	206/222	3.1/2.7	222/237	3.5/3.8	177/181	1.6/1.9	101/108
34	Motril	-3°31'12.00"	36°43'12.00"	15.4/13.3	35/49	6.1/5.3	62/72	3.3/3.7	142/156	1.9/2.2	116/114
35	Napoli	14°16'12.00"	40°48'36.00"	11.6/10.9	220/231	4.2/4.1	240/251	2.7/2.9	195/197	0.9/1.0	106/112
36	Nice	7°16'48.00"	43°41'24.00"	7.5/7.3	207/222	2.9/2.7	226/236	3.5/3.8	177/181	1.8/2.0	102/107
37	Ortona	14°24'36.00"	42°21'00.00"	6.7/6.1	49/64	4.7/4.2	58/73	8.8/9.0	60/64	3.0/2.9	49/48
38	Otranto	18°29'24.00"	40°09'00.00"	7.0/6.1	49/64	4.0/3.3	67/77	2.3/2.4	56/47	1.0/1.0	42/32
39	Palermo	13°22'12.00"	38°07'12.00"	11.1/10.3	221/234	4.1/4.0	243/254	2.8/3.2	187/196	1.0/1.3	112/118
40	Palinuro	15°16'12.00"	40°01'48.00"	12.2/ 11.1	218/232	4.5/4.2	238/251	2.9/3.0	194/199	0.8/0.9	115/118
41	Palma De Mallorca	2°37'48.00"	39°33'36.00"	2.8/3.0	196/217	1.1/1.0	210/235	3.7/3.9	159/170	2.2/2.4	100/105
42	Porto Empedocle	13°31'12.00"	37°16'48.00"	4.8/4.2	59/63	3.5/2.8	56/55	1.8/1.6	83/84	1.2/1.2	62/64
43	Portomaso	14°29'24.00"	35°55'12.00"	6.3/5.7	54/48	3.9/3.3	63/51	1.0/1.0	30/12	0.8/0.6	66/64
44	Portotorres	8°24'00.00"	40°50'24.00"	7.3/7.2	228/227	2.8/2.7	248/243	3.6/3.9	188/185	1.6/1.9	114/109
45	Port Vendres	3°06'36.00"	42°31'12.00"	5.7/5.8	203/220	1.9/1.9	222/239	3.5/3.7	165/169	2.2/2.4	97/103
46	Ravenna	12°16'30.00"	44°29'31.20"	16.9/15.7	264/271	9.8/9.2	271/277	15.9/16.5	63/62	5.0/4.9	54/49
47	Reggio Calabria	15°38'24.00"	38°07'12.00"	7.5/5.0	270/61	4.5/2.4	269/64	9.6/1.4	58/21	3.3/1.0	50/27
48	Rhodes	28°13'58.80"	36°26'49.20"	4.2/5.0	259/242	2.4/3.0	276/250	1.7/2.2	301/302	1.0/1.3	284/271
49	Sagunto	-0°12'00.00"	39°37'48.00"	1.9/2.3	184/218	0.5/0.6	182/241	3.7/4.0	151/163	2.5/2.8	102/105
50	Salerno	14°45'36.00"	40°40'12.00"	11.8/11.0	217/232	4.4/4.2	238/251	2.8/3.0	192/198	0.9/1.0	111/115
51	Senetosa	8°48'46.80"	41°33'00.00"	7.2/7.2	228/267	4.4/4.2	238/251	3.5/4.0	193/184	1.6/1.9	113/110
52	Sete	3°42'00.00"	43°24'00.00"	5.9/6.4	194/219	1.6/2.2	197/237	4.3/3.7	140/170	2.0/2.3	91/105
53	Solenzara	9°24'00.00"	41°51'36.00"	9.7/9.5	214/229	3.9/3.4	241/250	2.6/2.7	180/184	1.3/1.6	94/103
54	Taranto	17°13'12.00"	40°28'12.00"	6.7/5.6	55/66	3.5/2.8	59/67	2.1/2.1	31/33	0.9/1.0	23/22
55	Tasucu	33°49'48.00"	36°16'48.00"	9.8/9.1	240/232	5.9/5.0	251/242	2.3/2.7	286/283	1.8/2.0	265/258
56	Touloun	5°54'36.00"	43°07'48.00"	6.5/6.6	209/222	2.6/2.4	231/237	3.6/3.8	180/177	1.8/2.2	101/106
57	Trieste	13°45'00.00"	45°39'00.00"	26.5/24.0	233/251	15.9/14.4	240/237	17.7/17.9	49/54	5.3/5.0	39/38
58	Valencia	-0°18'36.00"	39°26'24.00"	0.9/2.2	108/217	0.5/0.6	105/243	3.4/4.1	149/163	2.3/2.8	102/105
59	Venezia	12°25'12.00"	45°24'36.00"	23.5/21.3	248/259	14.1/12.8	255/265	17.6/17.7	57/59	5.4/5.1	45/44
60	Vieste	16°10'48.00"	41°52'48.00"	9.5/8.6	57/70	6.0/5.3	66/77	5.2/5.1	67/69	1.9/1.8	49/47

TABLE 3.2: Observed (obs) and modelled (mod) amplitudes (A) in *cm* and phases
(ϕ) in degrees for the control set of 61 tide gauges.

No	Station	longitude	latitude	M2(obs/mod)		S2(obs/mod)		K1(obs/mod)		O1(obs/mod)	
				A(cm)	$\phi(deg)$	A(cm)	$\phi(deg)$	A(cm)	$\phi(deg)$	A(cm)	$\phi(deg)$
61	Zadar	15°14'06.00"	44°07'22.80"	5.0/7.3	215/200	2.8/4.0	220/195	11.8/13.1	53/42	3.5/3.9	43/27

Going now to a local level, for sake of brevity, only the comparison relative to the tide gauge sites of Trieste, Otranto, Lampedusa, and Motril are shown in figure 3.3. The four sites have been chosen as representative of a different tidal regime and because continuous time series are available during the simulation year (2016). In order to make sure of the consistency of the observed and modelled time series, and thus to make them comparable, the mean value of each dataset has been subtracted to the respective instantaneous values of SSH. The analysis has been done for all the year 2016 on a 1 hour-frequency time series, but for sake of readability only the time series relative to the months of April (from the 1 to the 24, according to the availability of measured data) and September are shown in figure (3.3).

The site of Trieste represent the shallow North Adriatic region, the spring-neap cycle is evident for both months and the modelled and observed time series are perfectly in phase. For what concerns the tidal amplitudes, the model is in a good agreement with the observations, even if it is unable to represent the high peaks reached during spring tides (60 *cm* in the month of September). At the contrary the SSH is not well represented at the Motril site, suggesting that further calibration of the bathymetry at the Gibraltar Strait is needed.
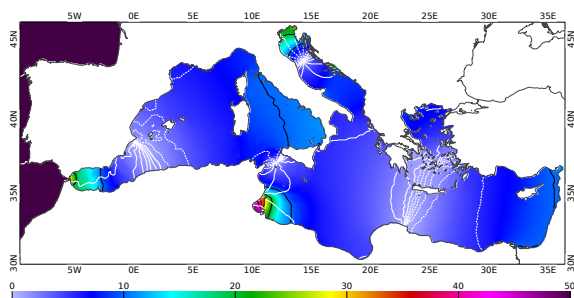
(a) M2 tidal elevation amplitude and phase
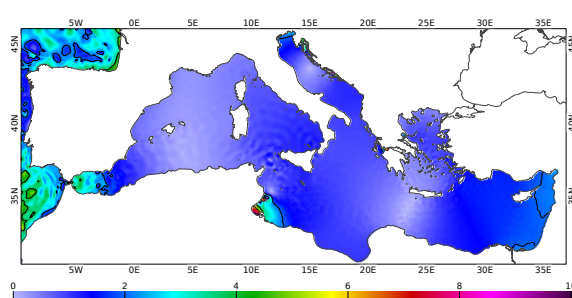
(b) M2 complex difference d with FES2014
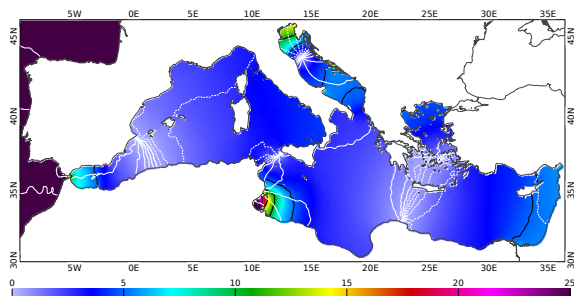
(c) S2 tidal elevation amplitude and phase
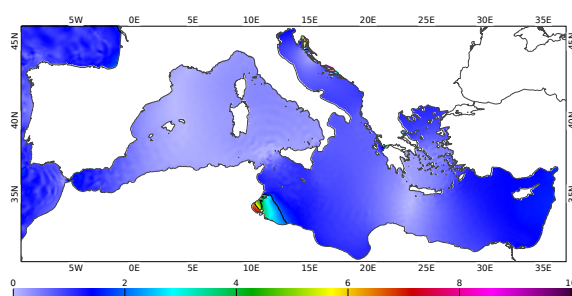
(d) S2 complex difference d with FES2014
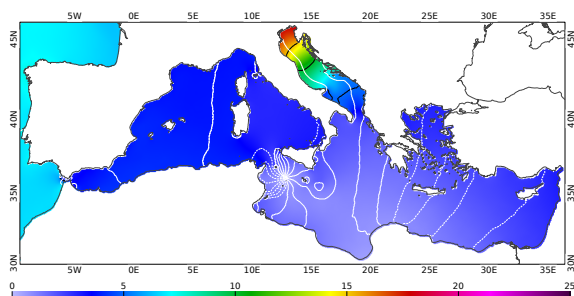
(e) K1 tidal elevation amplitude and phase
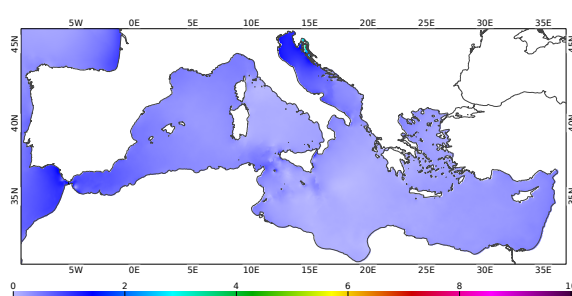
(f) K1 complex difference d with FES2014
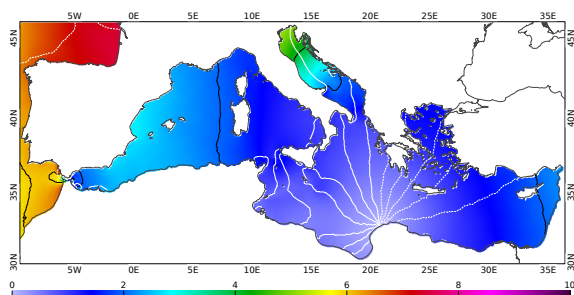
(g) O1 tidal elevation amplitude and phase
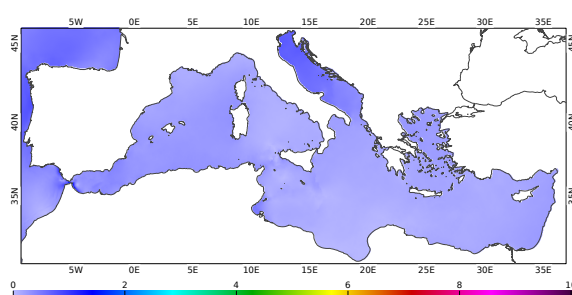
(h) O1 complex difference d with FES2014

FIGURE 3.2: M2, S2, K1 and O1 tidal components in the Mediterranean Sea. The left panels represent $NEMO24_{tide}$ M2 elevation amplitude in cm (black contours, interval $= 10$ cm) and phase in degrees (white solid contours for positive phases and white dashed contours for negative phases, interval $= 20°$) while the right panels show the complex amplitude error d (cm) of NEMO24 respect to FES2014 for M2 elevation in the Mediterranean Sea

(a) Trieste SSH, April 2016   (b) Trieste SSH, September 2016

(c) Otranto SSH, April 2016   (d) Otranto SSH, September 2016

(e) Lampedusa SSH, April 2016   (f) Lampedusa SSH, September 2016

(g) Motril SSH, April 2016   (h) Motril SSH, September 2016
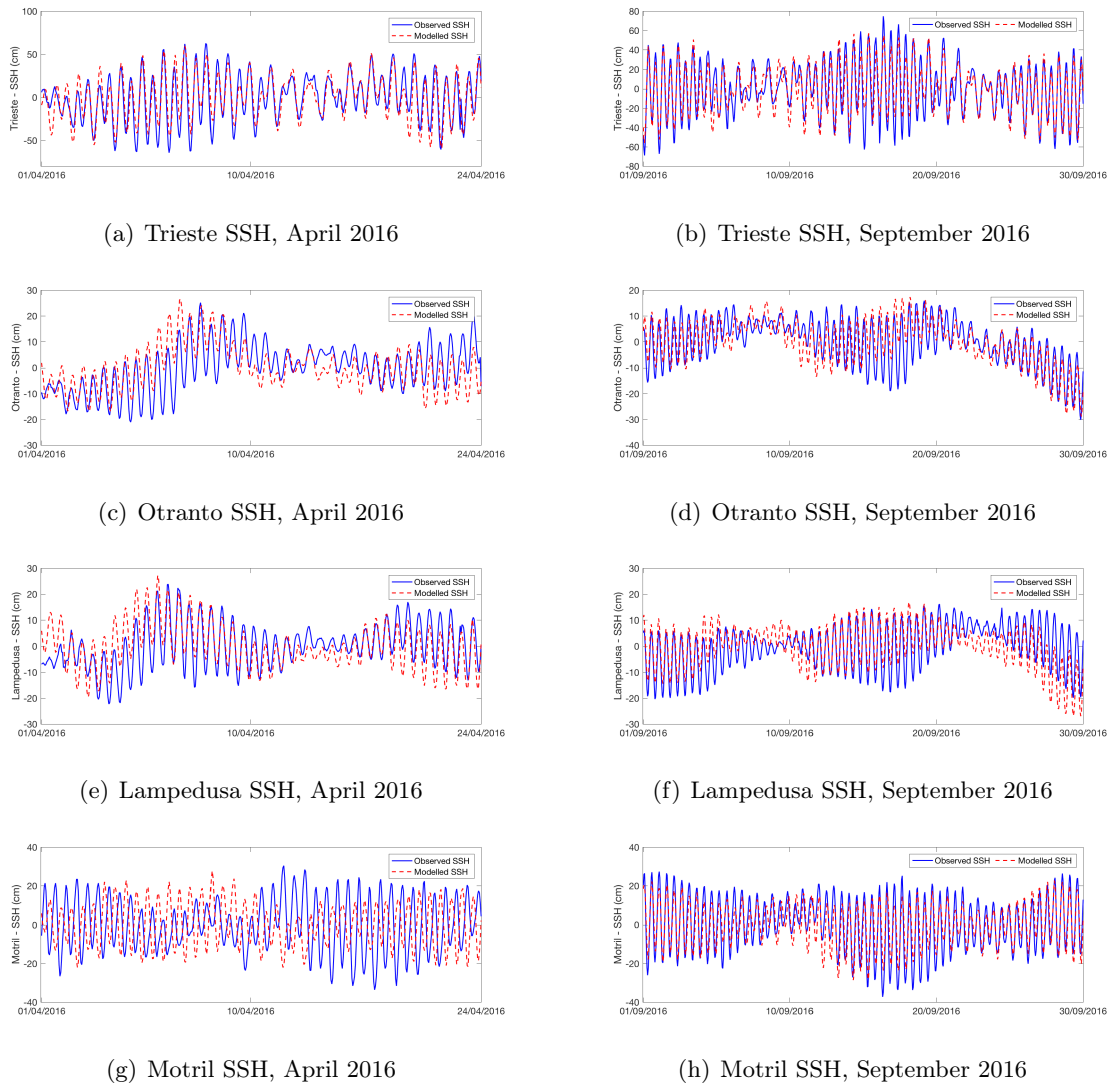
FIGURE 3.3: Comparison between modelled SSH of $NEMO24_{tide}$ (red dashed line) and observed SSH (solid blue line) in cm, at four mareographic stations of the control dataset. The dataset are on an hourly basis.

3.3   Tidal effects on the Mediterranean Sea

So far, several publications have discussed the local role of the semidiurnal tides at the Strait of Gibraltar, describing the phenomenology of tidal waves (Tejedor et al., 1999) and quantifying the effects of tidal forcing on transport of the Atlantic and Mediterranean waters (Sannino *et al.*, 2004).

All these studies come to the conclusion that the strait dynamics is strongly influenced by tides, which are responsible for the amplitude modulation of water transport and for the substantial vertical mixing. In addition to a barotropic tidal wave, tidal forcing also generates internal

baroclinic waves due to the interactions between the baroclinic shear of currents and the intense tidal currents and the steep local topography (Sannino *et al.*, 2004).

Tidal effetcs on the large scale Mediterranean Sea circulation have been studied by Naranjo et al. (2014), in which the impact of tides on the Western Mediterranean circulation is discussed. The authors find that the tidal increased exchange flow volume transport at the Strait of Gibraltar modifies the hydrological properties of the Atlantic inflowing waters, through the enhancement of mixing and facilitate the outflow of Mediterranean deep water. In particular, they argue that the tidal motion can favor the deep convention in the Gulf of Lyon.

In the same year, Harzallah *et al.* (2014) use a coarse resolution model of the Mediterranean Sea, with higher resolution at the Gibraltar Strait, to study the local tidal effects at the Strait and in all the basin. Coherently with Naranjo et al. (2014), the authors find that the tidal enhanced mixing at the Strait of Gibraltar reduces the tracer gradients between the Mediterranean basin and the Atlantic Ocean, the entering water in the Mediterranean resulting cooler on average. Similarly, the local mixing at the Strait of Gibraltar, induces more saline waters entering the basin and less saline waters leaving it. Finally they conclude that the Mediterranean Sea is cooled and saltened by tides, with the largest changes occurring in the upper and intermediate layers, leading to more homogenised waters.

In 2015 Sannino et al. investigate the importance of tides in determining the main features of the Mediterranean circulation. For this purpose they used a $1/16°$ of horizontal resolution model, with higher resolution at the Strait of Gibraltar. Basically they find that the inclusion of tidal explicit forcing in a eddy resolving Mediterranean model, has non negligible effects on the simulated circulation, in addiction to the intensification of local mixing processes. They find that the western basin exhibits an immediate response to the different characteristics of the inflowing Atlantic water and they also point out some effects of tidal wave in the Gulf of Lyon, in the Tyrrhenian Sea and in the Levantine basin.

In our work we examine different effects of tides on the Mediterranean Sea and we compare our findings with the literature ones.

3.3.1 Tidal effects on transports

The first assessment shown here, concerns the transport of the Atlantic inflowing water and the Mediterranean outflowing Water at Gibraltar Strait. For $NEMO24$ and $NEMO24_{tides}$, transports are computed integrating the along-strait velocity vertically, from the bottom up to

the depth where the along-strait velocity reverts its direction, for the outflow and from this depth up to the surface for the inflow, at a constant longitude section placed at $5.5°$ W. The net transport is calculated as the sum between these two components.
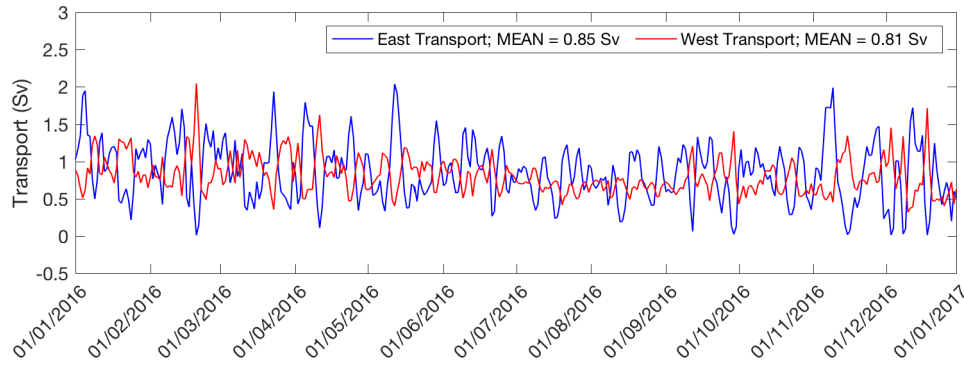
(a) Atlantic (blue) and Mediterranean (red) transports computed from the experiment $NEMO24$.
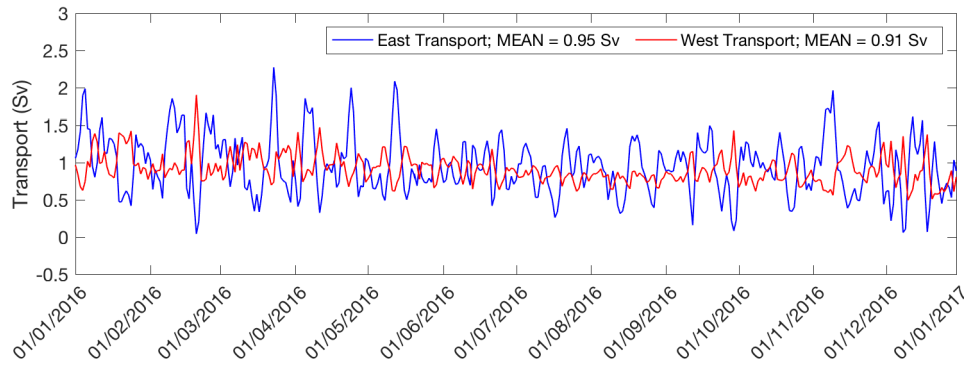
(b) Atlantic (blue) and Mediterranean (red) transports computed from the experiment $NEMO24_{tide}$.
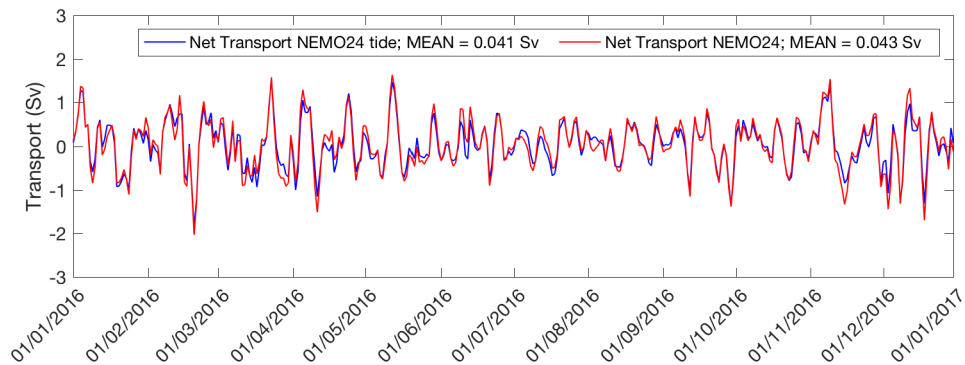
(c) Net transport of $NEMO_{tide4}$ (blue) and $NEMO24$ (red)

FIGURE 3.4: Atlantic, Mediterranean and net transports (Sv) calculated for a section at $5.5°$ W for the two experiments $NEMO24_{tide}$ and $NEMO24$. The absolute values of the mean transports, during the year 2016 are written in panels (a), (b) and (c).
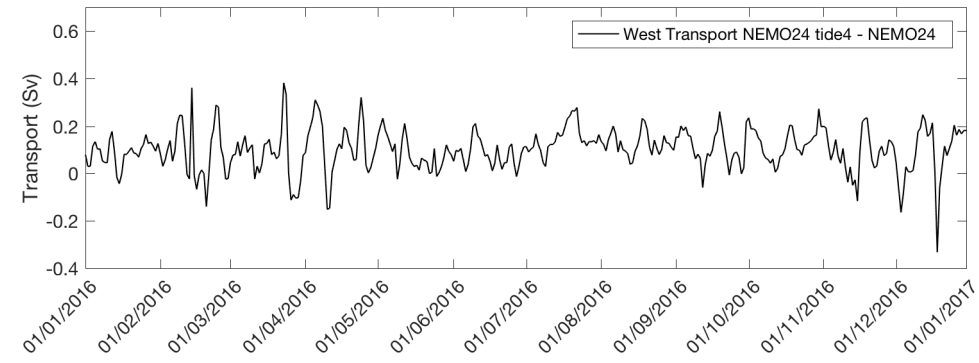
(a) Difference between the Mediterranean transports $NEMO24_{tide}$ - $NEMO24$
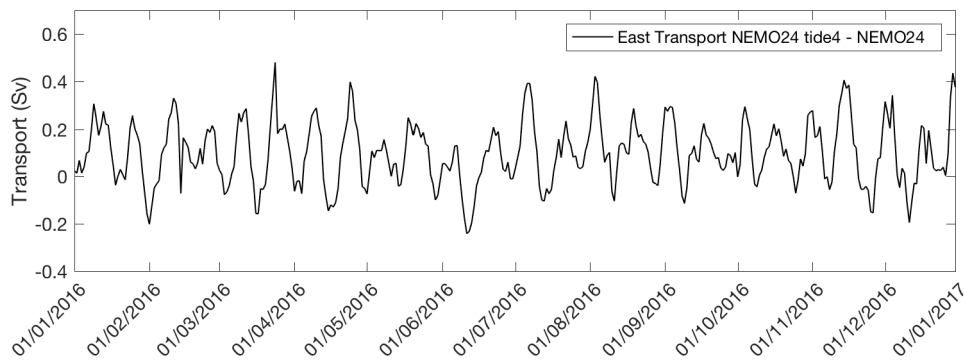
(b) Difference between the net transports $NEMO24_{tide}$ - $NEMO24$
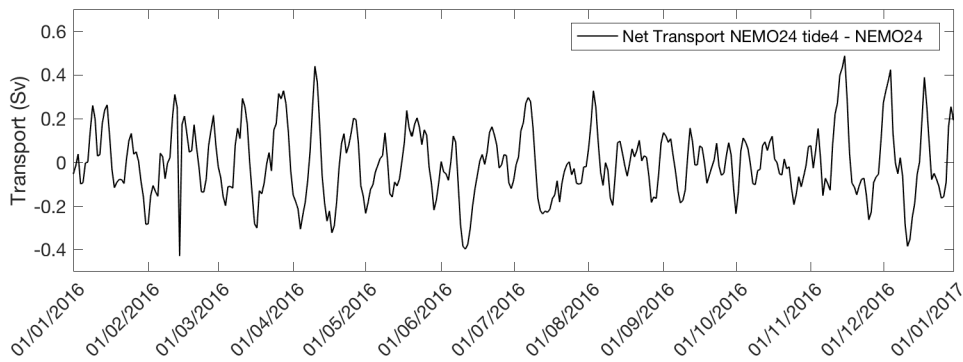
(c) Difference between the Atlantic transports $NEMO24_{tide}$ - $NEMO24$

FIGURE 3.5: Atlantic, Mediterranean and net transports differences (Sv) calculated for a section at 5.5° W for the two experiments $NEMO24_{tide}$ and $NEMO24$.

The panel (a) of figure 3.4 shows the East and West transports for the $NEMO24$ experiment, while analogous results for the $NEMO24_{tide}$ experiment are represented in panel (b) in order to point out their reciprocal pattern. The yearly mean East and West transports for the experiment $NEMO24$ are respectively 0.85 Sv and - 0.81 Sv, while the corresponding values result enhanced for the experiment $NEMO24_{tide}$ (0.95 Sv and - 0.91 Sv). The differences in terms of West and

East transports, between the two experiments, can be appreciated in panels (a) and (b) of figures 3.5, where the amplitude modulation of the tidal signal (with its period of 14 days) is clearly visible for the Atlantic inflowing Water. Our results show that both the Mediterranean and Atlantic baroclinic transports are increased by about 10% when tides are prescribed. However the most important difference is that eastward and westward transports have qualitatively different fluctuations. The increasing of both transports and their estimates are in general agreement with the results of Sannino *et al.* (2004).

The mean increment for both the inflow and outflow, in presence of the semidiurnal tidal forcing respect to a non-tidal experiment, imply that the mean net transport doesn't change for the experiments $NEMO24$ and $NEMO24_{tide}$ and it is in agreement with the reference value of 0.04 Sv found in Soto-Navarro et al. (2015).

3.3.2   Tidal effects on temperature and salinity

This section is dedicated to the assessment of the effects of tides on the tracers fields in the Mediterranean Sea. The present analysis starts by comparing the basin average sea surface salinity (SSS) and temperature (SST) trends during the year 2016, for the two experiments $NEMO24_{tide}$ and $NEMO24$.
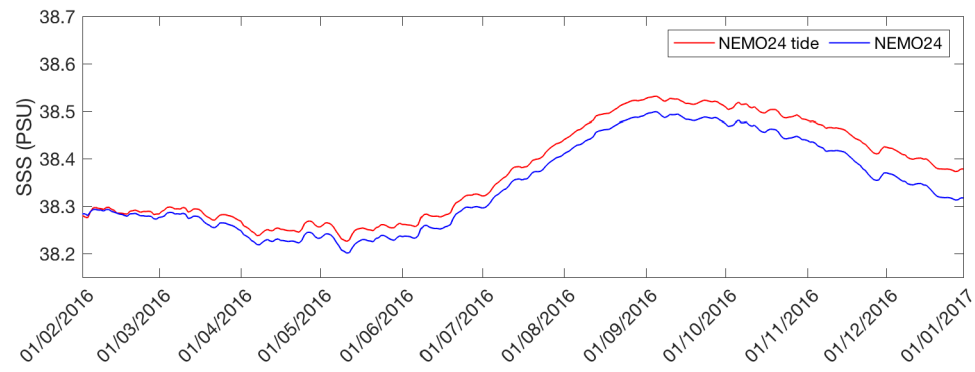
(a) $NEMO24$ and $NEMO24_{tide}$ SSS time serie (2016)
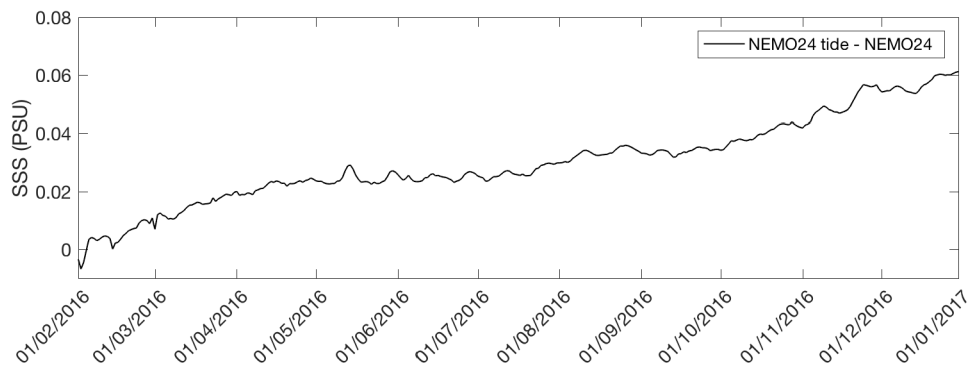
(b) Difference between $NEMO24_{tide}$ and $NEMO24$ SSS time series (2016)

FIGURE 3.6:   Average Sea Surface Salinity (PSU) over the year 2016.   Panels are shown along east-west vertical section of all the domain, at 36 N of latitude, crossing the Gibraltar Strait.

(a) $NEMO24$ and $NEMO24_{tide}$ SST time serie (2016)

(b) Difference between $NEMO24_{tide}$ and $NEMO24$ SST time series (2016)
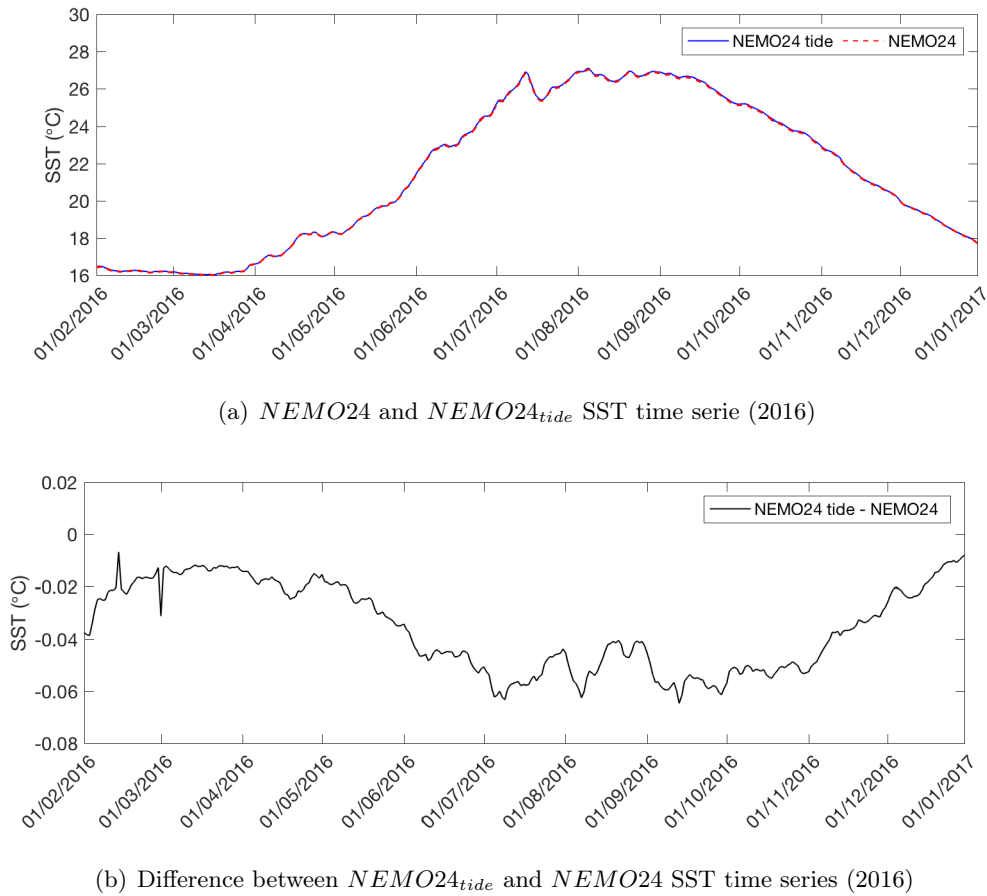
FIGURE 3.7: Average Sea Surface Temperature over the year 2016. Panels are shown along east-west vertical section of all the domain, at 36 N of latitude, crossing the Gibraltar Strait.

Figure 3.6 represents the time series of the mean-basin sea surface salinity (SSS) values, during the year 2016, showing a progressive increase of SSS when tides are considered. The two time series start witht the same value, less than 38.3 PSU, and gradually diverge, reaching at the end of the 2016, respectively the values of 38.31 PSU and 38.38 PSU for the experiments $NEMO24$ and $NEMO24_{tide}$. Moreover from the panel (b) of figure 3.6, the mean surface salinity difference seems to oscillate with the typical tidal fortnightly cycle, this is particularly evident for the month of November and for the summer period.

In the work of Harzallah *et al.* (2014), a similar analysis is performed on the salinity water volume average, on a 50-yr long simulation, showing a similar trend. From this long experiment, it results that the difference between the mean volume salinity in the tidal and non tidal experiments increases but slowly tends to a limit value.

For what concerns the mean sea surface temperature (SST), the comparison between the two

$NEMO24$ and $NEMO24_{tide}$ time series, during the year 2016, is shown in figure 3.7. Due to the great temperature excursion, the differences of surface temperature can't be distinguished in the upper panel of figure 3.7. Nevertheless, the difference between $NEMO24_{tide}$ and $NEMO24$ SST time series indicate a lower surface temperature in the Mediterranean basin, for the experiment that include the tidal waves, with a difference that is more pronounced during the summer period. These results are physically conceivable, although a validation is needed, and a longer simulation is necessary in order to compare this preliminary result with literature ones.

After the assessment of surface SST and SSS time series, an evaluation of how tides affect the temperature and salinity, in the upper and intermediate layers, fields is given.

The temperature and salinity fields relative to both experiments $NEMO24$ and $NEMO24_{tide}$ have been averaged over the year 2016 and five vertical transects are shown in figures: 3.9, 3.10, 3.11, 3.12 and 3.13, from the surface down to 1500 m. The positions of vertical transects are shown in figure 3.8 and their coordinates, the main Seas and Straits are listed in table 3.3. The horizontal transects (A, B and C) extend from West to East, while the meridional ones (D and E) extend from South to North.
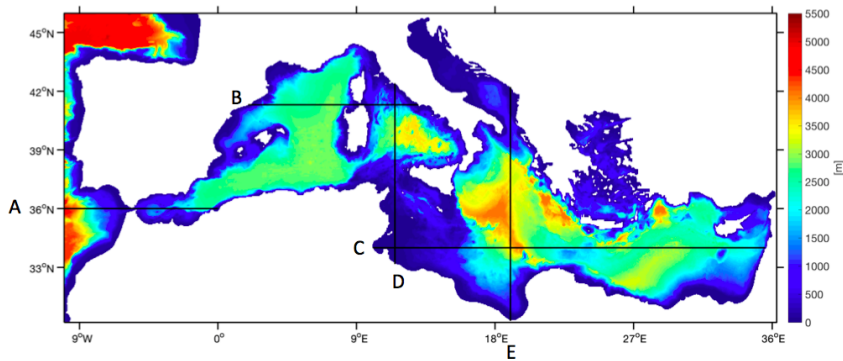
FIGURE 3.8: Model bathymetry in (m) and vertical transects A, B, C, D and E positions.

Transect	Crossed Seas and Straits	Longitude	Latitude
A	Atlantic - Gibraltar St. - Alboran	10°W - 0°	36°N
B	Balearic - Bonifacio St. - Tyrrhenian	2°E - 13°E	41.3°N
C	Libyan - Ionian - Levantine	10°E - 35.5°E	34°N
D	Libyan - Sicily St. - Tyrrhenian	11.5°E	33°N - 42°N
E	Libyan - Ionian - Otranto St.	19°E	30°N - 42°N

TABLE 3.3: Names, main Seas and Strait crossed by the vertical transects represented in figure 3.8 and their coordinates.

The transect A, crosses part of the Atlantic box, the Strait of Gibraltar and the Alboran Sea (figure 3.9). As aspected, we find that the effect of tides in the Strait of Gibraltar is the lowering of surface temperature and the enhancement of surface salinity of the Atlantic inflow water in the Alboran Sea, up to a depth of about 150 m and that below a thick interfacial layer the trend is opposite, up to a depth of about 300 m. From panel (b) of figure 3.9 is evident that the temperature stratification is weakened in $NEMO24_{tide}$ with respect to $NEMO24$ (panel (a)). Moreover a saltier Mediterranean Water outflows in the Atlantic Ocean, when tidal forcing is considered. These results are in agreement with the ones achieved by the model of Harzallah *et al.* (2014) and of Sannino *et al.* (2004).

(a) $NEMO24$ (b) $NEMO24_{tide}$ (c) $NEMO24_{tide}$ - $NEMO24$

(d) $NEMO24$ (e) $NEMO24_{tide}$ (f) $NEMO24_{tide}$ - $NEMO24$
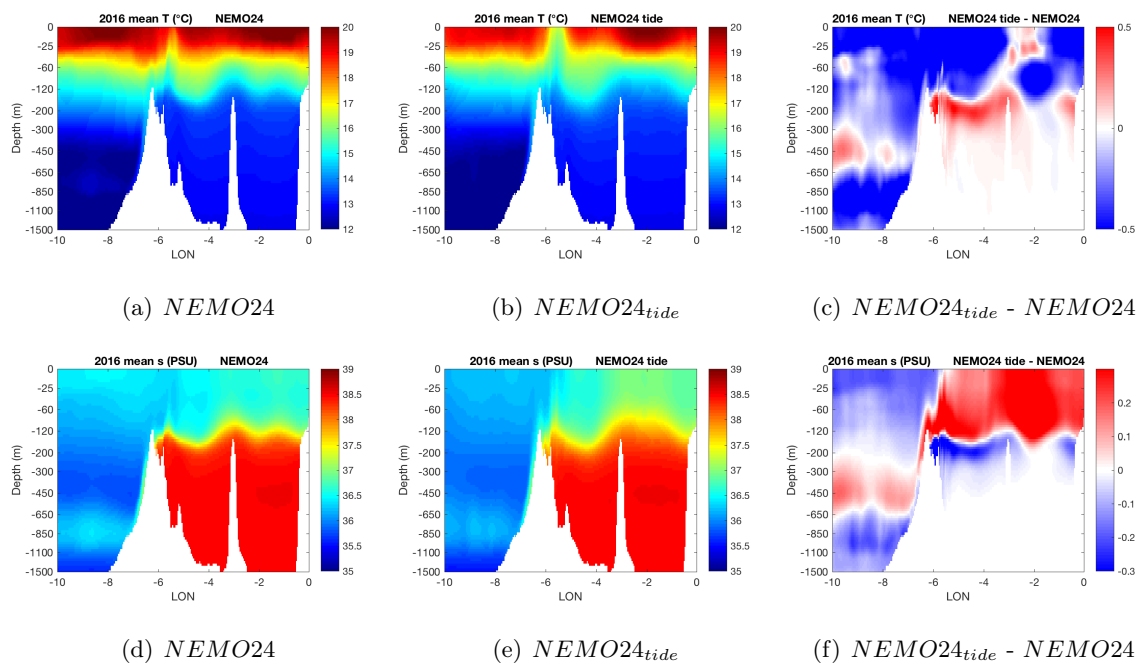
FIGURE 3.9: Yearly average tracers fields: (a), (b) and (c) for temperature, (d),(e), (f) for salinity corresponding to the transect A at a latitude of 36°N.

The transect B, crosses the Western Mediterranean basin, from the Balearic Sea up to the Tyrrhenian Sea, passing through the Strait of Bonifacio, at about 9°W (figure 3.10). The effects of tides show again the salinity increase in the upper layer of 100 m and but temperature contains an eddy-like signal and the cooling is not as evident as in the Gibraltar Strait. Some spots with decreased salinity can be observed in the underlying layer (panel (f) of figure 3.10). East to the Strait of Bonifacio, in the North Tyrrhenian Sea, both salinity and temperature are variable.

(a) $NEMO24$ (b) $NEMO24_{tide}$ (c) $NEMO24_{tide}$ - $NEMO24$

(d) $NEMO24$ (e) $NEMO24_{tide}$ (f) $NEMO24_{tide}$ - $NEMO24$
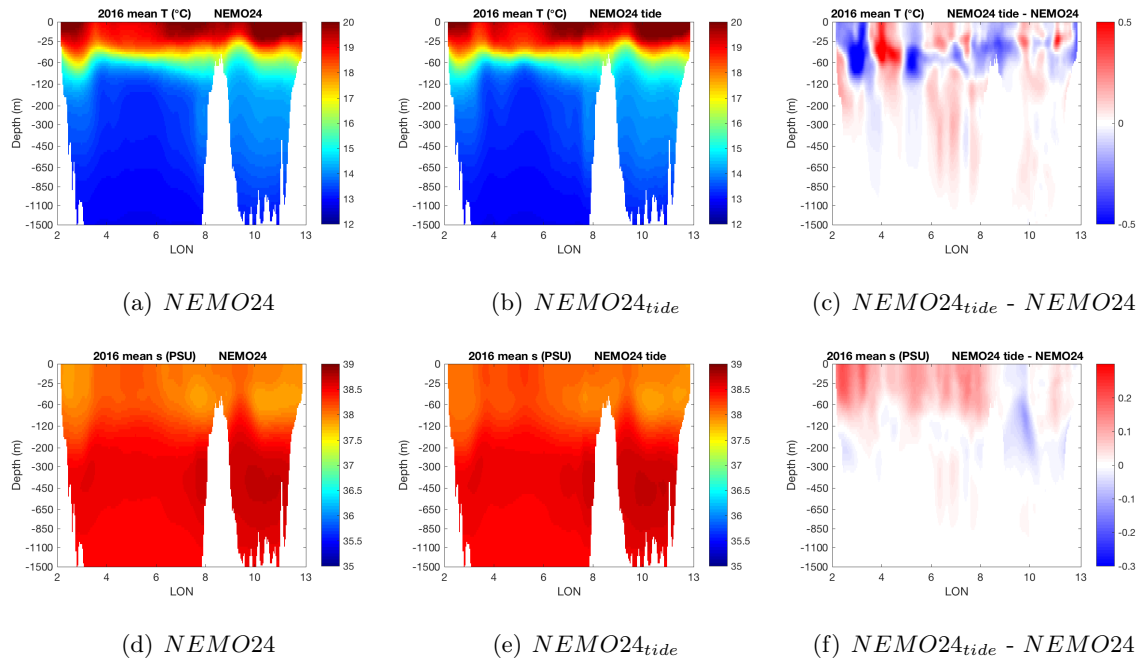
FIGURE 3.10: Yearly average tracers fields: (a), (b) and (c) for temperature, (d),(e), (f) for salinity corresponding to the transect B at a latitude of 41.3° N.

The transect C starts in the Tunisian shelf, crosses the Libyan Sea and all the Levantine Sea.

The main effect of tides seem to be connected to a different penetration of Modified Atlantic Water (the subsurface salinity minimum around $60\,m$) into the Levantine and a different thickness of the 16°C layer. Further investigations are needed to understand what the tides have changed here. From the present analysis it seems that impacts range from tracer advection to mixing.

(a) $NEMO24$ (b) $NEMO24_{tide}$ (c) $NEMO24_{tide}$ - $NEMO24$

(d) $NEMO24$ (e) $NEMO24_{tide}$ (f) $NEMO24_{tide}$ - $NEMO24$
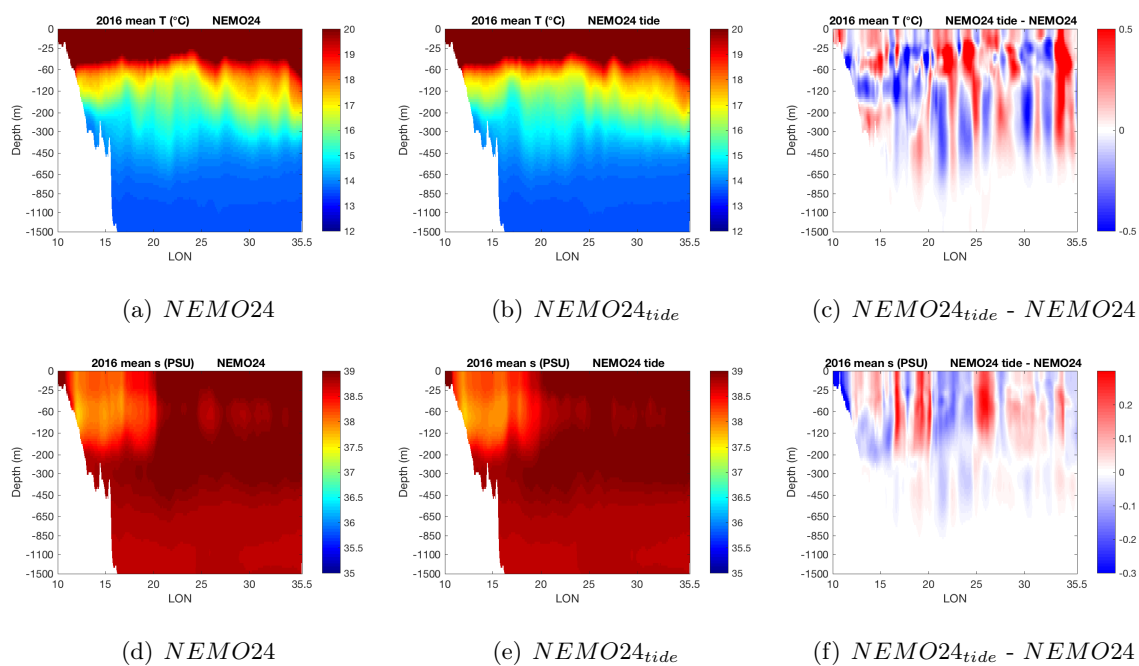
FIGURE 3.11: Yearly average tracers fields: (a), (b) and (c) for temperature, (d),(e), (f) for salinity corresponding to the transect C at a latitude of 34°N.

The meridional transect D crosses the Tunisian Shelf, the Sicily Strait and the Tyrrhenian Sea. In this transect it is evident the change in the salinity of the Modified Atlantic Water which is saltier due to the saltying process occurred at the Gibraltar Strait. The propagation of this subsurface low salinity tongue is different in the case with and without tides. Temperature does not have a specific cooling or warming effect due to tides but the overall stratification is changed.

(a) $NEMO24$ (b) $NEMO24_{tide}$ (c) $NEMO24_{tide}$ - $NEMO24$

(d) $NEMO24$ (e) $NEMO24_{tide}$ (f) $NEMO24_{tide}$ - $NEMO24$
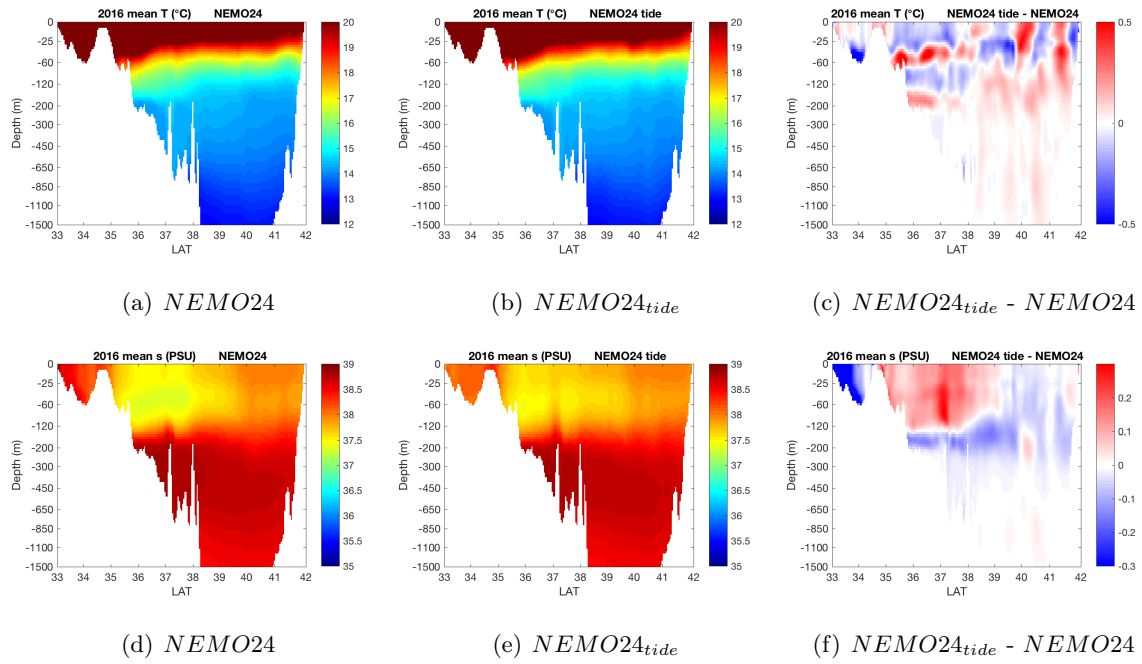
FIGURE 3.12: Yearly average tracers fields: (a), (b) and (c) for temperature, (d),(e), (f) for salinity corresponding to the transect D at a longitude of 11.5°W.

East of the panel D, at the longitude of 19°W, the vertical transect E starts from the coast of the Libyan Sea, crossing the Ionian Sea and the Strait of Otranto (figure 3.13). As for the other meridional transect saltier, northward Modified Atlantic Waters are evident at around 60 m while no precise trend in temperature is found (panel (f) of figure 3.13).

(a) $NEMO24$ (b) $NEMO24_{tide}$ (c) $NEMO24_{tide}$ - $NEMO24$

(d) $NEMO24$ (e) $NEMO24_{tide}$ (f) $NEMO24_{tide}$ - $NEMO24$
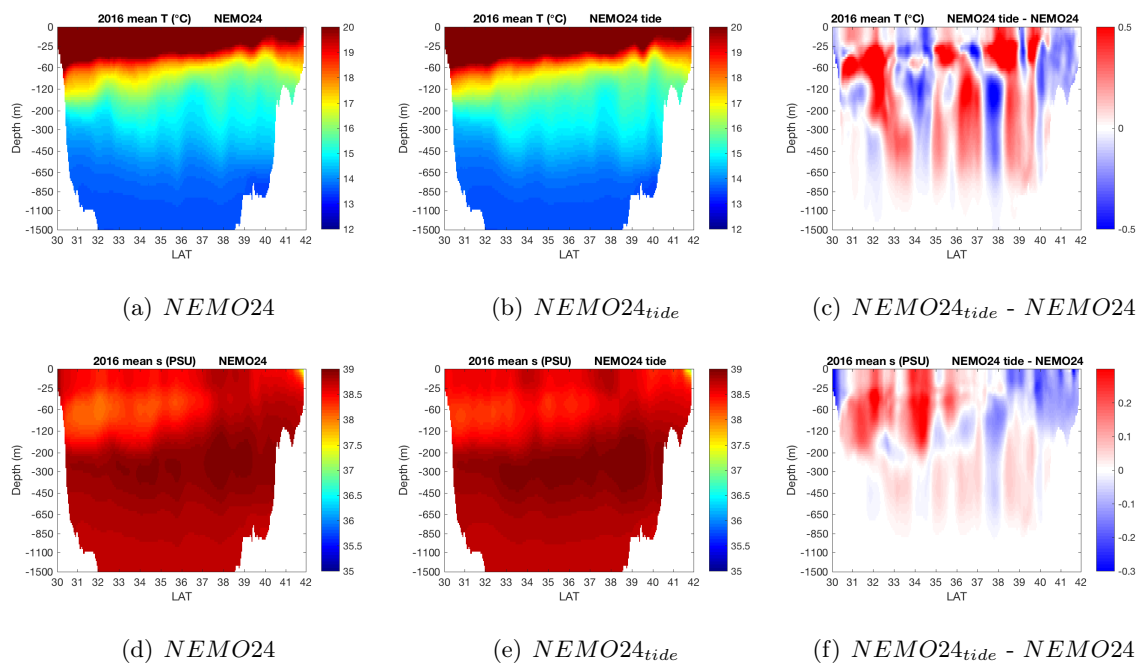
FIGURE 3.13: Yearly average tracers fields: (a), (b) and (c) for temperature, (d),(e), (f) for salinity corresponding to the transect E at a longitude of 19° W.

3.3.3 Effects of tides on the mean circulation

Tidal forcing effects are expected to be visible in the 2016 average currents. For what concerns the surface circulation, the figure 3.14 shows the difference between the two experiments, at a depth of 10 m. Basically each $NEMO24$ velocity component has been subtracted from the $NEMO24_{tides}$ one and these differences are plotted as a vector. The main differences are found in the southern Mediterranean Sea where the Modified Atlantic Water propagates from the Gibraltar Strait.
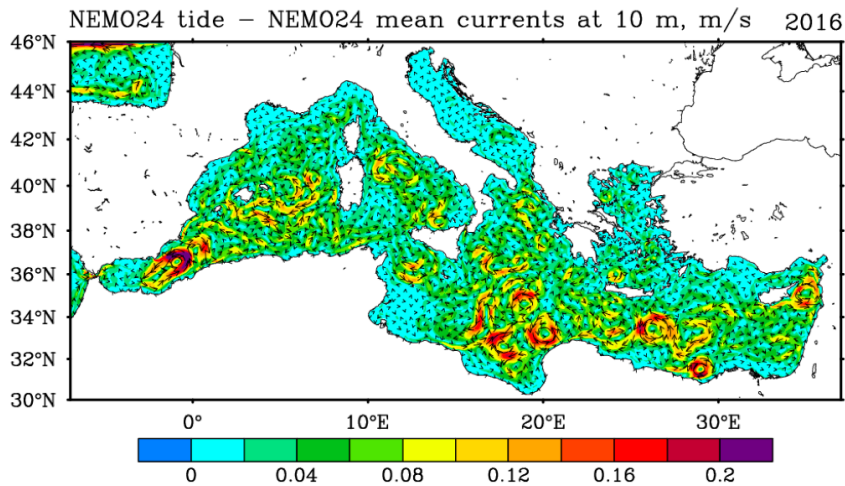
FIGURE 3.14: Mediterranean Sea 2016 time-mean circulation (m/s) difference, at 10 m between the experiments $NEMO24$ panel and $NEMO24_{tides}$.

In order to discuss the differences in mean currents between the two experiments $NEMO24$ and $NEMO24_{tides}$, the results are shown in three domains: the first spanning from the Gibraltar Strait until the Sardinian and Corsica islands (figure 3.15), the second covering the Tyrrhenian and the Adriatic Sea (figure 3.16) and a third one that covers the Strait of Sicily, the Libyan Sea and the Levantine and the Aegean Sea (figure 3.17).

The mean currents of the Western Mediterranean basin, from the entrance of the Strait of Gibraltar, up to the Sardinian and Corsica islands are shown in figure 3.15. Starting with the Alboran Sea, the circulation is characterized by the Atlantic Water current entering from Gibraltar and meandering around the two Alboran gyres, the western Gyre and the smaller amplitude eastern one (Pinardi et al., 2015). While both the western and eastern anticyclonic Alboran Gyres are similar between tides and no-tides, the third gyre, so-called Almeran-Oran cyclonic eddy, it is stronger in the tidal case and at all depths.

Immediately to the East, between between 3°W and 8°W, the instability region of the Algerian starts, a region characterized by a mean flow weak and without a precise direction (Millot, 1990). Several differences between the mean currents in the experiments $NEMO24$ and $NEMO24_{tides}$ are found in this region but they are related to positions and strength of mesoscale eddies that have been averaged out so it is difficult to extract a general rule. Our conclusion here is that the Algerian current instabilties are different but an in depth analysis of the mesoscale fields is required here. In the Northern part of the western basin, the mean circulation seem to be less affected by the forcing of tides.

Figure 3.16 shows the mean circulation in the Tyrrhenian, Adriatic Sea and part of the Ionian Sea. In the Tyrrhenian Sea, the circulation is dominated by three cyclonic gyres: the South-Western Tyrrhenian Gyre (SWTG), the South-Eastern Tyrrhenian Gyre (SETG) and the Northern Tyrrhenian Gyre (NTG) (Artale et al., 1994). Only two of the three are well known in the literature, while the SETG is weak in the mean most probably because this is an area of frequent anticyclonic eddies that weaken the cyclonic mean circulation (Pinardi et al., 2015).

The main differences between the experiments $NEMO24$ and $NEMO24_{tides}$ are that, the SETG is more structured and the NTG is smaller in extent but with amplified, when tides are considered. This last feature is evident both in surface and in the intermediate layer.

The Adriatic Sea is dominated by a cyclonic circulation composed of the Middle and Southern Adriatic cyclonic gyres and by the Eastern Adriatic Current and the Western Adriatic Coastal Current systems (Artegiani et al., 1997). These features are visible in both, $NEMO24$ and $NEMO24_{tides}$. As already shown by Cushman-Roisin et al., 2013 residual currents in the Adriatic Sea have low amplitude and our results confirm that.

An interesting difference appears in the Strait of Otranto, where a small anticlyclonic gyre can be appreciated in the mean surface currents when tides are prescribed (experiment $NEMO24_{tides}$). This implies that the Northward coastal current which enters in the Adriatic Sea is deviated Westward and part of the exiting Western Adriatic Coastal Current inverts its path and recirculates Northward.

In general, the eastern basin is the area in which the two experiments show largest difference in currents structures at both the considered depth. From the Sicily Strait up to the Levantine, currents are heavily modified in terms of cyclonic and anticyclonic gyres and mesoscales. This might be connected to the different Modified Atlantic Water forcing found in the previous section but again more investigations are required to interpret the circulation differences.

(a) *NEMO24*

(b) *NEMO24*

(c) *NEMO24$_{tide}$*

(d) *NEMO24$_{tide}$*

(e) *NEMO24$_{tide}$ - NEMO24*

(f) *NEMO24$_{tide}$ - NEMO24*
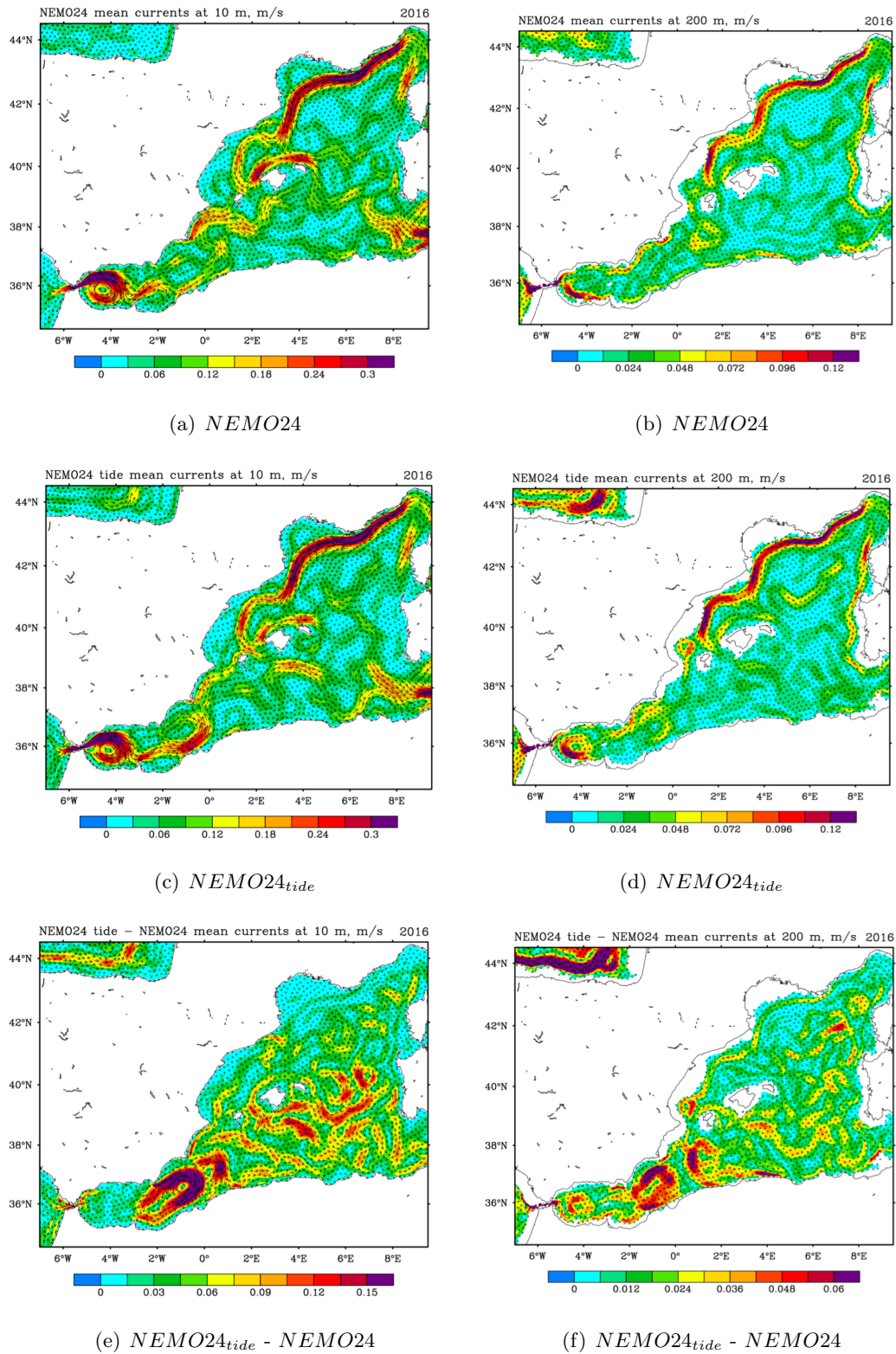
FIGURE 3.15: Western Mediterranean basin averaged circulation on the year 2016 (m/s), at 10 m of depth for the experiment $NEMO24$ panel (a), $NEMO24_{tides}$, panel (c) and their difference, panel (e) and at at 200 m for the experiment $NEMO24$ panel (b), $NEMO24_{tides}$, panel (d) and their difference, panel (f).

(a) *NEMO*24

(b) *NEMO*24

(c) *NEMO*24$_{tide}$

(d) *NEMO*24$_{tide}$

(e) *NEMO*24$_{tide}$ - *NEMO*24

(f) *NEMO*24$_{tide}$ - *NEMO*24
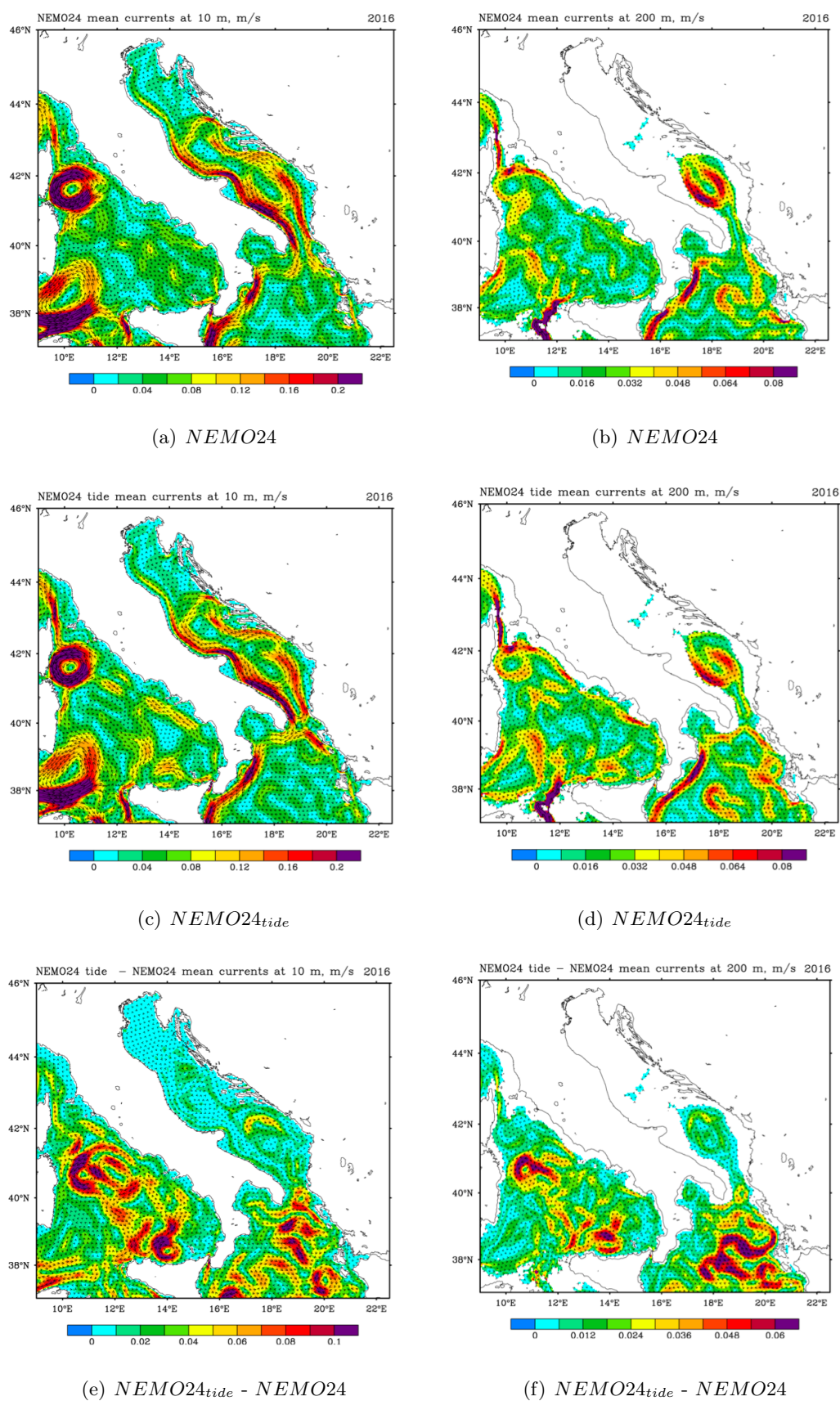
FIGURE 3.16: Central Mediterranean basin averaged circulation on the year 2016 (m/s), at 10 m for the experiment *NEMO*24 panel (a), *NEMO*24$_{tides}$, panel (c) and their difference, panel (e) and at at 200 m for the experiment *NEMO*24 panel (b), *NEMO*24$_{tides}$, panel (d) and their difference, panel (f).

(a) *NEMO*24

(b) *NEMO*24

(c) *NEMO*24$_{tide}$

(d) *NEMO*24$_{tide}$

(e) *NEMO*24$_{tide}$ - *NEMO*24

(f) *NEMO*24$_{tide}$ - *NEMO*24
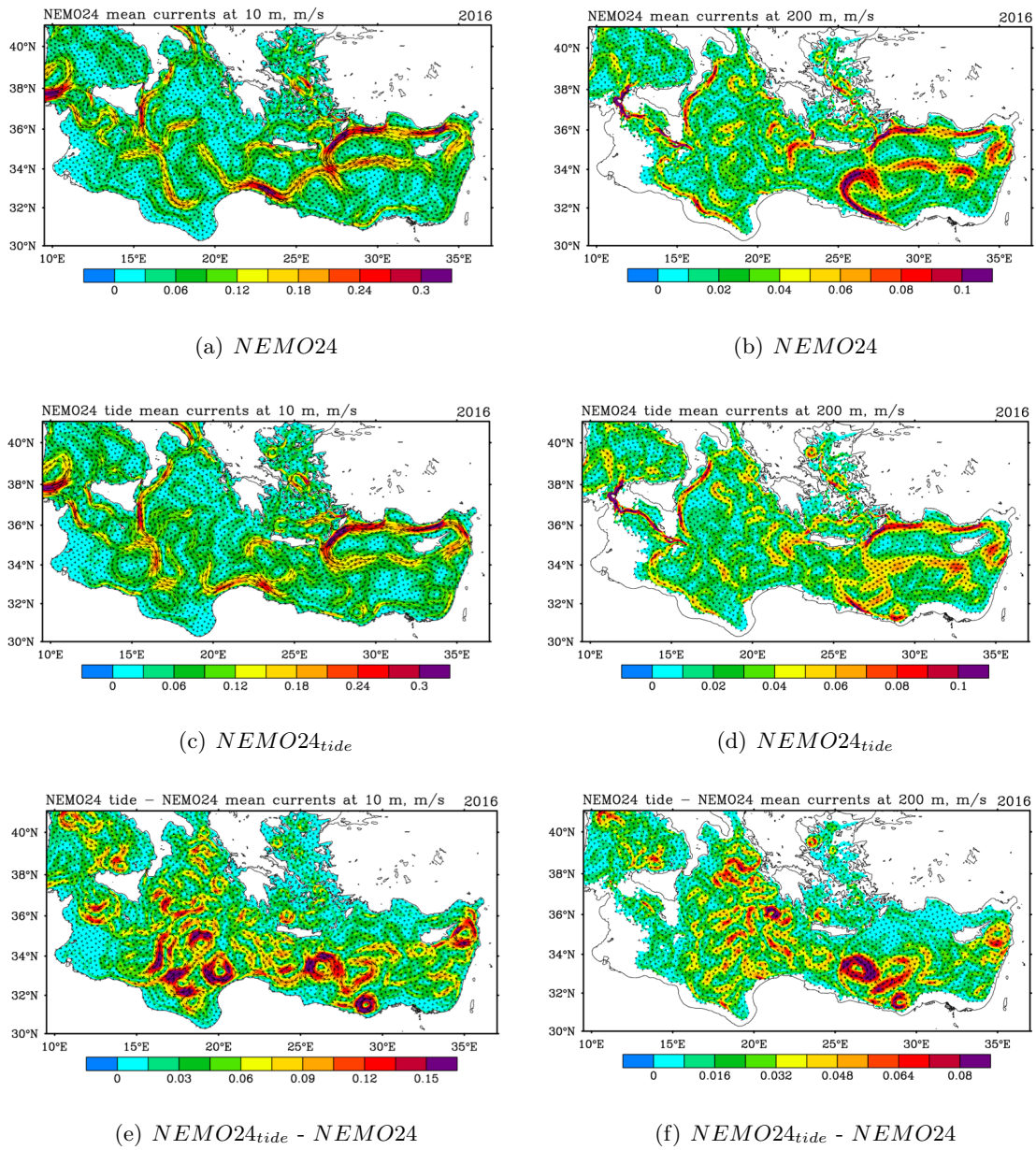
FIGURE 3.17: Eastern Mediterranean basin averaged circulation on the year 2016 (m/s), at 10 m for the experiment *NEMO*24 panel (a), *NEMO*24$_{tides}$, panel (c) and their difference, panel (e) and at at 200 m for the experiment *NEMO*24 panel (b), *NEMO*24$_{tides}$, panel (d) and their difference, panel (f).

3.4 Summary and conclusions

This chapter is the first assessment of the impact of tides in a pre-operational forecasting model of the Mediterranean Sea, with complete and realistic air-sea atmospheric forcings, lateral open boundary conditions in the Atlantic and an eddy resolving model, $1/24° \times 1/24°$ degrees horizontal resolution and 141 levels. The simulation is validated with the harmonics derived from the measured time series of Sea Surface Height at the tide gauge stations and with the harmonics derived from the satellite altimetry data. The results of this validation are compared to the harmonics obtained with a barotropic-equivalent and the errors associated to the baroclinc model result slightly reduced, in case of the semidiurnal tidal constituent and strongly reduced in case of diurnal ones. This means that even if the simplified two dimensional model is capable to reproduce most of the structures of the tidal dynamics it is less accurate then a model that considers all atmospheric forcings and a baroclinic structure of the currents. We argue that in the barotropic-equivalent model we have parametrized the missing effects of baroclinic tides and for this reason we have enforced two areas of larger bottom drag coefficient. This is the case of the northern Adriatic Sea and the Gulf of Gabes for the barotropic-equivalent model.

Despite many studies have focused on the effects of tides at the Strait of Gibraltar, few studies have addressed the issue of analysing the effects of tides in the Mediterranean Sea stratification and circulation, and no one with the current horizontal resolution of about $4\ km$ and with 141 vertical levels. The work of Sannino et al. (2015) has an increased resolution at the Strait of Gibraltar but an horizontal resolution of 6.5 km in the rest of the basin which makes the model only eddy permitting.

From our study it is confirmed that the interaction of the barotropic tides with the Strait of Gibtraltar generate an internal tidal variability, that produces an enhancement of the vertical mixing in the Alboran Sea. An important result of this work is that these local processes, are reproduced with the complete $NEMO24_{tide}$ model: the Atlantic Water entering in the Mediterranean Sea is saltier and colder, with respect to an experiment where tides are neglected, and the opposite behaviour is found in the underlying layer.

Our work focus on the study of the stratification variations in many Seas and Straits of the Mediterranean Sea in the upper and intermediate layers. The time series of the basin mean Sea Surface Salinity and Temperature, show an increase and cooling respectively similarly to the findings of Harzallah *et al.* (2014). Vertical sections of temperature and salinity fields in the basin show enhanced salinity in the upper layer of western basin, with the exception of the

Tyrrehnian Sea, while in the Eastern basin the main effect is the higher salinity of the Modified Atlantic water in the subsurface, advected eastward by different currents in the tidal experiment. Even if this study should be considered a preliminary evaluation of the effect of tidal waves in the Mediterranean Sea, it is already evident that tides have measurable effects in the surface and intermediate currents of the Mediterranean Sea. The main features highlighted by the comparison of the tides-no-tides experiments is the intensification of different gyres especially in the southern part of the basin where mesoscale and semi-permanent gyres are present.

Further analysis and validations are needed in order to complete the assessment of the effects of tides on the vertical mixing, stratification and currents together with a longer simulation.

Chapter 4

Conclusions and future research

4.1 Conclusions

Ocean tides are one of the most important dynamical processes in shelf and coastal seas, as well in terms of sea surface elevation and currents. Along topographic slopes and over some abyssal plains, internal tides generate strong currents, ocean stratification oscillations and the interaction with the ocean circulation, through locally enhanced mixing and isopycnal displacements. If external tides are know very well in most part of the ocean, the internal tides realistic representation is still a highly challenging issue.

Mediterranean barotropic tides have reduced amplitudes respect to the ocean tides. With the exception of the Adriatic Sea, the Aegean Sea and the Gulf of Gabès where tides have important ranges and are amplified by resonance phenomena, tides in the Mediterranean Sea have amplitudes of the order of centimetres.

The objectives of this work is the as accurate as possible reconstruction of the Mediterranean tides with the NEMO model and the study of tidal effects on the general circulation of the basin. To this purpose two models are built: a barotropic-equivalent model $NEMO24_{2D}$ and a stratified and realistic $NEMO24_{tide}$ model. A third model ($NEMO24$), which is the corresponding of $NEMO24_{tide}$ without tides, allows to highlight the features of tidal prescription in terms of transports, salinity, temperature and currents, by means of a comparison.

In general the validation of $NEMO24_{2D}$ and $NEMO24_{tide}$ in the Mediterranean basin, respect both the satellite altimetry derived harmonics and a set of 61 tide gauges gives small errors, of the order of mm for the main tidal components M2, S2, K1 and O1. As aspected, the errors are slightly higher respect to tide gauges harmonics than respect to satellite altimetry, since they are representative of coastal areas, where tides reach the most important amplitudes. We must

keep in mind that the control set of tide gauges used for the validation is quite inhomogeneous with a lack of data on the African coasts and with few data on the Eastern basin.

From the comparison between $NEMO24_{2D}$ and $NEMO24_{tide}$ it is evident that a better correspondence is found for the baroclinic $NEMO24_{tide}$ model, especially for the diurnal tidal components. This result is also coherent with the comparison with FES2014 tidal solution. It is worth saying that the $RMS_{misfits}$ associated to the $NEMO24_{2D}$ are greater if the enhancement of the bottom drag coefficient in the Gulf of Gabès and in the North Adriatic is non considered. The fact that much larger differences arise when no stratification effects are present can be a sign of a barotropic tidal energy transfer to baroclinic one but more investigations are needed. We also argue that this difference can be due to the atmospheric pressure effects that are not adequately subtracted from tide gauges and satellite altimetry because in the Mediterranean pressure effects are very different from inverse barometer effects. This probably makes the baroclinic model closer to the observations.

The revisited barotropic-equivalent tidal model of the Mediterranean Sea ($NEMO24_{2D}$), relies on several sensitivity tests, respect the one of Tsimplis *et al.*, (1995), since after almost 20 years, more sophisticated dataset and global tidal models are available. Moreover during the last years, the availability of more and more computational power has allowed to increase the resolution of ocean models and to take explicitly into account several physical processes that was parameterized in previous coarser models. This work has shown that the most important factors to build a robust tidal model of the Mediterranean Sea are basically the high resolution, an accurate bathymetry and a careful nesting into a global tidal model. In particular the Strait of Gibraltar deserves much attention since the simulation of tides in the Mediterranean Sea is strongly affected by the incoming Atlantic tide. With the current horizontal resolution of about 4 *km* the Strait of Gibraltar is solved with a minimum number of three grid cells on the meridional direction. Thanks also to the high number of vertical levels, the analysis of the Strait of Gibraltar of $NEMO24_{tide}$ model has given results that are comparable to high resolution models on the Strait of Gibraltar domain (such as the one of Sannino *et al.*, 2004), in terms of transports, salinity and temperature profiles and currents.

The originality of this work consists also in the setting up of a modelling chain, used to downscale the FES2014 tidal currents to the Med Sea model lateral open boundary which allows to reduce the errors on tidal representation. In particular an intermediate simulation with the TUGO model, forced only with FES2014 tidal elevations and using $NEMO24_{2D}$ bathymetry, allows to extract tidal currents on the boundary that are adapted to $NEMO24_{2D}$ bathymetry.

Once a satisfying tidal barotropic-equivalent model of the Mediterranean Sea is achieved, the results of this implementation are added to a pre-operational forecasting model of the Mediterranean Sea. This allows to study the interactions of tides with the complex dynamics of the Mediterranean Sea with an horizontal resolution never achieved so far. This is the true strength of $NEMO24_{tide}$ model. In fact, global assimilative models such as FES2014 or TPXO-8 have high resolution in the Mediterranean Sea but they are essentially barotropic models and they cant't be used to perform this kind of analysis.

In this work, the comparison of two tide and no-tides experiments has allowed to highlight non-neglecting features on both surface and intermediate currents. The interaction of the Atlantic barotropic tide with the complex bathymetry of the Strait of Gibraltar generates an internal wave which effect is the enhancing of the vertical mixing in the Alboran Sea with a saltening and cooling of surface water and the opposite occurring on the underlying layer. The signature of tides in the rest of the Mediterranean Sea can be mainly associated to the propagation of the saltier Atlantic modified water, this is the reason why the most evident changes are found on the Southern part of the Mediterranean Sea, where permanent cyclonic and anticyclonic gyres are present. The intensification of these circulation structures in $NEMO24_{tide}$ respect to $NEMO24$ is evident. The results of this work are preliminary and give an overview of the main features deriving from the introduction of the potential forcing. At this stage it seems that the main tidal impact in the Mediterranean derives from the changes on the Atlantic Water that enter in the Mediterranean Sea which is saltier. More in depth investigations are needed on the mesoscale fields together with a comparison with the observed currents, salinity and temperature fields.

4.2   Future work

In this section we want to point out which are the aspects of this work that could be improved and which are further analysis that we plan as future work.

For what concerns tidal implementation, the shape and size of the Atlantic box could be an interesting aspect to investigate in future. The current shape poses some modelling issues, since its northern boundary crosses the Bay of Biscay shelf, where the tidal amplitudes and currents are very huge. This fact requires a careful calibration and the lowering of the time step of integration, in order to ensure the stability of the model, especially when a high number of tidal constituents is taken into account. In particular, the lowering of the time step of integration could be a problem in terms of computational coasts for a possible operational forecasting system

including tides. Considering that the propagation of tidal waves in the Atlantic is northward, this high currents, should not influence the tidal inflow in the Mediterranean Sea if we consider an Atlantic reduced buffer zone, crossing the Spanish North-Western corner instead of the French shelf. On the other hand, reducing the shape of the current domain could imply a worsening of the non-tidal dynamics. Several sensitivity tests should be done in order to find an optimal size and shape for the Atlantic box. The possibility to use unstructured open boundary conditions (already implemented in NEMO model) which offer a multitude of possible shapes should be also considered, since it could allow to use a larger buffer zone without the necessity of crossing the French or England shelves, where tides are huge, by means of a curve open boundary section.

An issue of $NEMO24_{tide}$ model is the fact that tidal amplitude in the Alboran Sea is underestimated when the GEBCO bathymetry interpolated on the $1/24° \times 1/24°$ grid is used. In the barotropic-equivalent $NEMO24_{2D}$ tidal model, the bathymetry system of sub-marine sills at the Strait of Gibraltar have been modified by hand and smoothed in order to simulate properly the tidal amplitude in the Alboran Sea which are otherwise underestimated. On the other hand, at this stage, we prefer to use the original bathymetry in the $NEMO24_{tide}$ model since it ensure a good estimate of transports, in agreement with the literature ones. In future, more sensitivity tests should be done on the bathymetry at the Strait of Gibraltar, in order to find a compromise between the right simulation of tidal amplitude at the Alboran Sea and the correct estimate of Eastern and Western transports. In particular a combination of the two mentioned sensitivity tests on the size of the Atlantic box and on the bathymetry at the Strait of Gibraltar could improve the tidal solution in the Alboran Sea.

In this work an increasing of bottom friction is introduced in the shelf areas, in $NEMO24_{2D}$ tidal model in order to make it comparable with the assimilative FES2014 tidal model. On the other hand, the more realistic $NEMO24_{tide}$ model gives satisfying results without this parameterisation. This fact suggest that a non negligible baroclinic component is present in the Mediterranean Sea. We argue that an estimate of the tidal energy budget associated to tides in Mediterranean Sea should be done in order to better understand the tidal mixing processes and the associated energy distributions and to highlight possible tidal energy conversion processes.

The reason why a significative improvement is reached in diurnal tidal components by the comparison between $NEMO24_{2D}$ and $NEMO24_{tide}$ still remain unsolved. At this stage the main four tidal components are considered in the $NEMO24_{tide}$ model which are responsible of most part of the tidal signal in the Mediterranean Sea. We prefer to increase the number of tidal components gradually, in order to highlight their specific contribution on the effects of the Mediterranean Sea.

From the literature we know that that the M2 and S2 components are responsible for most part of the Atlantic tide hence for the processes occurring at the Gibraltar Strait and that modify the Atlantic incoming Water. The diurnal components K1 and O1 could have non negligible effects on the basin too, so another in depth analysis could be the comparison of the results of $NEMO24$ model with other two experiments forced only by the semidiurnal and the diurnal components separately in order to understand their own signature.

The results discussed in Chapter 3 are preliminary consideration on the effects of tides on the circulation of the Mediterranean Sea on a basin scale, while the accurate study of local processes, such as a more in deep analysis of the internal tide at the Gibraltar Strait, will be the object of future research.

Appendix A

CTOH tidal constant validation dataset

Altimetry data used in this study were developed, validated, and distributed by the CTOH/LEGOS, France. The aim of Center of Topography of the Ocean and Hydrosphere (CTOH) is to provide the scientific community with a large collection of tidal constant estimates from the satellite altimetry data on both continental shelves and costal regions.

These regionals products are available over more than twenty areas including the Mediterranean Sea, [1]. Tidal constant products for each region are amplitudes, phase lags and accuracy estimates for a a wide spectrum of tidal constituents, every 6 - 7 km along the satellite ground tracks.

The tidal constant database is computed using the CTOH regional Sea Level Anomalies database, taking advantage of the TOPEX-Poseidon, Jason-1 and Jason-2 long time series and the X-TRACK costal processing tool. In fact due to the interaction of radar signal with land topography, satellite altimetry data processing and interpretation is very difficult in costal areas. The X-TRACK is a post-processing software, that has been developed by the CTOH in order to optimise the completeness and the accuracy of the sea surface height information, derived from satellite altimetry in coastal ocean areas. It is tailored for extending the use of altimetry data to coastal ocean applications and provides freely available along-track Sea Level Anomaly time series that cover today all the coastal oceans.

The X-TRACK tool and the results derived from its last version (2016) in costal areas is widely discussed in Birol et al., 2017.

X-TRACK main products are along track sea surface heights (SSH), mean sea surface (MSS) and sea level anomalies (SLA) along the satellite ground track. These products are available at both a 1Hz rate and a higher rate (10/20 Hz) for the TOPEX/Poseidon, Jason-1, Geosat-Follow-On and Envisat altimeter missions.

---

[1] http://ctoh.legos.obs-mip.fr/products/coastal-products/coastal-products-1/tidal-constants
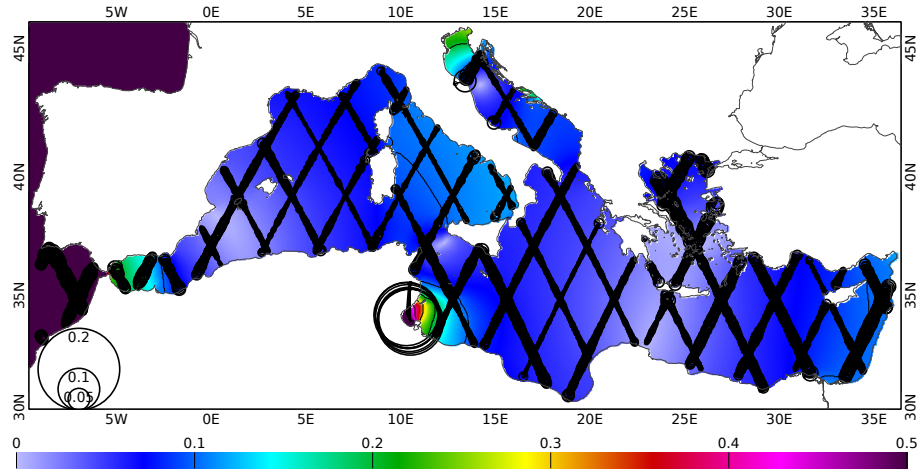
FIGURE A.1: Tidal misfits in the Mediterranean Sea for M2 tidal constituent:
background chart represents the tidal amplitude in m from NEMO-24 barotropic
model. The size of the black circles is proportional to the modulus of the complex
difference between NEMO modelled amplitude and CTOH tidal one.

In figure A.1 the CTOH tidal amplitude is compared to the M2 solution of NEMO-24 barotropic
tidal model over all the Mediterranean Sea. Altimeter-derived tidal constituents are computed
from a harmonic analysis of the X-TRACK SLA onto mean tracks products. For the Mediter-
ranean Sea, X-TRACK altimeter products are de-aliased by a combination of regional modelling
of tides and short-period ocean response to meteorological forcing (Roblou et al., 2007). On the
M2 tidal constituent, the overall RMS_{misfit} is of cm.

The size of the black circles is proportional to the modulus of the complex difference between
NEMO modelled amplitude and CTOH tidal amplitude. In general it is lower than 5 cm over
all the basin with the exception of the Gulf of Gabès, where the error can be interpreted as
the combination of, in one hand, residual modelling errors in NEMO-24 solutions and, in the
other hand, residual noise in the altimeter measurements. For this reason, the validation with
CTOH altimetry data, gives an overall estimate of tidal accuracy in open-ocean ares while for the
assessment of tides in costal areas the comparison with tidal gauges harmonics must be preferred
B.

Appendix B

Tide gauge validation dataset

In this appendix a short description of the control set of tide gauges used to validate the harmonics modelled by NEMO is given. The figure B.1 shows the locations of tide gauge sites, while in the table B.1 the list sites in alphabetic order, the associated numbers, their coordinates and their source can be found.
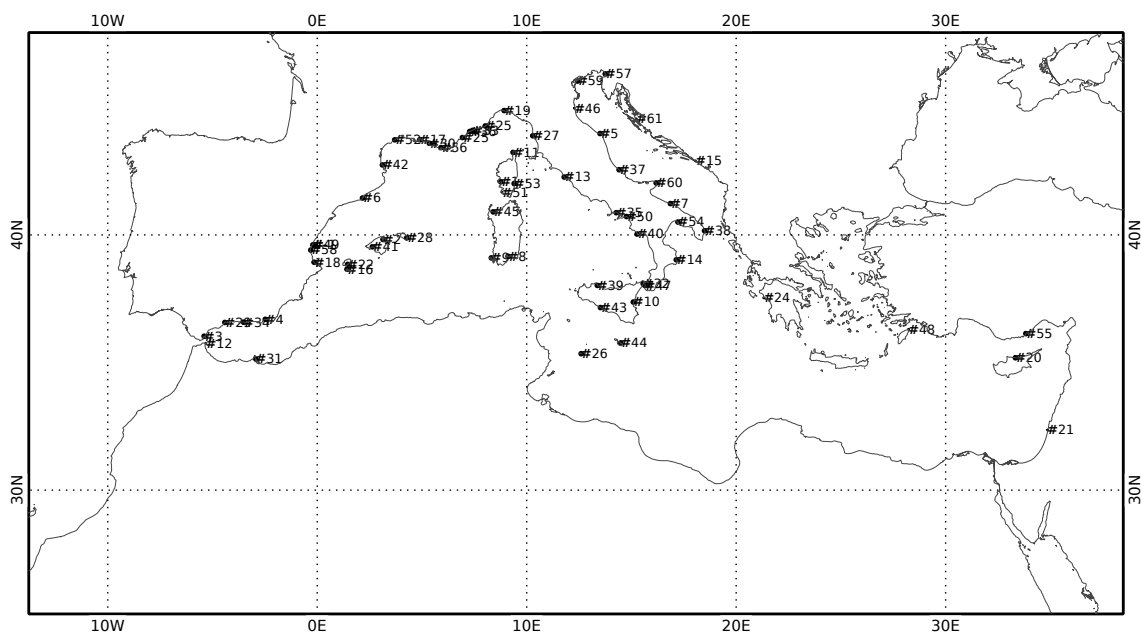
FIGURE B.1: Control dataset of tide gauges

The institutes which provides the hourly time series are basically:

- Puerto del Estado, for the Spanish tide gauges;

- ISPRA - Istituto Superiore per la Protezione e la Ricerca Ambientale, for the Italian tide gauges;

- SHOM Service Hydrographique et Océanographique de la Marine, for the French tide gauges.

Starting from these time hourly series the harmonics have been calculated with the T-UGO Tidal Toolbox, the same tool used to harmonically analyse the modelled time series.

Ten other tidal harmonics are added to this dataset. They are kindly provided by LEGOS, France (Florent Lyard, personal communication).

TABLE B.1: Tide gauges sites and associated numbers, coordinates and source of the SLA data.

No	Station	longitude	latitude	Source
1	Ajaccio	8°45'36.00"	41°55'12.00"	SHOM
2	Alcudia	3°08'24.00"	39°49'48.00"	Puerto del Estado
3	Algeciras	-5°24'00.00"	36°10'48.00"	Puerto del Estado
4	Almeria	-2°28'48.00"	36°49'48.00"	Puerto del Estado
5	Ancona	13°30'00.00"	43°37'12.00"	ISPRA
6	Barcelona	2°09'36.00"	41°20'24.00"	Puerto del Estado
7	Bari	16°51'36.00"	41°08'24.00"	ISPRA
8	Cagliari	9°06'36.00"	39°12'36.00"	ISPRA
9	Carloforte	8°18'36.00"	39°09'00.00"	ISPRA
10	Catania	15°05'24.00"	37°29'24.00"	ISPRA
11	Centuri	9°21'00.00"	42°57'36.00"	SHOM
12	Ceuta	354°40'58.80"	35°54'00.00"	LEGOS
13	Civitavecchia	11°47'24.00"	42°05'24.00"	ISPRA
14	Crotone	17°08'24.00"	39°04'48.00"	ISPRA
15	Dubrovnik	18°03'46.80"	42°39'28.80"	LEGOS
16	Formentera	1°25'12.00"	38°43'48.00"	Puerto del Estado
17	Fos Sur Mer	4°53'24.00"	43°24'00.00"	SHOM
18	Gandia	-0°09'00.00"	38°59'24.00"	Puerto del Estado
19	Genova	8°55'12.00"	44°24'36.00"	ISPRA
20	Girne	33°19'48.00"	35°20'24.00"	LEGOS
21	Hadera	34°52'01.20"	32°28'01.20"	LEGOS
22	Ibiza	1°27'00.00"	38°54'36.00"	Puerto del Estado
23	Imperia	8°01'12.00"	43°52'48.00"	ISPRA
24	Katakolo	21°18'54.00"	37°39'00.00"	LEGOS
25	La Figueirette	6°55'48.00"	43°28'48.00"	SHOM
26	Lampedusa	12°36'00.00"	35°30'00.00"	ISPRA
27	Livorno	10°17'24.00"	43°32'24.00"	ISPRA
28	Mahon	4°16'12.00"	39°53'24.00"	Puerto del Estado
29	Malaga	-4°24'36.00"	36°42'36.00"	Puerto del Estado
30	Marseille	5°21'00.00"	43°16'48.00"	SHOM
31	Melilla	-2°55'48.00"	35°17'24.00"	Puerto del Estado
32	Messina	15°33'36.00"	38°11'24.00"	ISPRA
33	Monaco	7°25'12.00"	43°43'48.00"	SHOM
34	Motril	-3°31'12.00"	36°43'12.00"	Puerto del Estado
35	Napoli	14°16'12.00"	40°48'36.00"	ISPRA
36	Nice	7°16'48.00"	43°41'24.00"	SHOM
37	Ortona	14°24'36.00"	42°21'00.00"	ISPRA
38	Otranto	18°29'24.00"	40°09'00.00"	ISPRA
39	Palermo	13°22'12.00"	38°07'12.00"	ISPRA
40	Palinuro	15°16'12.00"	40°01'48.00"	ISPRA
41	Palma De Mallorca	2°37'48.00"	39°33'36.00"	Puerto del Estado
42	Porto Empedocle	13°31'12.00"	37°16'48.00"	ISPRA
43	Portomaso	14°29'24.00"	35°55'12.00"	ISPRA
44	Portotorres	8°24'00.00"	40°50'24.00"	ISPRA
45	Port Vendres	3°06'36.00"	42°31'12.00"	SHOM
46	Ravenna	12°16'30.00"	44°29'31.20"	ISPRA
47	Reggio Calabria	15°38'24.00"	38°07'12.00"	ISPRA
48	Rhodes	28°13'58.80"	36°26'49.20"	LEGOS
49	Sagunto	-0°12'00.00"	39°37'48.00"	Puerto del Estado

TABLE B.1: Tide gauges sites and associated numbers, coordinates and source of the SLA data.

No	Station	longitude	latitude	Source
50	Salerno	14°45'36.00"	40°40'12.00"	ISPRA
51	Senetosa	8°48'46.80"	41°33'00.00"	LEGOS
52	Sete	3°42'00.00"	43°24'00.00"	SHOM
53	Solenzara	9°24'00.00"	41°51'36.00"	SHOM
54	Taranto	17°13'12.00"	40°28'12.00"	ISPRA
55	Tasucu	33°49'48.00"	36°16'48.00"	LEGOS
56	Touloun	5°54'36.00"	43°07'48.00"	SHOM
57	Trieste	13°45'00.00"	45°39'00.00"	ISPRA
58	Valencia	-0°18'36.00"	39°26'24.00"	Puerto del Estado
59	Venezia	12°25'12.00"	45°24'36.00"	ISPRA
60	Vieste	16°10'48.00"	41°52'48.00"	ISPRA
61	Zadar	15°14'06.00"	44°07'22.80"	LEGOS

Bibliography

Adani, Mario, Srdjan Dobricic, and Nadia Pinardi (2011). "Quality assessment of a 1985–2007 Mediterranean Sea reanalysis". In: *Journal of Atmospheric and Oceanic Technology* 28.4, pp. 569–589.

Adcroft, Alistair and Jean-Michel Campin (2004). "Rescaled height coordinates for accurate representation of free-surface flows in ocean circulation models". In: *Ocean Modelling* 7.3, pp. 269–284.

Allain, Damien J (2016). *TUGOm Tidal ToolBox*. Tech. rep.

Arabelos, DN et al. (2011). "A new tide model for the Mediterranean Sea based on altimetry and tide gauge assimilation". In: *Ocean Science* 7.3, pp. 429–444.

Artale, V et al. (1994). "Seasonal variability of gyre-scale circulation in the northern Tyrrhenian Sea". In: *Journal of Geophysical Research: Oceans* 99.C7, pp. 14127–14137.

Artegiani, A et al. (1997). "The Adriatic Sea general circulation. Part I: Air–sea interactions and water mass structure". In: *Journal of physical oceanography* 27.8, pp. 1492–1514.

Ayoub, Nadia, Pierre-Yves Le Traon, and Pierre De Mey (1998). "A description of the Mediterranean surface variable circulation from combined ERS-1 and TOPEX/POSEIDON altimetric data". In: *Journal of Marine Systems* 18.1, pp. 3–40.

Bernard, Barnier et al. (2006). "Impact of partial steps and momentum advection schemes in a global ocean circulation model at eddy-permitting resolution". In: *Ocean dynamics* 56.5-6, pp. 543–567.

Birol, F et al. (2017). "Coastal applications from nadir altimetry: example of the X-TRACK regional products". In: *Advances in Space Research* 59.4, pp. 936–953.

Candela, Julio (1991). "The Gibraltar Strait and its role in the dynamics of the Mediterranean Sea". In: *Dynamics of Atmospheres and Oceans* 15.3-5, pp. 267–299.

Carrère, L et al. (2012). "FES 2012: a new tidal model taking advantage of nearly 20 years of altimetry measurements". In: *Ocean Surface Topography Science Team 2012 meeting, Venice-Lido, Italy*.

Carter, Glenn S and Mark A Merrifield (2007). "Open boundary conditions for regional tidal simulations". In: *Ocean Modelling* 18.3, pp. 194–209.

Cushman-Roisin, Benoit et al. (2013). *Physical oceanography of the Adriatic Sea: past, present and future*. Springer Science & Business Media.

Defant, Albert (1961). "Physical Oceanography". In: *Pergamon Press, New York*.

Egbert, Gary D, Andrew F Bennett, and Michael GG Foreman (1994). "TOPEX/POSEIDON tides estimated using a global inverse model". In: *Journal of Geophysical Research: Oceans* 99.C12, pp. 24821–24852.

Egbert, Gary D and Svetlana Y Erofeeva (2002). "Efficient inverse modeling of barotropic ocean tides". In: *Journal of Atmospheric and Oceanic Technology* 19.2, pp. 183–204.

Egbert, Gary D and Richard D Ray (2001). "Estimates of M2 tidal energy dissipation from TOPEX/Poseidon altimeter data". In: *Journal of Geophysical Research: Oceans* 106.C10, pp. 22475–22502.

Egbert, GD and RD Ray (2000). "Significant dissipation of tidal energy in the deep ocean inferred from satellite altimeter data". In: *Nature* 405.6788, pp. 775–778.

Flather, RA (1976). "A tidal model of the northwest European continental shelf". In: *Mem. Soc. Roy. Sci. Liege* 10, pp. 141–164.

Foreman, MGG et al. (1993). "A finite element model for tides and resonance along the north coast of British Columbia". In: *Journal of Geophysical Research: Oceans* 98.C2, pp. 2509–2531.

Green, JA Mattias and Jonas Nycander (2013). "A comparison of tidal conversion parameterizations for tidal models". In: *Journal of Physical Oceanography* 43.1, pp. 104–119.

Guarnieri, A et al. (2013). "Impact of tides in a baroclinic circulation model of the Adriatic Sea". In: *Journal of Geophysical Research: Oceans* 118.1, pp. 166–183.

Harzallah, Ali, Mohamed Alioua, and Laurent Li (2014). "Mass exchange at the Strait of Gibraltar in response to tidal and lower frequency forcing as simulated by a Mediterranean Sea model". In: *Tellus A: Dynamic Meteorology and Oceanography* 66.1, p. 23871.

Hicks, Steacy D and Paul Schureman (1984). *Tide and current glossary*. US Department of Commerce, National Oceanic and Atmospheric Administration, National Ocean Service.

Kang, Dujuan (2012). "Barotropic and Baroclinic Tidal Energy". In: *Energy Conservation*. InTech.

Lascaratos, A and K Nittis (1998). "A high-resolution three-dimensional numerical study of intermediate water formation in the Levantine Sea". In: *Journal of Geophysical Research: Oceans* 103.C9, pp. 18497–18511.

Le Provost, C et al. (1994). "Spectroscopy of the world ocean tides from a finite element hydro-dynamic model". In: *Journal of Geophysical Research: Oceans* 99.C12, pp. 24777–24797.

Le Traon, Pierre-Yves et al. (1994). "Global statistical analysis of TOPEX and POSEIDON data". In: *Journal of Geophysical Research: Oceans* 99.C12, pp. 24619–24631.

Lefevre, Fabien et al. (2002). "FES99: a global tide finite element solution assimilating tide gauge and altimetric information". In: *Journal of atmospheric and oceanic technology* 19.9, pp. 1345–1356.

Levier, B et al. (2007). "Free surface and variable volume in the NEMO code". In: *MERSEA IP report WP09-CNRS-STR03-1A*.

Lozano, CJ and Julio Candela (1995). "The M (2) tide in the Mediterranean Sea: Dynamic analysis and data assimilation". In: *Oceanologica acta* 18.4, pp. 419–441.

Lyard, Florent et al. (2006). "Modelling the global ocean tides: modern insights from FES2004". In: *Ocean Dynamics* 56.5-6, pp. 394–415.

Lynch, Daniel R and William G Gray (1979). "A wave equation model for finite element tidal computations". In: *Computers & fluids* 7.3, pp. 207–228.

Madec, Gurvan (2008). "NEMO reference manual, ocean dynamic component: NEMO-OPA". In: *Note du Pôle de modélisation, Institut Pierre Simon Laplace, France, Technical Report* 27.

Maraldi, Claire et al. (2013). "NEMO on the shelf: assessment of the Iberia-Biscay-Ireland con-figuration." In: *Ocean Science* 9, pp. 745–771.

Millot, Claude (1990). "The gulf of Lions' hydrodynamics". In: *Continental Shelf Research* 10.9, pp. 885–894.

Munk, Walter and Carl Wunsch (1998). "Abyssal recipes II: energetics of tidal and wind mixing". In: *Deep Sea Research Part I: Oceanographic Research Papers* 45.12, pp. 1977–2010.

Naranjo, C et al. (2014). "How much do tides affect the circulation of the Mediterranean Sea? From local processes in the Strait of Gibraltar to basin-scale effects". In: *Progress in Oceanography* 127, pp. 108–116.

Oddo, P and N Pinardi (2008). "Lateral open boundary conditions for nested limited area models: a scale selective approach". In: *Ocean modelling* 20.2, pp. 134–156.

Oddo, P et al. (2009). "A nested Atlantic-Mediterranean Sea general circulation model for oper-ational forecasting". In: *Ocean science.*

Oddo, P et al. (2014). "Sensitivity of the Mediterranean sea level to atmospheric pressure and free surface elevation numerical formulation in NEMO". In: *Geoscientific Model Development* 7.6, pp. 3001–3015.

O'dea, EJ et al. (2012). "An operational ocean forecast system incorporating NEMO and SST data assimilation for the tidally driven European North-West shelf". In: *Journal of Operational Oceanography* 5.

Pacanowski, RC and SGH Philander (1981). "Parameterization of vertical mixing in numerical models of tropical oceans". In: *Journal of Physical Oceanography* 11.11, pp. 1443–1451.

Pairaud, Ivane L et al. (2008). "Dynamics of the semi-diurnal and quarter-diurnal internal tides in the Bay of Biscay. Part 1: Barotropic tides". In: *Continental Shelf Research* 28.10, pp. 1294–1315.

Pettenuzzo, D, WG Large, and N Pinardi (2010). "On the corrections of ERA-40 surface flux products consistent with the Mediterranean heat and water budgets and the connection between basin surface total heat flux and NAO". In: *Journal of Geophysical Research: Oceans* 115.C6.

Pinardi, N and G Coppini (2010). "Preface" Operational oceanography in the Mediterranean Sea: the second stage of development"". In: *Ocean Science* 6.1, pp. 263–267.

Pinardi, Nadia and Antonio Navarra (1993). "Baroclinic wind adjustment processes in the Mediterranean Sea". In: *Deep Sea Research Part II: Topical Studies in Oceanography* 40.6, pp. 1299–1326.

Pinardi, Nadia et al. (2003). "The Mediterranean ocean forecasting system: first phase of implementation (1998-2001)". In: *Annales Geophysicae*. Vol. 21. 1, pp. 3–20.

Pinardi, Nadia et al. (2015). "Mediterranean Sea large-scale low-frequency ocean variability and water mass formation rates from 1987 to 2007: a retrospective analysis". In: *Progress in Oceanography* 132, pp. 318–332.

Pinardi, Nadia et al. (2017). "From weather to ocean predictions: an historical viewpoint". In: *Journal of Marine Research* 75.3, pp. 103–159.

Pugh, David T (1996). *Tides, surges and mean sea-level (reprinted with corrections)*. John Wiley & Sons Ltd.

Robinson, Allan R et al. (1992). "General circulation of the Eastern Mediterranean". In: *Earth-Science Reviews* 32.4, pp. 285–309.

Roblou, Laurent et al. (2007). "X-TRACK, a new processing tool for altimetry in coastal oceans". In: *Geoscience and Remote Sensing Symposium, 2007. IGARSS 2007. IEEE International*. IEEE, pp. 5129–5133.

Roblou, Laurent et al. (2011). "Post-processing altimeter data towards coastal applications and integration into coastal models". In: *Coastal altimetry*. Springer, pp. 217–246.

Sammari, Chérif, Vladimir G Koutitonsky, and Mahmoud Moussa (2006). "Sea level variability and tidal resonance in the Gulf of Gabes, Tunisia". In: *Continental Shelf Research* 26.3, pp. 338–350.

Sánchez-Garrido, José Carlos et al. (2011). "Numerical modeling of three-dimensional stratified tidal flow over Camarinal Sill, Strait of Gibraltar". In: *Journal of Geophysical Research: Oceans* 116.C12.

Sannino, G, A Bargagli, and V Artale (2004). "Numerical modeling of the semidiurnal tidal exchange through the Strait of Gibraltar". In: *Journal of Geophysical Research: Oceans* 109.C5.

Sannino, G et al. (2015). "On the relevance of tidal forcing in modelling the Mediterranean thermohaline circulation". In: *Progress in Oceanography* 134, pp. 304–329.

Sannino, Gianmaria, Lawrence Pratt, and Adriana Carillo (2009). "Hydraulic criticality of the exchange flow through the Strait of Gibraltar". In: *Journal of Physical Oceanography* 39.11, pp. 2779–2799.

Sannino, Gianmaria et al. (2009). "An eddy-permitting model of the Mediterranean Sea with a two-way grid refinement at the Strait of Gibraltar". In: *Ocean Modelling* 30.1, pp. 56–72.

Sannino, Gianmaria et al. (2014). "Mediterranean model response to enhanced resolution at Gibraltar and tidal forcing". In: *BLACK SEA/MEDITERRANEAN ENVIRONMENT*, p. 41.

Schureman, Paul (1940). *Manual of harmonic analysis and prediction of tides*. U. S. DEPARTMENT OF COMMERCE, COAST and GEODETIC SURVEY.

Shriver, JF et al. (2012). "An evaluation of the barotropic and internal tides in a high-resolution global ocean circulation model". In: *Journal of Geophysical Research: Oceans* 117.C10.

Shum, CK et al. (1997). "Accuracy assessment of recent ocean tide models". In: *Journal of Geophysical Research: Oceans* 102.C11, pp. 25173–25194.

Soto-Navarro, Javier et al. (2015). "Evaluation of regional ocean circulation models for the Mediterranean Sea at the Strait of Gibraltar: volume transport and thermohaline properties of the outflow". In: *Climate Dynamics* 44.5-6, pp. 1277–1292.

Stammer, Detlef et al. (2014). "Accuracy assessment of global barotropic ocean tide models". In: *Reviews of Geophysics* 52.3, pp. 243–282.

Tejedor, Luis et al. (1999). "Simulation of the semidiurnal tides in the Strait of Gibraltar". In: *Journal of Geophysical Research: Oceans* 104.C6, pp. 13541–13557.

Tonani, M et al. (2008). "A high-resolution free-surface model of the Mediterranean Sea". In: *Ocean Science* 4.1, pp. 1–14.

Tonani, Marina et al. (2014). "The Mediterranean Forecasting System: recent developments". In: *EGU General Assembly Conference Abstracts*. Vol. 16, p. 16899.

Tsimplis, MN (1994). "Tidal oscillations in the Aegean and Ionian Seas". In: *Estuarine, Coastal and Shelf Science* 39.2, pp. 201–208.

Tsimplis, MN, R Proctor, and RA Flather (1995). "A two-dimensional tidal model for the Mediterranean Sea". In: *Journal of Geophysical Research: Oceans* 100.C8, pp. 16223–16239.

Zavatarielli, Marco and George L Mellor (1995). "A numerical study of the Mediterranean Sea circulation". In: *Journal of Physical Oceanography* 25.6, pp. 1384–1414.